Design, Fabrication and Performance of Silicon Monolithic Monochromators and its Application for Lattice Spacing Measurements of Si and GaAs Single Crystals with Synchrotron Radiation

Mohammed Obaidur Rahman

Doctoral Thesis

Department of Material Structure Science
School of Mathematical and Physical Sciences
The Graduate University for Advanced Studies

March 2002

Contents

Chapter 1

Motivation

The aim and scope of the present research is to illustrate the potential of Silicon monolithic monochromators and its applications for lattice spacing measurements of Si and GaAs and associated defects in it using brilliant Synchrotron radiation.Monolithic monochromators are critical ingredients where fixed wavelength plays the key role. In the monolithic structure the interplanar angle between the concerned diffraction planes are fixed, thus the wavelength emerging from this device are highly stable and we exploit this feature in the measurements of lattice spacing of Si and GaAs in our present study.

The lattice spacing of crystalline solids are sensitive to a wide variety of phenemenon such as elastic strains by variation in the temperature,pressure, mechanical stress, impurity, vacancy, electric and magnetic fields. These are mainly sensitive in the region of few parts per million. For example if one is interested only in the strains below$\Delta d/d \leq 10^{-3}$ and if a precision of order 1 percent is required, then sensitivity to $\Delta d/d \leq 10^{-5}$ must be achieved. The absolute and relative measurement of lattice spacing of silicon crystal is important for the establishment of precision wavelegth scale for various spectroscopies and also for the determination of fundamental physical constants like Avogadro constant and atomic mass unit. Determination of avo-

gadro number with high accuracy is needed to define the mole, kilogram and electric standards. There are many defects in semiconductor materials those are at the order of 10^{-5} to 10^{-8}. Therefore our aim is to measure the lattice parameter of Si and GaAs with high precision and accuracy using Synchrotron radiation from 2.5 GeV facility of Photon factory,KEK, Japan. In this regard a 4-reflection channel-cut monolithic monochromator has been realized to achieve the unique wavelength which is one of the key ingredients for high precision lattice parameter measurement. We have developed several new methods of different optics for the lattice parameter measurement systems at BL-3C2 of Photon Factory.

1.0.1 Synchrotron x-rays

As is well-known some of the advantages of SR compared to conventional x-ray generator tubes are, higher intensity, the wavelength selectivity and well-colliminated beam. Many devices have and are being developed to further increase the intensity such as wigglers and undulators and x-ray FEL's. We used the standard bending magnet radiation which gave at least an order of magnitude higher intensity and better resolution than the X-ray tube. The much higher statistics and lower background obtained with SR are important factors in the measurements.

1.1 Previous study:

The starting point of lattice spacing measurements by x-ray diffraction methods and evaluation of their accuracy and precision is the Bragg's law, combining diffraction conditions with the parameters of the lattice to be determined by $2dsin\theta = n\lambda$ where d is the interplanar distance being a function of direct lattice parameters and n is the order of interference, a correction for refraction of X-rays should be introduced. Measurement of lattice spacings can be divided into absolute in which lattice spacings are determined under defined enviornmental conditions, and relative, in which compared to a reference crystal, small changes of lattice spacings due to the temperature, pressure, mechanical stress etc are examined. In the particular case when the lattice parameter of the reference crystal has been very accurately determined, precise determination of the ratio of two lattice spacing will enable one to obtain an accurate value of the speciman parameter. Absolute method can be characterized by the accuracy Δd defined as the difference between measured and real interplanar spacings or more frequently by using the relative accuracy, $\Delta d/d$ defined by the formula obtained as a result of differentiation of the Bragg law: $\Delta d/d = \Delta\lambda/\lambda - cot\theta\Delta\theta$ where $\Delta\lambda/\lambda$ is relative accuracy of the wavelength determination in relation to the

commonly accepted wavelength standard, and $\Delta\theta$ is the error in the Bragg angle determined. There are many ways by which one can measure the lattice parameter depending on the need of the experimenter, the details are given elsewhere, they can classified mainly in the following way:

(1) Single Crystal Methods:

(a) The Bond Method

(b) The Kossel Method

(c) Energy dispersive methods

(d) High angle diffraction of X-rays

(2) Multiple Crystal Methods:

(a) Double Crystal rocking curve

(b) Rocking curve from epitaxial layer

(c) Three reflection comparator

(d) Double beam comparators

(3)Topographic Methods:

(a) Bragg angle mapping

(b) Bragg angle contours.

In the crystal diffraction methods, which give accurate determinations of the Bragg angles and intensities, several instrumental and physical factors should be taken into account. .The effect of some can be diminished by the use of soller slits and effects of most can be reduced by the Bond geometry, in its basic forms or its various modifications in particular in combination with double or triple crystal spectrometers. Another arrangement giving a partial reduction of systematic errors phenomena are applied. In most one or double crystal assymetric spectrometers , the uncertainty of the origin of the angular scale is the important problem, which can be resolved by Bond symmetrical arrangement or triple axis arrangement or a second beam in the multiple beam method or in various combined method. The other important

problem in the single-crystal methods, in the case when high accuracy is required, is the mis-alignment of the crystals and some element of the device. The errors due to the mis-alignment can be reduced to some extent experimentally if a respective dependence is known.

Along with an increase of Bragg angle determination, the error due to the wavelength determination becomes more important and a correction for the refraction should be introduced. Among others measurement performed in the case of Kossel method and divergent-beam techniques can be strongly affected by uncertainty of wavelength, especially when the exact value of the wavelength is to be determined[1-10] from the experiment. Combination of X-ray and optical interferrometry gives new possibilities of very accurate lattice spacing measurements. For obtaining high precision a monochromatic and well collimated X-ray beam is desired . Some authors have managed to reduce the cost of the experiment using simple equipment. An example may be the triple-crystal scheme realized by the use of a double-axis spectrometer. Considering all the methods we found a method which reduce the error in Bragg angle measurement and reduce the error in wavelength selection[10-19], both are achieved in our lattice spacing measurement system which are by monolithic monochromator for particular wavelength and particular sample indexes and thus we demonstrate the potential of Monolithic monochromator x-ray optics.

1.2 Present Study

The aim and scope of the present research is to illustrate the potential of Silicon monolithic monochromators and its applications for lattice spacing measurements of Si and GaAs and associated defects in it using brilliant Synchrotron radiation. The precise and accurate determination of lattice spacing attract scientists for decades as there is a continuous need for the establishment of precision wavelength scale for

x-ray, determination of Avogadro number and atomic mass unit with high accuracy. In addition the production of silicon wafers free enough of both defects and contamination for use in the semiconductor industry is becoming increasingly difficult. The industry is working on the problems associated with detecting, identifying and specifying these features. Our goal is to understand the very small strain in silicon and in silicon wafer with a precision of $\Delta d/d = 10^-7$to 10^-8. Many works has been reported using optical/x-ray interferrometry and conventional x-ray tube in this connection. On the otherhand we have used synchrotron x-ray which is extremely high intense, collimated, forward directed and tunable in comparison with conventional x-ray tube. In addition we have introduced an monolithic monochromator x-ray optics as a fixed wavelength device for the first time. We have designed and fabricated several monolithic monochromators of different wavelengths, resolution, geometry and energy dispersive settings from the notion that monolithic monochromators can play an important role in the development of synchrotron radiation x-ray optics and can provide the precision information about the materials. Monolithic monochromators (MM/MDCM) are made from a single piece of silicon slot and perhaps this is the significant difference from the Double crystal monochromator (DCM)where the crystals are seperated. Due to this difference there are lot of improvements in the x-ray optics can be obtained by MM than DCM. Notably we can get an excellent 'stability' by MM than DCM due to its mono lithic structure. In the monolithic structure the interplanar angle between the concerned diffraction plane is fixed therefore the wavelength emerging from this device can retain its high stability. Thus MM can be used as an excellent precision wavelength device.

Therefore MM are a citical ingredient where fixed wavelength plays the key role. The 'continuous' properties and 'good natural collimation' of synchrotron x-rays in addition to the large distance from the source allows monolithic monochromators to provide a high energy resolution using a high index reflection. Using this high

resolution features of MM, one can achieve an excellent x-ray optics. So far our knowledge no technological details about MM is reported in the literature.
We have designed and fabricated several monolithic monochromators, here we reported their design principle, fabrication and applications .We applied some of the MM in the high precision measurement of Si and GaAs lattice spacing with synchrotron radiation, mainly two methods (1) Precision Bond Method with MDCM optics (2) Bragg method from pair of diffraction. The results demonstrate their potential use as a precision wavelength device as well as an excellent SR x-ray optics.

In our study Chapter 2 describes details of monolithic monochromator (MM) design, fabrication and etching techniques. A code for wavelength generation has been also described in this chapter.

Chapter 3 describes the development of dynamical X-ray diffraction theory. We present analytical expressions for diffraction curves in Bragg (reflection) geometry. Several examples are presented as an implementation of the theory in this chapter. Chapter 3 also contains the refraction and temperature corrections that are necessary for high precision lattice spacing measurement with theoretical details.

Chapter 4 describes the characterization of all MM's which include the wavelength callibration and details descriptions of Dumond diagrams for all MM's. Further Chapter 4 discusses with the 3-beam and many beam effect in the simultaneous diffraction from the monochromator that uses the Bragg diffraction of two same planes of (513) and (153) ,detail calculation shows that overall Bragg peak shift around 12 micro-radians. The Triplet phase have been determined to be zero degree for the coplanar three beam (000), (513) and (153).

In Chapter 5 we describe X-ray optic systems that have been developed at beam line BL-3C2 of Photon factory,KEK for the study of the relative lattice spacings of Si-wafers using synchrotron radiation (SR). Since, unlike a X-ray tube, SR has no characteristic [wavelength] spectral lines, a new tool of (+,+) high resolution

channel-cut monolithic monochromators (MM) are introduced in the systems as a wavelength selective device. Using two types of MM, two schemes are proposed and applied to the study of the lattice spacings of Si-wafers. The lattice spacing differences are determined in the range of sub ppm level, for example in scheme-1 we obtain 0.6 ppm and 0.2 ppm in scheme-2. One of the practical advantages of this system is that it can be applied for a fast and precise measurement of the lattice spacing changes due to the doping and defects in Si, GaAs and other single crystals. Scheme-1 describes the introduction MM optics as a wavelength selection device while using the modified Bond method , thus the method provides the absolute determination of lattice spacing values, the precision of the method increases with the increase of higher Bragg angle,MM plays the role of Cu,Mo labratory x-ray source for wavelength selection. The proposed method is unique for precision d-spacing measurement using the state-of the are SR technology. In scheme-2 uses the Bragg diffraction of two same planes of a sample, in this scheme lattice spacing differences are determined from the measured differences in two quasi-simultaneous Bragg diffractions of two equivalent atomic planes in a crystal. If we select a particular x-ray wavelength and pair of planes in the crystal with interplanar angle between the planes matching the diffraction condition, the Bragg angle can be obtained by measuring a small angle in a range of few arcseconds instead of measuring a wide angle of few tens degrees in the Bond method. Asmall angle can be measured quickly and accurately, therefore the the method provides high accuracy as well as speedy.

Chapter 6 describes the lattice spacing measurement fron GaAs single crystal. The lattice spacing of GaAs has been measured using the modified Bond method at the order of ppm level.

As a conclusion, several monolithic monochromators of (+,+) type has been designed and fabricated as a energy selective device and is classified into two types

which provides two schemes for lattice spacing measurement . We have achieved the relative lattice value at the order of 10^{-7} to10^{-8} in this study as overall precision of the proposed system. Further three beam cases have been described in details for the type-2 monochromator where equivalent planes are excited simultaneously showing the Bragg peak shift for N-beam interactions with (000),(513) and (153) co-planar three beam cases. More elaborately, conclusions are given after each chapter.

Chapter 2

Monolithic Monochromator(MM) Design and Fabrication

2.1 Introduction

High energy resolution Monolithic monochromator are a critical ingredient in the measurement where fixed wavelengths[26,27] play the key role such as determination of lattice spacing of Si with high precision and accuracy, and in the inelastic scattering for example to study the phonon spectrum and in nuclear resonant scattering experiments. In these experiments it is necessary to reduce the energy bandwidth of the beam from the high heat load monochromator from a few eV to the required few meV level with very high efficiency. We can produce meV beams including cystals in the dispersive arrangements (+,-,-,+) and scattering at High Bragg angles.

We fabricate the monolithic double crystal monochromator from a single perfect crystal as a means of obtaining an X-ray beam of well defined wavelength

Monolithic double crystal monochromator(MM), in effect a single perfect crystal where two sets of Bragg planes play the role of two seperate crystals. The angleβ_0 between the two crystals of the MM is therefore fixed.Since the dihedral angle between

the diffracting planes is fixed, the wavelength of the emerging beam is completely determined by the geometry of the crystal structure when one imposes the conventional condition that the beam must lie in the plane defined by the two diffraction vectors.

We can obtain the longest wavelength by rotating the double crystal monochromator around an axis normal to the first set of planes. Thus the angle of incidence on the first set of planes does not vary. The incidence angle in the second set of planes, however varies with the angle of rotation α, is the angle of rotation around the normal of the first diffraction plane of monolithic monochromator. The maximum point in this rotation corresponds to the central wavelength or the longest wavelength transmitted by the monochromator.

2.2 Theory:

The starting point of our MM design is the Bragg's law. In order to obatain suitable wavelength for experiments from MM, we solved the the following four equations:

$$\lambda_1 = 2d_1 sin\theta_1(1 - \delta/\sin^2\theta_1).....(2.1)$$

$$\lambda_2 = 2d_2 sin\theta_2(1 - \delta/\sin^2\theta_2).....(2.2)$$

$$\theta_1 + \theta_2 + \beta_0 = \pi.....(2.3)$$

$$\lambda_1 = \lambda_2$$

where δ represents the refraction related correction and β_0 is the interplanar angle between the two planes.d_1 and d_2 are the two lattice planes of monochromator and θ_1 and θ_2 are corresponding two Bragg angles in vacuum

let$sin\theta_1 = x$ and $\sin\theta_2 = y$ then

$$\lambda_1 = 2d_1x(1 - \delta/x^2)$$

$$\lambda_2 = 2d_2y(1 - \delta/y^2)$$

$$\theta_1 + \theta_2 + \beta_0 = \pi$$

Now from (2.3) we can write

$$\theta_1 + \beta_0 = 180 - \theta_2$$

$$sin(\theta_1 + \beta_0) = sin(180 - \theta_2) = sin\theta_2 = y$$

$$sin\theta_1 cos\beta + cos\theta_1 sin\beta = y$$

$$sin\theta_1 cos\beta + \sqrt{(}1 - x^2)sin\beta = sin\theta_2$$

$$\lambda = 2d_2 sin\theta_2 = 2d_2 sin\theta_1 cos\beta + \sqrt{(}1 - x^2)sin\beta$$

$$\lambda = 2d_2 sin(\theta_1 cos\beta + cos\theta_1 sin\beta)(1 - \delta/(sin\theta_1 cos\beta + cos\theta_1 sin\beta)^2 ...(2.4)$$

Equation (2.4) provides wavelength with δ value. Now considering δ equals 0, the equations can be written as

$$\lambda_1 = 2d_1 sin\theta_1 .....(2.1)$$

$$\lambda_2 = 2d_2 sin\theta_2 .....(2.2)$$

$$\theta_1 + \theta_2 + \beta_0 = \pi .....(2.3)$$

$$\lambda_1 = \lambda_2$$

From(2.1) and (2.2)

$$sin\theta_1/sin\theta_2 = d_1/d_2 .....(2.5)$$

From (2.3)

$$\pi - \theta_1 = \theta_2 + \beta$$

$$sin\theta_1 = sin\theta_2 cos\beta + cos\theta_2 sin\beta$$

Now putting the value in (2.1) and (2.5)

$$\lambda = 2d_1 sin\theta_1$$

$$\lambda = 2d_1[(d_1/d_2)sin\theta_1 cos\beta + cos\theta_2 sin\beta]$$

$$>= 2d_1 sin\theta_1[(d_1/d_2)cos\beta + (cos\theta_2/sin\theta_1)sin\beta]$$

$$\lambda = 2d_1 sin\theta_1[xcos\beta + (1/sin^2\theta_1 - x^2)^{1/2} sin\beta]$$

using $\lambda = 2d_1 sin\theta_1$,$herex = d_1/d_2$ (let).

$$1 = xcos\beta + (1/sin^2\theta_1 - x^2)^{1/2} sin\beta$$

squaring bothe the sides

$$(1 - xcos\beta)^2 = (1/sin^2\theta_1 - x^2)sin^2\beta$$

$$sin^2\beta/sin^2\theta_1 = x^2 + 1 - 2xcos\beta$$

$$>= (d_1/d_2)^2 + 1 - 2d_1/d_2 cos\beta$$

$$>= (d_1/d_2 - cos\beta)^2 + sin^2\beta$$

$$4d_1^2 sin^2\beta/\lambda^2 = (d_1/d_2 - cos\beta)^2 + sin^2\beta$$

$$\lambda = \frac{2d_1 sin\beta}{[(d_1/d_2 - cos\beta)^2 + sin^2\beta]^{1/2}}$$

(1) Solving the 4 equations yields after further simplificaytions,$\beta = \beta_0$:

$$\lambda = \frac{2d_1 sin\beta_0}{[\sqrt{(h_2^2 + k_2^2 + l_2^2/h_1^2 + k_1^2 + l_1^2)} - cos\beta_0)^2 + sin^2\beta_0]^{1/2}} \tag{2.5}$$

(2) if $d_1 = d_2 = d$ we can further modify the above equations as follows:

$$\lambda = \frac{2dsin\beta_0}{[(1 - cos\beta_0)^2 + sin^2\beta_0]^{1/2}} \tag{2.6}$$

MM have been designed following the above equations.

2.3 MCMD (Monolithic Crystal Monochromators Design) Code

2.3.1 Table of H_1, K_1, L_1 and H_2, K_2, L_2

A simulation code MMCD (Monolithic Monochromator Crystal Design) has been realized which can generate different wavelengths using$(h_1, k_1, l_1)$and(h_2, k_2, l_2) combinations using the wavelengths equations written previously.Our Code rely on the lattice parameter value a=5.431061 angstrom at 25^0C.

Tables are given in chapter 5 and programme Codes are shown in Appendix

2.4 MM Design and fabrication:

Several monolithic monochromators of different wavelengths $\lambda = 1.612607a^o$ (Fig-1), $1.410846a^o$ (Fig-2) $1.356949a^o$ (Fig-3) $1.542079a^o$ (Cu-K monochromtor, Fig-4) $0.694067a^o$ (M0-K monochromator, Fig-5). has been designed and fabricated by ourselves. Technical details of their design and fabrication described below. (a) Wavelength $\lambda = 0.1612nmMM$

This is a very significant monochromator that we have designed having same Bragg angle for $(h_1, k_1, l_1) and (h_2, k_2, l_2)$, the index being used are (5,1,3) and (1,5,3). This is an implementation of eqn(2.6) special case. The reason of choosing this wavelength and these indexes originates from the application for precision lattice spacing measurement for Si. Conventional Bond method usually provides very high precision value but we need a rotation of the sample in the bond method. If we choose (513) and (153) indexes we can achieve simultaneous diffraction and therefore effect of temperature can be neglected and better precision data can be obtained than conventional bond method at room temperature.

Table I. Type-1 different indexes, MMCD Code generated wavelengths

$h_1k_1l_1$	$h_2k_2l_2$	HKL	β_0	θ_1	θ_2	λ	δ
1 5 5	-5 3 1	-4 8 6	69.2044	63.1437	47.6519	1.356950	.57719E-05
3 5 5	-3 3 1	0 8 6	70.8196	75.8031	33.3772	1.370938	.58915E-05
3 3 5	-3 5 1	0 8 6	73.5280	57.1730	49.2990	1.391940	.60734E-05
1 1 3	-5 -3 5	-4 -2 8	74.0515	25.2230	80.7255	1.395642	.61057E-05
1 1 3	-3 -5 5	-2 -4 8	74.0515	25.2230	80.7255	1.395642	.61057E-05
1 5 5	5 1 5	6 6 10	46.6641	66.6680	66.6680	1.396621	.61143E-05
1 1 3	-5 3 1	-4 4 2	104.7631	25.3769	49.8599	1.403594	.61755E-05
3 5 5	1 5 -1	4 10 4	54.8119	83.0088	42.1792	1.403614	.61757E-05
1 1 5	1 1 7	2 2 12	42.4407	68.3502	69.2091	1.410846	.62686E-05

Table II. Type-2 same indexes, MMCD Code generated wavelengths

$h_1k_1l_1$	$h_2k_2l_2$	HKL	β_0	θ_1	θ_2	λ	δ
1 3 5	3-5 -1	4 -2 4	119.0593	30.4704	30.4704	.931039	.27172E-05
3 5 5	-5 -3 5	-2 2 10	94.8614	42.5693	42.5693	.956631	.28686E-05
1 3 5	5 -1 -3	6 2 2	111.8037	34.0981	34.0981	1.029302	..33210E-05
3 3 5	-3 5 -3	0 8 2	102.0815	38.9593	38.9593	1.041527	.34004E-05
1 5 5	-1 -5 5	0 0 10	91.1235	44.4382	44.4382	1.064914	.35548E-05
1 3 5	-5 -3 1	-4 0 6	104.9006	37.5497	37.5497	1.118970	.39249E-05
1 5 5	-5 5 -1	-4 10 4	72.8954	53.5523	53.5523	1.223493	.46924E-05
3 3 5	-3 -3 5	0 0 10	80.6311	49.6854	49.6854	1.263037	.50006E-05
1 3 5	-5 3 -1	-4 6 4	91.6373	44.1814	44.1814	1.279591	.51325E-05
1 5 5	5 5 1	6 10 6	46.6641	66.6680	66.6680	1.396621	.61143E-05
1 3 5	-3 5 -1	-2 8 4	78.4630	50.7685	50.7685	1.223493	.46924E-05
3 3 5	-3 -3 5	0 0 10	80.6311	49.6854	49.6854	1.422186	.63402E-05
1 1 5	-1 5 -1	0 6 4	92.1226	43.9387	43.9387	1.450516	.65953E-05
1 3 5	-1 -3 5	0 0 10	64.6231	57.6885	57.6885	1.551732	.75479E-05
1 3 5	5 3 1	6 6 6	57.1216	61.4392	61.4392	1.612607	.81517E-05

MMCD code provides wavelength of 1.612607 angstrom which satisfies the simultaneous Bragg condition for the indexes (5,1,3), (-5,-1,-3),(1,5,3),and (-1,-5,-3). The Bragg angles for both indexes is 61.4392 degree with interplanar angle 57.1216 degree. In this design the third reflection is not allowed therefore the many beam effects is avoided. In order to realize the monochromator, in brief we did the following steps: (1) First we find the perpendicular vector for the indexes (5,1,3)and(1,5,3), this is (-1,-1,2) which is the vector product$(5i + 1j + 3k) \times (1i + 5j + 3k)$ of the above indexes. A stereogram is drawn for the pole (-1,-1,2) . From the pole figure we identify the major direction (-1,1,0), (1,1,1) and (-1,-1,2). (3) Accordingly we design our MM , we choose the beam gap 35mm between the incident and diffracted beam so that direct beam is avoided without any shielding.

As we know the major directions , then we find the angle between (153)/or(513) with any major direction say (111),28.5603 degree in this case and we cut the first index by Diamond saw with a precision of 1micro m. As a next step we just rotate the saw by the interplanar angle 57.1216^0 and cut the second plane. According to the design we move the saw parallely for the cutting of a conjugate plane. We check the major direction and choosen indexes by X-ray diffraction in order to confirm the direction.

Geometry:

Once at least the two direction is known with respect to the choosen diffraction vectors then one can choose any geometry one likes. We have choosen $L \times B \times H = 45mm \times 45mm \times 45mm$. For making MM adjustment easier for the experiment we have choosen different height of the diffraction legs, the second leg is smaller than the first leg so that we can catch the first diffraction easily and hence after necessary adjustment we can get the 4th cosecutive reflections. For etching we use

the solutions of HF,HNO3 and CH3CH2OH with appropriate ratio.

(b) Wavelength $\lambda = 1.410846a^{o}MM$

This monolithic monochromator has been made using the reflection indexes (1,1,7), (1,5,1),(-1,-1,-7),and (-1,-5,-1). The motivation behind for fabrication of this monochromator is to study the d-spacing of the GaAs(800) single crystal doped with Boron(B) using the Bond method. As the high bragg angle provides high precision there fore we found the above indexes from the MMCD code which provides 86.5 degree for GaAs(800) sample. MM has been made following the same procedure that has been described for the previous monochromator, here the perpendicular vector is (17,-3,-2). The diffraction plane has been checked by X-ray. .

The Bragg angles are 42.4 degree(151) and 68.1 degrees(117) respectively and the interplanar angle turns out to be 69.5 degree.The beam gap is 15 mm between incident and diffracted beam.

(c) Wavelength $\lambda = 1.356949a^{o}MM$

This monochromator has been made to study the d-spacing of Si. For Si(800) sample this provides 88 degrees using the indexes(155),(-1-5-5),(-531)and (5-3-1).Bragg angles are 53.1437 degree and 47.6519 degree respectively,the interplanar angle is 69.2044 degree. The perpendicular vector (5,13,-14) is perpendicular to both index and thus the index planes are parallel. Fig 6 shows schematic design for 0.135nm wavelengths MM and Fig 7 shows for the O.161nm MM and its steregram is shown in Fig 8.

2.5 Conclusion

(1) Three independent equations has been solved and two types of wavelength has been derived, using the solved equations (eqn 2.5,2.6) a computer code MMCD has been developed to generate the two types of wavelength.

(2) From the two wavelength equations monolithic monochromator classified into type-1 (a) $d_1 \neq d_2$ and (b) type-2, $d_1 = d_2$

(3) Several monolithic monochromators of different wavelengths $\lambda = 1.612607a^{o}$ (Fig-1), $1.410846a^{o}$ (Fig-2) $1.356949a^{o}$ (Fig-3) $1.542079a^{o}$ (Cu-K monochromtor, Fig-4) $0.694067a^{o}$ (M0-K monochromator, Fig-5) have been designed and fabricated by ourselves. Technical details of their design and fabrication have been described. Design and fabrication of 1.612607 angstrom MM is reported as an illustration.

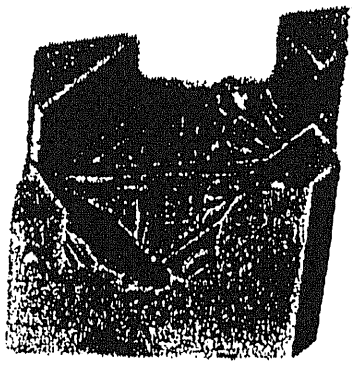

Figure 1
Type 1 monolithic monochromator designed for a wavelength of 0.1410 nm with index $(1, 5, 1)$, $(1, 1, 7)$, $(\bar{1}, \bar{5}, \bar{1})$, $(\bar{1}, \bar{1}, \bar{7})$.

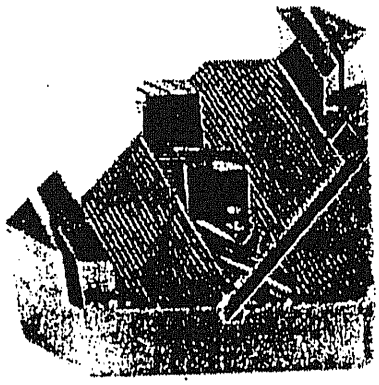

Figure 2
Type 2 monolithic monochromator for a wavelength of 0.1612 nm with index $(5, 1, 3)$, $(1, 5, 3)$, $(\bar{5}, \bar{1}, \bar{3})$, $(\bar{1}, \bar{5}, \bar{3})$.

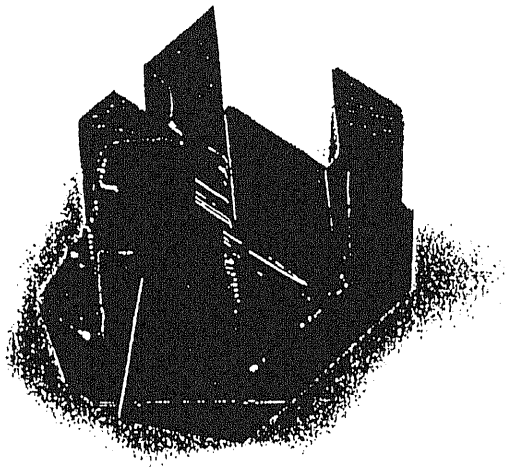

Fig 5 Type-1 Monochromator designed for wavelength 0.13525 nm with index (1,5,1),(-5,3,1), (-1,-5,-1) , (5,-3,-1)

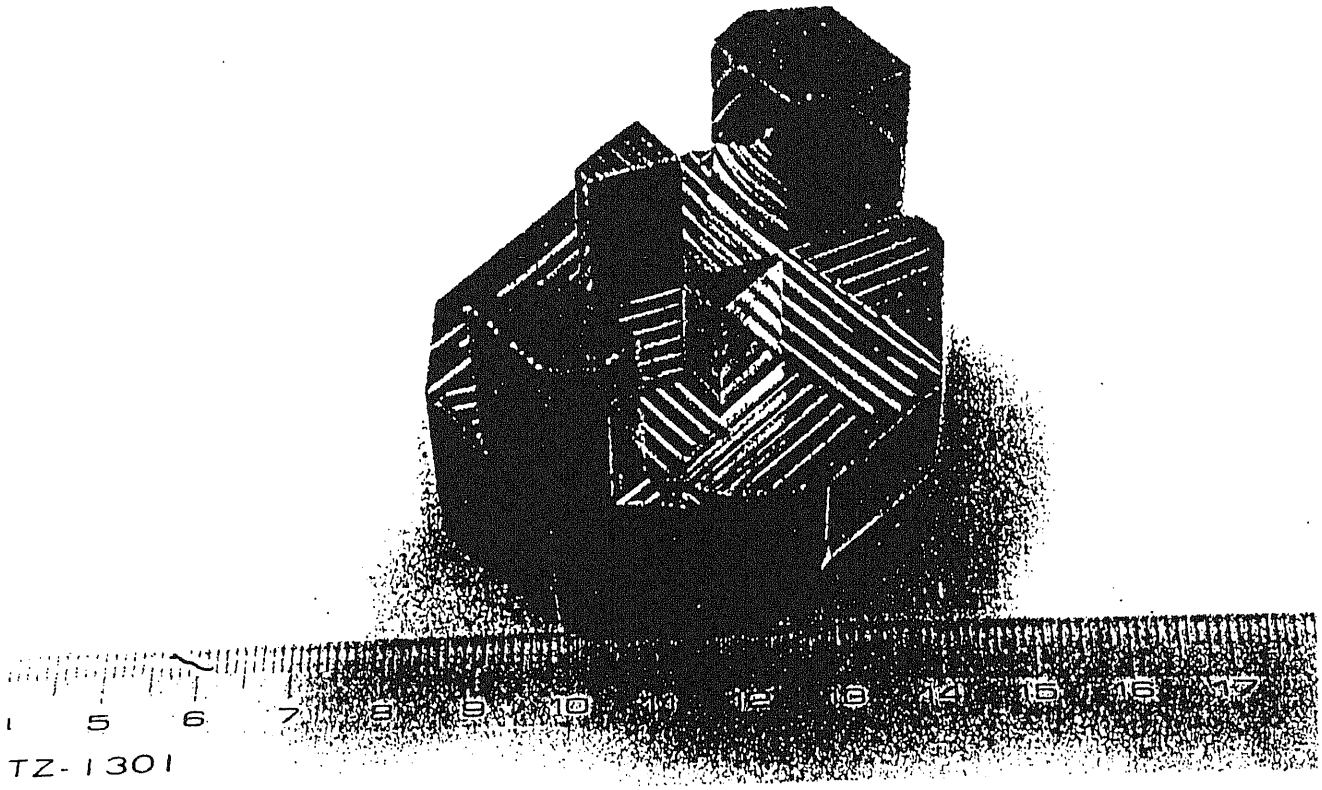

Fig 3 Type-1 Monochromator designed for wavelength 0.15420 nm with index (3,3,-3),(-3,-5,-3), (-3,-3,3) , (3,5,3).

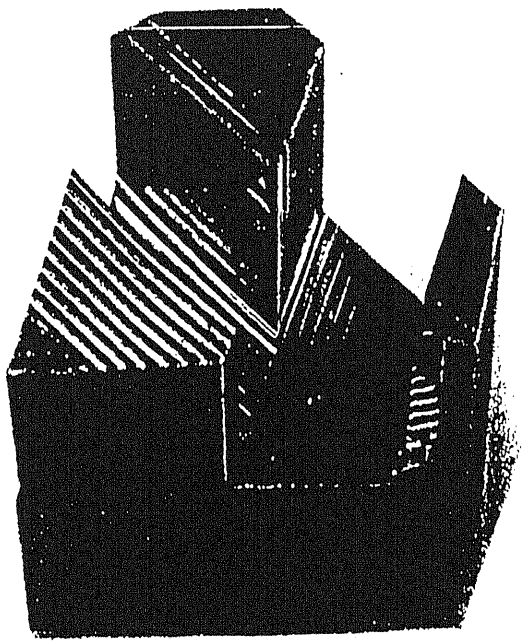

Fig 4 Type-1 Monochromator designed for wavelength 0.0690 nm with index (5,9,11),(7,-7,-7), (-5,-9,-11) , (-7,7,7).

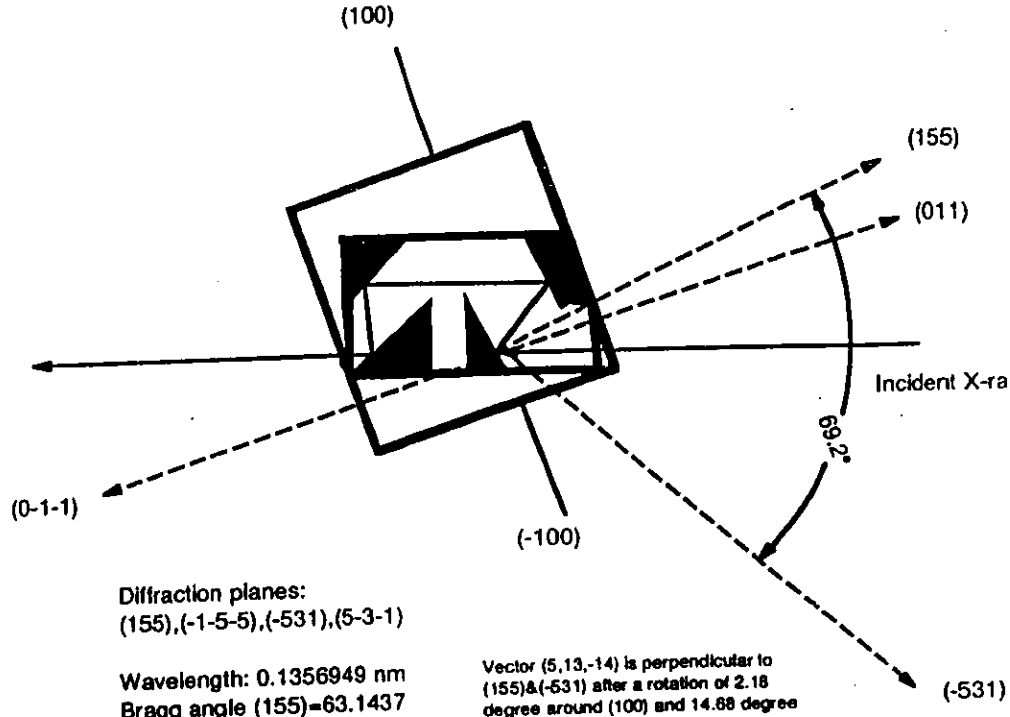

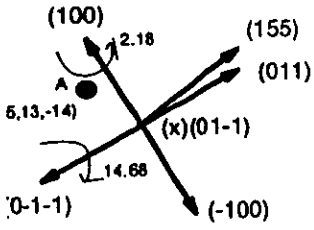

Diffraction planes:
(155),(-1-5-5),(-531),(5-3-1)

Wavelength: 0.1356949 nm
Bragg angle (155)=63.1437
Bragg angle (-531)=47.6519
Interplanar angle=69.2044
Setting=(+.-.-+)

Vector (5,13,-14) is perpendicular to (155)&(-531) after a rotation of 2.18 degree around (100) and 14.68 degree around (0-1-1) as shown .

Fig 6 Schematic design for 0.13569 MM showing Crystallographic direction (100), (011) an (155)

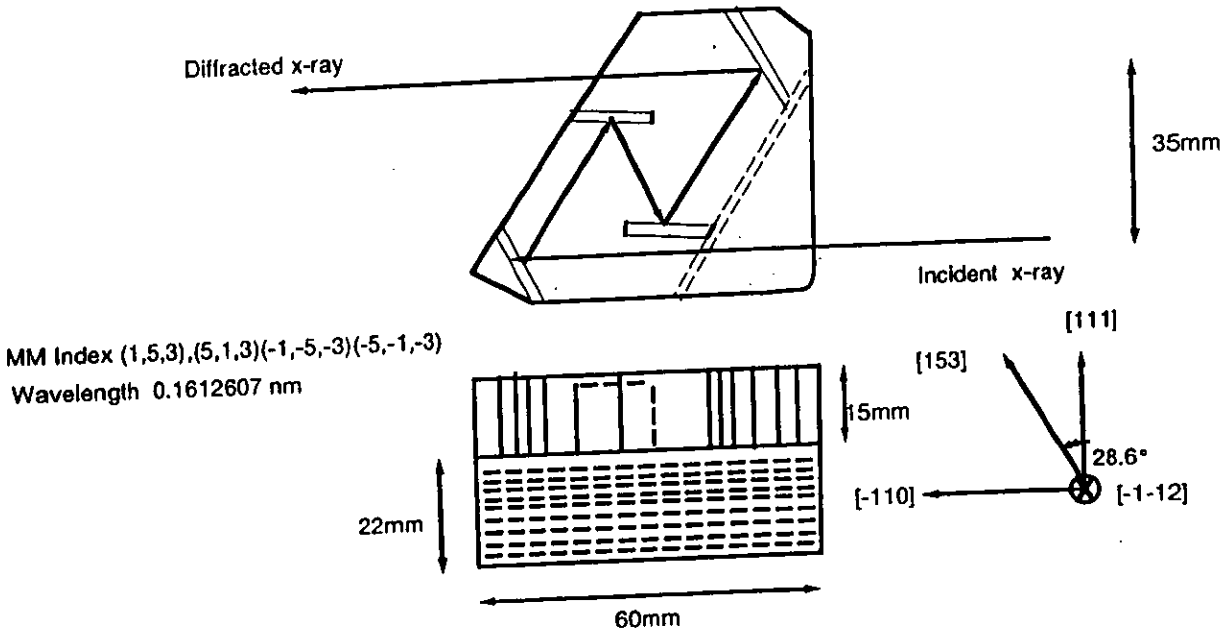

Fig 7 Design for 0.16126nm MM side view.

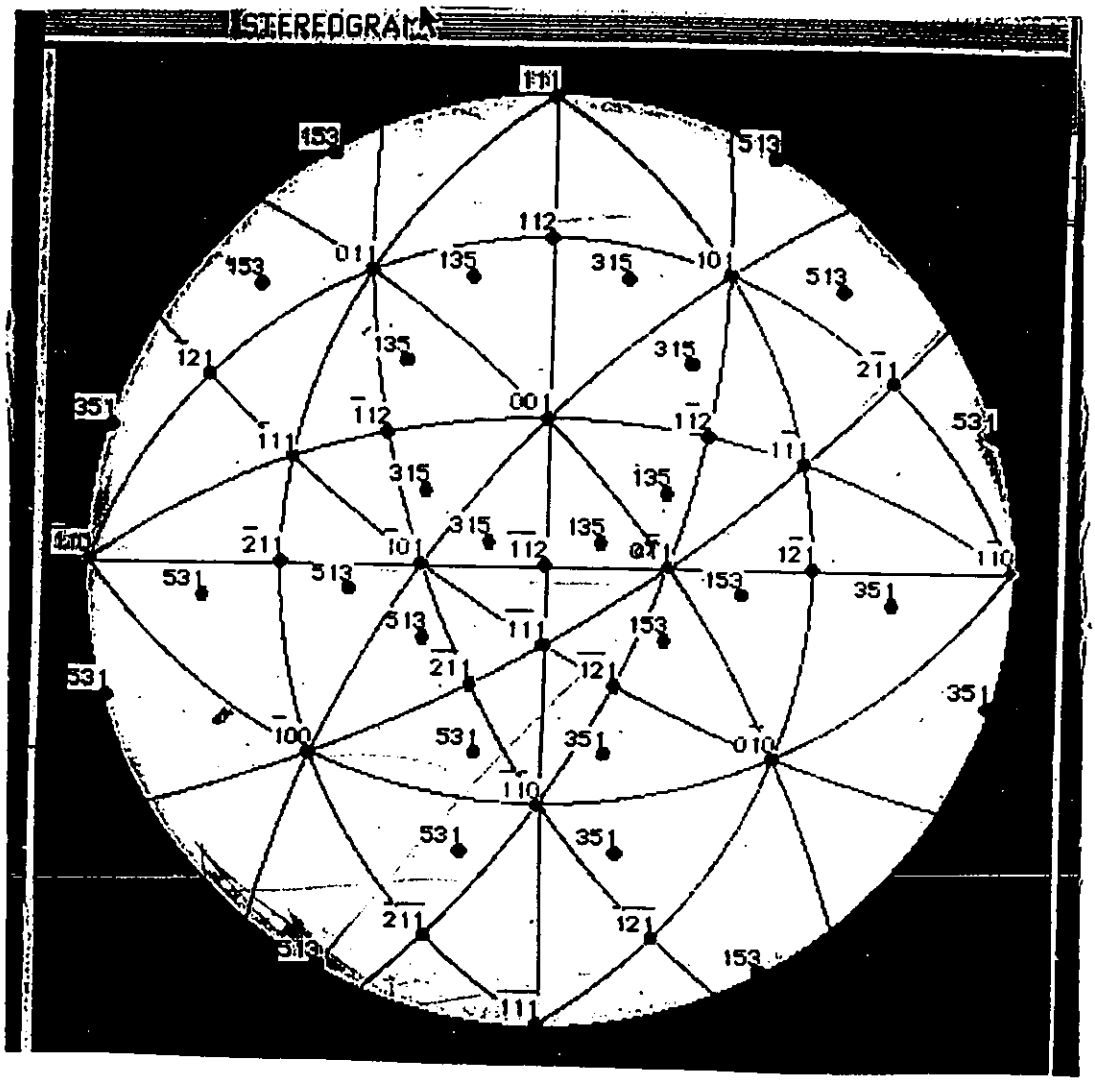

Fig 8 Sterogram for 0.16126 nm wavelength MM design.

Chapter 3

Dynamical theory of X-ray Diffraction

3.1 Introduction

We present analytical expressions for diffraction curves in Bragg (reflection) geometry[31,32]. Detailed various aspects of dynamical theory and their various applications are reported in [56,57,58,59,60,61,62,63,64,65,66,67] and many others,

Several examples are presented as an implementation of the theory. In describing the dynamical theory of X-ray diffraction, from Maxwell equations , we can derive the following two differential equations for the field strength D_0 and D_h which are related to the waves propagating along the incident-beam direction and diffracted-beam direction inside a perfect crystal. The electromagnetic waves are transverse waves, and we assume that we can treat the π and σ polarization components independently, viz.,

$$\partial D_h/\partial s_h = -i\pi KC\chi_h D_0 + (i2\pi K\beta_h^{'} + \pi K\chi_0^{''})D_h \text{.....}(1)$$

$$\partial D_0/\partial s_0 = \pi KC\chi_0^{''}D_0 - (i\pi KC\chi_{h^{'}} D_h) \text{.....}(2)$$

Here, we use the oblique cordinate system (s0,sh). The directions of s0 and sh correspond to those of the incident wavevector and diffracted wavevector, respectively. C is the parameter distinguishing the polarization states and usually referred to as the "polarization factor".

C=1 for σ polarization .....(3)

C=$cos(2\theta_B)$ for π polarization.....(4)

where θ_B is the Bragg angle.

The χ_h's are related to the hth Fourier component of the susceptibility and are represented as follows in terms of the crystal structure factor F_h.

$$\chi_h = -\lambda^2 r_e F_h/\pi V \text{.....}(5)$$

here $\lambda$is the X-ray wavelength, r_e the classical electron radius ($r_e = 2.8179 \times 10^{-13}$) and V is the volume of the unit cell. The Crystal structure factor F_h is represented in terms of the atomic scattering factor

$$f_j = f_j^0 + f_j^{'} + if_j^{''} \text{.....}(6)$$

by

$$F_h = F_h^{'} + iF_h^{''} = \sum_j (f_j^0 + f_j^{'} + if_j^{''}) exp(2\pi i\mathbf{h.r})\mathbf{e}^{-\mathbf{M_j}} \text{.....}(\mathbf{7})$$

. where the summation is over all the atoms in the unit cell. Here the two parameters $F_h^{'}$ and $F_h^{''}$ are defined by the following equations:

$$F_h^{'} = \sum_j (f_j^0 + f_j^{'}) exp(2\pi i\mathbf{h.r})\mathbf{e}^{-\mathbf{M_j}} \text{.....}(\mathbf{8})$$

$$F_h^{''} = \sum_j (f_j^{''}) exp(2\pi i\mathbf{h.r})\mathbf{e}^{-\mathbf{M_j}} \text{.....}(\mathbf{9})$$

The Debye-Waller factor e^{-M_j}, arising from thermal vibrations and static displacements , We can re-write the susceptibility as follows:

$$\chi_h = \chi_h^{'} + i\chi_h^{''} \text{.....}(10)$$

$$\chi_h^{'} = -\lambda^2 r_e F_h^{'}/\pi V \text{.....}(11)$$

$$\chi_h^{''} = -\lambda^2 r_e F_h^{''}/\pi V \text{.....}(12)$$

$\beta_h^{'}$ is the parameter representing the angular deviation from the Bragg condition and is related to $\theta_0 - \theta_B$ through another parameter W,

$$\beta_h^{'} = \epsilon\sqrt{(\epsilon\gamma_h/\gamma_0)}C\chi_h^{'}W \text{.....}(13)$$

$$W = \frac{\epsilon\sqrt{(\gamma_0/\epsilon\gamma_h)}[2(\theta_0 - \theta_B)sin(2\theta_B) + \chi_0^{'}(1 - \gamma_h/\gamma_0)]}{2C\chi_h^{'}} \text{.....}(14)$$

γ_h and γ_0 are scalar products of s_h and s_0 with the inner surface normal n. For Bragg geometry ϵ=-1 and for Laue +1. The solutions of egn(1) and (2) will be following form:

$$D_0(z) = d_0 exp(2\pi i\delta k_{zz}) \text{.....}(15)$$

$$D_h(z) = d_h exp(2\pi i\delta k_{zz}) \text{.....}(16)$$

Let us introduce new parameters ζ and g as

$$d_h = \zeta d_0$$

$$g = \frac{\epsilon\chi_0^{''}(\epsilon\sqrt{(\gamma_0/\epsilon\gamma_h} - \sqrt{\epsilon}\gamma_h/\gamma_0)}{2C\chi_h^{'}}$$

Inserting eqns(13),(15),(16) and (17) into egns(1) and (2) and using the relations

$$\delta/\delta_{s0} = \gamma_0 d/dz and$$

$$\delta/\delta_{sh} = \gamma_h d/dz$$

eqns (1) and (2) becomes

$$2\pi i\delta k_z\gamma_0 - \pi K\chi_0^{''} = -\pi iKC\chi_h^{\zeta}.....(21)$$

$$(2\pi i\delta k_z\gamma_h + 2\pi iKC\chi_h^{'}$$

$$\sqrt{(\epsilon\gamma_h)/\gamma_0)W - \chi_0^{''})\zeta} = -\pi iKC\chi_h.....(22)$$

Solving egns(21) and (22) for δk_z we can get the following expressions:

$$\delta k_z^j = -\epsilon KC\chi_h^{'}/[2\sqrt{(\epsilon\gamma_0\gamma_h)}]$$

$$\times[(W+ig) \pm \sqrt{((W+ig)^2 + \epsilon(1+ik)(1+ik^*))}] - (iK\chi_0^{''})/2\gamma_0.....(23)$$

The corresponding expression for ζ is derived from egn(21) and is given by:

$$\zeta^j = -1/(1+ik^*)\sqrt{(\gamma_0/\epsilon\gamma_h)}[(W+ig) \pm \sqrt{((W+ig)^2 + \epsilon(1+ik)(1+ik^*))}].....(24)$$

In eqns (23) and (24) k and k^* are given by

$$k = \frac{\chi_h^{''}}{\chi_h^{'}}$$

$$k^* = \frac{[\chi_h^{''}}{\chi_h^{'}]^*}$$

Now the solutions of egns(1) and (2) can be written as the form:

$$D_0(z) = d_0^1 exp(2\pi i\delta k_z^1 z) + d_0^2 exp(2\pi i\delta k_z^2 z)$$

$$D_h(z) = \zeta^1 d_0^1 exp(2\pi i\delta k_z^1 z) + \zeta^2 d_0^2 exp(2\pi i\delta k_z^2 z).....(28)$$

d_0^1 and $d_0^2$are to be determined from the boundary conditions for the X-ray wave-field at the entry and exit surfaces of the crystal.

3.1.1 Diffraction curves in the Bragg geometry

In Bragg geometry, $\gamma_0 > 0, \gamma_h < 0$ and $\epsilon = -1$

so that egn(23) and (24) can be written as

$$\delta k_z^j = -KC\chi_h^{'}/[2\sqrt{(\gamma_0\gamma_h)}]$$

$$\times[(W+ig) \pm \sqrt{((W+ig)^2 + (1+ik)(1+ik^*))}] - (iK\chi_0^{''})/2\gamma_0 .....(23.2)$$

The corresponding expression for ζ is given by:

$$\zeta^j = -1/(1+ik^*)\sqrt{\gamma_0}/\gamma_h[(W+ig)\pm$$

$$\sqrt{(W+ig)^2 + (1+ik)(1+ik^*)}] .....(24-2)$$

If we take the amplitude of the incident beam to be unity and that of the diffracted beam to be E_h the boundary conditions at the entrance surface is z=0 and also at the exit surface, thus we can write:

$$D_0(z=0) = d_0^1 + d_0^2 = 1 .....(29)$$

$$D_h(z=0) = \zeta^1 d_0^1 + \zeta^2 d_0^2 = E_h .....(30)$$

Since one of the δ_z^j has a negative imaginary part, resulting in a field amplitude which diverges to infinity as z increases, the coefficient d_0^2 must be zero. Accordingly , eqn(29) and (30) are reduced to:

$$E_h = \zeta^1$$

3.2 Reflectivity

and the Reflectivity is given by

$$R_{Bragg}(W) = \gamma_h/\gamma_0(\zeta^1)^2$$

3.2.1 Intensity

The rocking curve Intensity is the auto-correlation of the Reflectivity, the relationship between the rocking curve and reflection curve can be written as:

$$I(\omega) = K \int R(\theta R(\theta - \omega) d\theta$$

[for double crystal]

The general theory of X-ray diffraction, which properly accounts for normal absorption and extinction of wavefields in crystal medium, is called the dynamical x-ray diffraction theory. It is a first order theory in that it takes the deviation of the x-ray refractive index from unity up to first order, and the variation of the complex amplitudes over one x-ray wavelength to first order.

3.2.2 Computer Program

Using the dynamical theory a computer programme [30] have been developed to generate the rocking curves which incorporates the equations described above by FORTRAN 77 , one run takes several few minutes to calculate the rocking curves.

3.3 Simulated results:

3.3.1 Examples

Several simulated rocking curves has been generated Using the prorgramme above , Fig-1 and Fig 2 shows some simulated reflectivity curves for Si.

3.4 Discussion

Several simulated rocking curves has been generated Using the prorgramme above , Fig-1 and Fig 2 shows some simulated reflectivity curves for Si. Fig 3 shows the Intensity curves generated for Si(153) which shows good agreement between theory and experiment thus showing the good performance of the monochromator. The discrepency is due to the convolution effect. It is assumed in the theory that crystal is perfect but this may not be the true in real case. Further Fig 4 shows the dynamical effect after the 4th reflection for 0.16126 nm MM.

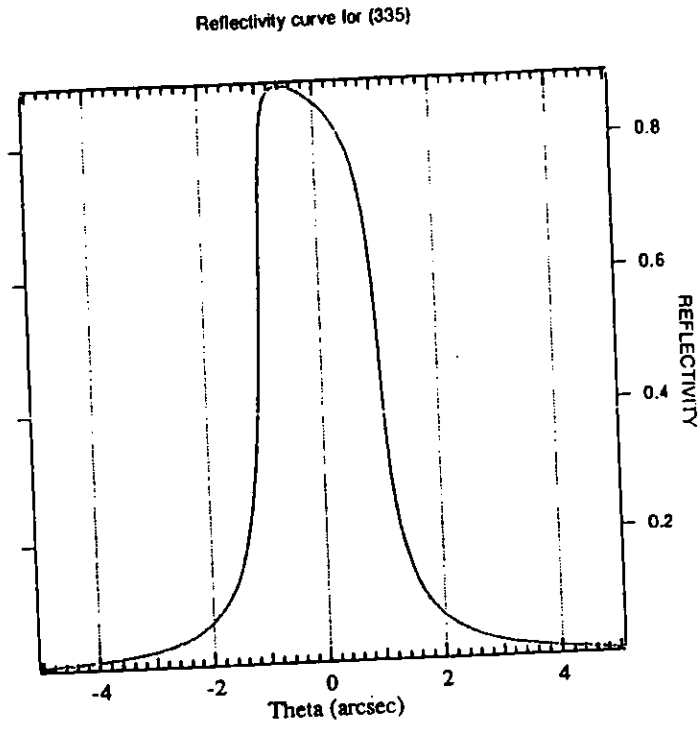

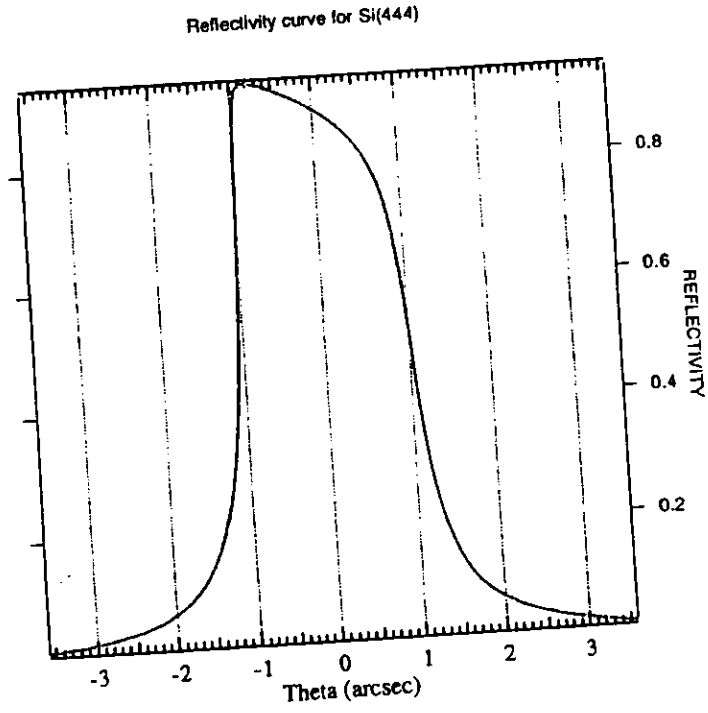

Fig 1 2 Reflectivity curve from Si(335) and Si(444)

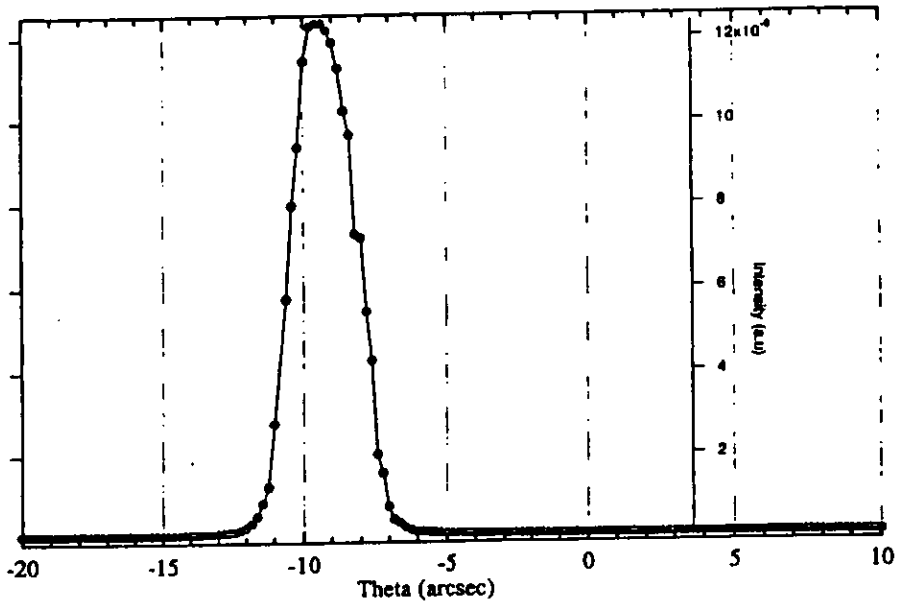

Fig 4 Experimentally observed curve after fourth reflection from MM with wavelength 0.16126nm

3.5 Corrections for Lattice Spacing Measurement

In this section we describe the necessary corrections for lattice spacings, these are mainly (1) Refraction (2) Assymetric and (3) Temperature corrections and all possible corrections depending on the experimenter and experiment. Lattice spacing can be corrected as $d = d_0$+all corrections.

3.5.1 Refractive Index

The refractive index is defined as the ratio of the phase velocities in vacuum and in the medium c/ν_q. because ν_q is complex, we get complex refractive indexμ_c. The partial refractive index for q-type electron :

$$\mu_{c,q} = \mu_q - i\mu i, q = 1 - \delta_q - i\beta_q .....(4.1)$$

$\mu_q = 1 - \delta_q$ is the real part of $\mu_{c,q}$. The unit decrement δ_q gives the departure ofμ_q from 1. for X-ray frequencies:

$$\delta_q = \frac{2\pi n_q e^2 m(\omega^2 - \omega_q^2)}{m^2(\omega^2 - \omega_q^2) + 4e^4\omega^6/9c^6}$$
$$\simeq \frac{2\pi n_q e^2}{m(\omega^2 - \omega^2)}$$

indexμ For the X-ray frequencies ($\omega \geq\geq \omega_q$)

$$\delta = \sum_q \delta_q = \frac{2\pi e^2 \sum_q n_q}{(\omega - \omega_q^2)m}$$
$$\simeq \frac{2\pi e^2 \sum_q n_q}{\omega^2 m}$$
$$= \frac{e^2 n\lambda^2}{2\pi mc^2}$$

For X-rays being dispersed by crystals, the unit decrement δ is a small positive quantity ,and $\mu = 1 - \delta \leq 1$(for x-rays) (In glass prism $\mu \geq 1$).It follows that for

X-rays the medium of a crystal is less dense than a vacuum If $N_A = 6.0225 \times 10^{23}$ is Avogadro number, A=Atomic wt,Z=Atomic number,ρ=density, then from the above equation gives with $n = \frac{ZN\rho}{A}$ and

$$\delta/\lambda^2 = e^2 N_A Z\rho/(2\pi mc^2 A.)$$

$$\delta/\lambda^2 = 2.7 \times 10^10 Z\rho/A = constant(\lambda \leq \lambda_k).....(4.4)$$

for most cases. From eqn(2) for$Al^{13}(A = 27, \rho = 2.7)\delta = 1.74 \times 10^{-6}$.
For $MoK_\alpha(0.708)$ radiation $\delta_{expt} = 1.68 \times 10^{-6}$(good agreement). Near the absorption edge $\frac{\delta}{\lambda^2}$ is not constant and anomalous dispersion occurs δ^2 varies with λ.
In our case:
we have $\lambda_{Si-513} = 1.612607$angstrom
Using eqn(2)$\delta/\lambda^2 = (2.7 \times 10^{10} Z\rho)/A$ we have

$$Z = 14$$

$$A = 28.085$$

$$\rho = 2.3290406 gm/cc$$

$$\lambda = 1.612607 Angstrom$$

$$so, \delta = 2.7 \times 10^{10} \times 14/28.085 \times 2.3290406 \times 1.612607^2 \times 10^{-8} \times 10^{-8}$$

$$\delta_{si-1.61} = 8.15 \times 10^{-6}$$

$$\delta_{si-1.41} = 6.23 \times 10^{-6}$$

$$\delta_{si-1.35} = 5.77 \times 10^{-6}$$

$$\delta_{si-1.54} = 7.45 \times 10^{-6}$$

3.5.2 Assymetry:

In the general case when the crystal surface is not parallel to the reflecting planes but is rotated from the atomic planes around the measuring axis by the angle μ , the corrections which relates directly to the determined interplanar distance, has the form $d = d_0[1 + \delta cos\mu/(sin(\theta + \mu)sin(\theta - \mu))]$ where $\delta = 4.48 \times 10^{-6} n_0 \lambda^2$,where $n_0 = 699nm^{-3}$ for Si. In order to incorporate the refraction and assymetry the additional term to the Bragg angle can be written more explicitly by the formula

$$\theta_{Assym} = 90^0 - \beta_0/2 - \delta/4[2 + 1/b + b]$$

where b is the assymetry factor. In another form in terms of small correction (ϵ) due to the assymetry arises from the miscut can be written as $\epsilon = \frac{\delta}{sin2\theta_b}[1+sin\theta/sin(2\theta_b - \theta)]$ where θ and θ_b are glancing angle of incidence and Bragg angle.

3.5.3 Temperature corrections:

Temperature correction to lattice spacing values follow the linearity equations $\Delta d/d = \alpha\Delta t$ where α is the thermal expansion co-efficient, usually 2.5×10^{-6} at 22.5 degree celcius. For example temperature fluctuation should be maintained 0.04 degree celcius for $\Delta d/d = 10^{-8}$ to be achieved. Usually corrections are standard procedure to be needed to follow depending on the experimental conditions.

3.5.4 Vibration Measurement

We have taken the vibration spectrum by Fourier spectrometer. Fig 5.1a shows the signal when the accelerometer is placed on the goniometer stage and Fig 5.1b shows the spectrum when the sensor is put on the sample holder, we see from the both spectrum there is no significant change, peak signals are due to the line signal. Fig 5.1c shows the spectrum when the Coarse motor of the sample goniometer moves

and Fig 5.1d shows the spectrum when the Fine motor of the sample goniometer moves, from the above study we see that Fig 5.1a,5.1b and 5.1d has no change in the spectrum and thus we take our all diffraction spectrum in the lattice measuring system by tuning the Fine motor.

Further it is estimated that for the source orbit movement of $100micron, comesas$ the effect of $(1/2)\alpha^2 tan\theta$ to the measured Bragg angle which attibutes approximately $1 \times 10\ -6$ to the $\Delta d/d$ value. Thus all effects need to be taken care for the measurements.

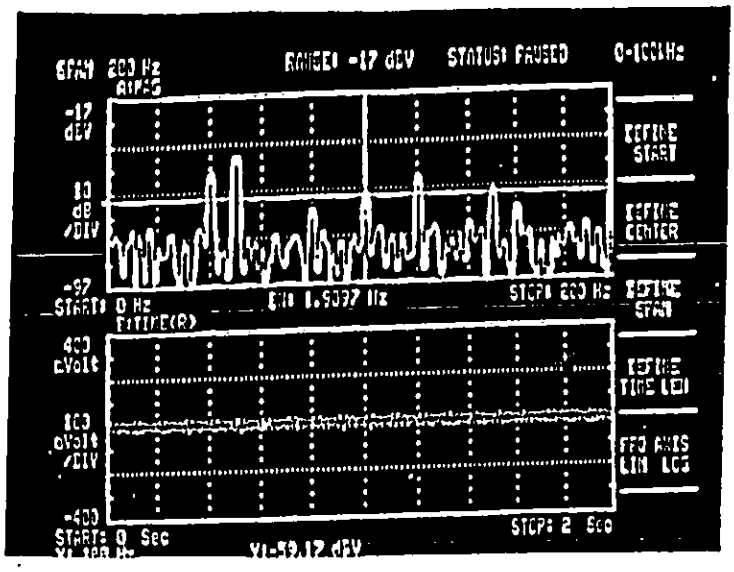

Fig 5.1a

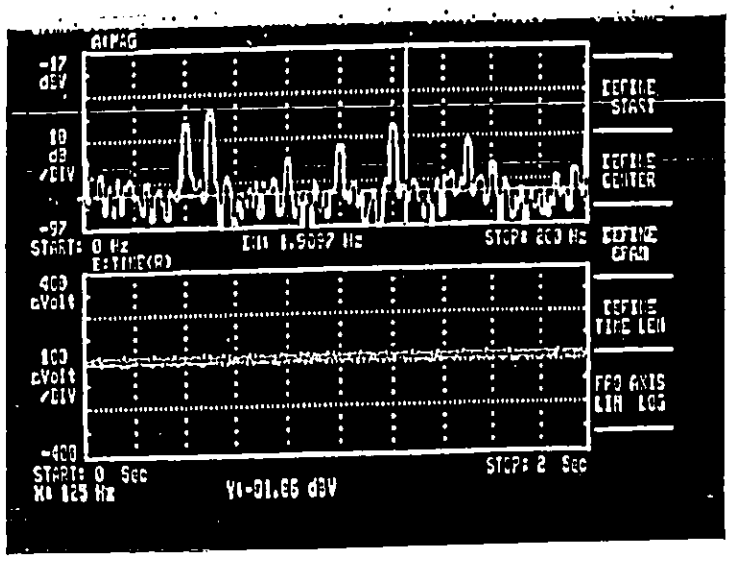

Fig 5.1b

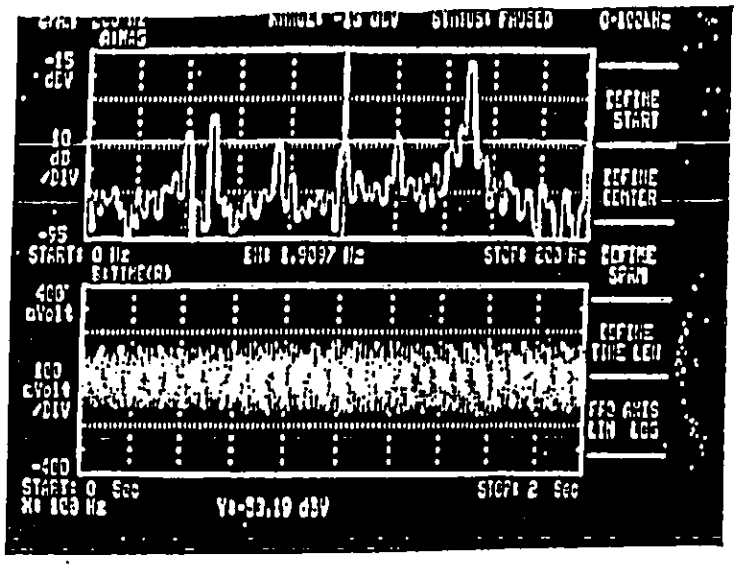

Fig 5.1c

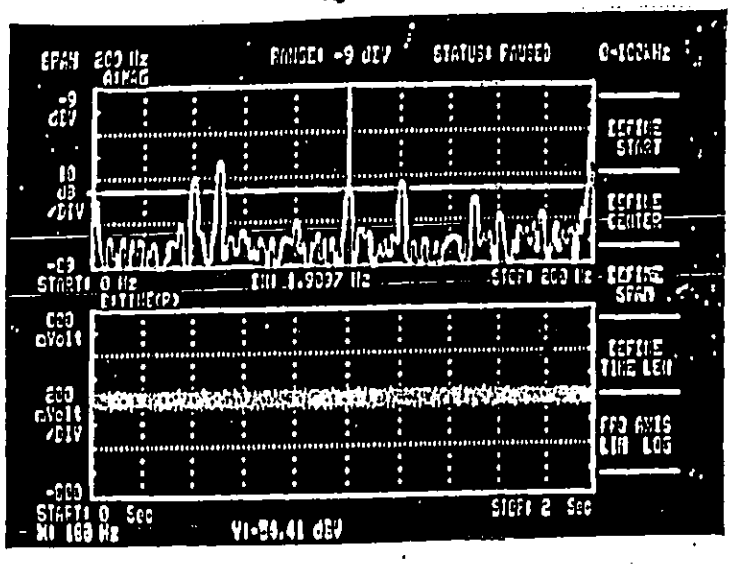

Fig 5.1d

Chapter 4

Charcaterization Of Monolithic Monochromator:

4.0.5 Wavelength Callibration:

The absolute wavelenghth have been callibrated first by DCM Si(111) with Bond method using an analyzer crystal and fine tuning of the wavelength have been performed by inserting the monolithic momonochromator and using two cross tilting stage of the goniometer where MM were fixed. Further as we fabricate the monolithic double crystal monochromator from a single perfect crystal as a means of obtaining an X-ray beam of well defined wavelength, the tilt dependence wavelength is defined by [45]

$$\lambda(\alpha) = \frac{2d_1 sin\beta_0 cos\alpha}{[\sqrt{(h_2^2 + k_2^2 + l_2^2/h_1^2 + k_1^2 + l_1^2)} - cos\beta_0)^2 + sin^2\beta_0 cos^2\alpha]^{1/2}} \tag{3.1}$$

where α is the rotation around the normal of the first plane and $\alpha = 0$ corresponds the maximum wavelength transmitted by the MM(MDCM). Our all MM has been chracterized to transmit the maximum wavelength as at $\alpha = 0$ position define the lattice constant precisely. To charaterize the wavelength we have used the analyzer crystal after the MM, MM was installed in a two stage goniometer by which we

can rotate the MM around the normal of the First plane and to obtain a maximum wavelength. Fig 3a shows the wavelength callibration of MM's, showing the $\alpha = 0$ positions which corresponds the maximum wavelength, either side from maximum position corresponds the spectral range of MM

4.0.6 Intensity

The general expression for the intensity transmitted by MM can be expressed[45] and many other references related to the dynamical theories are [26, 31, 32, 65, 56-66]:

$$I = \int\int\int G(\omega,\phi)J(\lambda)\sum_{\sigma} R^2_{1\sigma}[\Delta\theta_1(\phi,\omega) \\ -(\Delta\lambda/\lambda_0)tan\theta_1]R^2_{3\sigma}[\Delta\theta_3(\phi,\omega) \\ -(\Delta\lambda/\lambda_0)tan\theta_3]]d\lambda d\phi d\omega$$

where ω and ϕ are the horizontal and vertical divergences and R1 and R2 is the reflectivity from the 1st and 2nd index and θ are the Bragg angles from the crystal faces. The window function is defined as :

$$W(\lambda - \lambda_0) = \int\int G(\omega,\phi)J(\lambda)\sum_{\sigma} R^2_{1\sigma}[\Delta\theta_1(\phi,\omega) \\ -(\Delta\lambda/\lambda_0)tan\theta_1]R^2_{3\sigma}[\theta_3(\phi,\omega) \\ -(\Delta\lambda/\lambda_0)tan\theta_3]d\phi d\omega$$

where the symbols R1,2 are the Bragg reflectivity curves of the two crystals, P denotes the polarization state. the arguments of R are the deviations of the glancing angles of the rays θ and $\theta \pm \beta$ from respective Bragg angles θ_1 and θ_2, G is geometry of the instrument and J is the intensity distribution in the spectrum. We developed a programme using the dynamical diffraction theory to compare with the expt rocking curve.

4.1 Resolution provided by the Monolithic Monochromator

The full width at half maximum (FWHM) of the reflecting range is given by [59] :

$$\Delta\theta = 2C\chi_g(\gamma_g/\gamma_0)^{1/2}/sin2\theta_B$$

$$\chi_g = -\gamma_e\lambda^2 F_h/\pi V_c$$

where γ_e is the classical electron radius, F_h is the atomic structure factor, V_c is the volume of the unit cell, λ is the wavelength C is the polarization factor; 1 for σ polarization and $cos2\theta_B$ for π polarization and $(\gamma_g/\gamma_0) = 1$ for symmetry reflection. The energy resolution is usually determined using the relation:

$$\Delta E/E = cot\theta\Delta\theta$$

4.1.1 Dispersion:

Dispersion is an important parameter as how wavelength varies with Bragg-angle and the angular dispersion of MM is defined by

$$D = d\alpha/d\lambda = 4E1(a/\sqrt{(h1^2+k1^2+l1^2)}^2 sin^2(\beta_0)cos^3\alpha/[B^2(d2/d1)+cos\beta_0 sin\alpha]...(3.2)$$

where B=12398.4244eVangstrom. The general behavior of the dispersion function D is proportional to $cos^3\alpha/sin\alpha$ We have caculated the dispersion following the above equations for some of our monochromators. In order to callibrate wavelength resolution we have used the Fig- 3d where an analyzer crystal was used. Table 3f shows the beam size,wavelength, energy resolution and throughput of various MM. Theoretical Rocking curves has been generated using the X-ray dynamical diffraction theory for 0.1612nm wavelength MM, the experimental rocking curves correlate well with the theory.

4.2 Results and discussions

Fig 3 shows the X-ray photograph showing the incident and diffracted beam gap is in agreement with the designed value for the 0.1542 and 0.0694nm Monochromators. All monochromators has been callibrated at its maximum wavelengths following equation 3.1. Fig3b shows the relationship between the tilt angle of a channel-cut(α) and their wavelengths for monochromators of 0.0694 nm(Mo-K) , around the peak positions , we observed the zero tilt position which corresponds to the longest wavelength transmitted by the monochromator.

We further calculate the dispersion for the above two monochromators following eqn(3.2), Fig 3b and 3c shows the absolute callibration of the wavelengths and their correspondence dispersion relationship for MM design for 0.154nm and 0.069 nm wavelength. We observed the singularity at maximum wavelength position as expected and is clearly shown in fig 3c in case of 0.06940nm monochromator. Such relationship has been obtained for the first time and thus lattice constant at this maximum position defines with high precision. We further observed that for higher Bragg angle the dispersion is higher. We have tried both high and low Bragg angle MM, for higher Bragg angle the dispersion is higher, therefore one needs the optimum choice of wavelength. In fig 3a shows Callibration of wavelength of MM showing the maximum wavelength transmitted from 0.0694 nm. All MM has been set at this maximum position. Further wavelength have been callibrated using Bond method and FZ oxyzen free crystal.

Further Experimental rocking curves in Fig 3e for 0.1612nm monochromator fits well with the Dynamical diffraction theory thus showing the good performance of MM. From MM Characterization Table-3f we see that for higher index MM, the wavelength resolution is higher therefore number of photons on the sample is lower, in case of low index provides lower resolution but higher number of photons. Thus one needs to compromise the higher resolution at the cost of lower intensity and

higher intensity at the cost of lower resolution. Output after the 4th reflection from MM varies accordingly. Our main interest is to set the MM at its maximum position as it is related to the lattice constant value which is the longest wavelength value of MM according to the expression (2.5). All MM' were well characterized in terms of their wavelength, resolution, FWHM , beam gap and throughput.

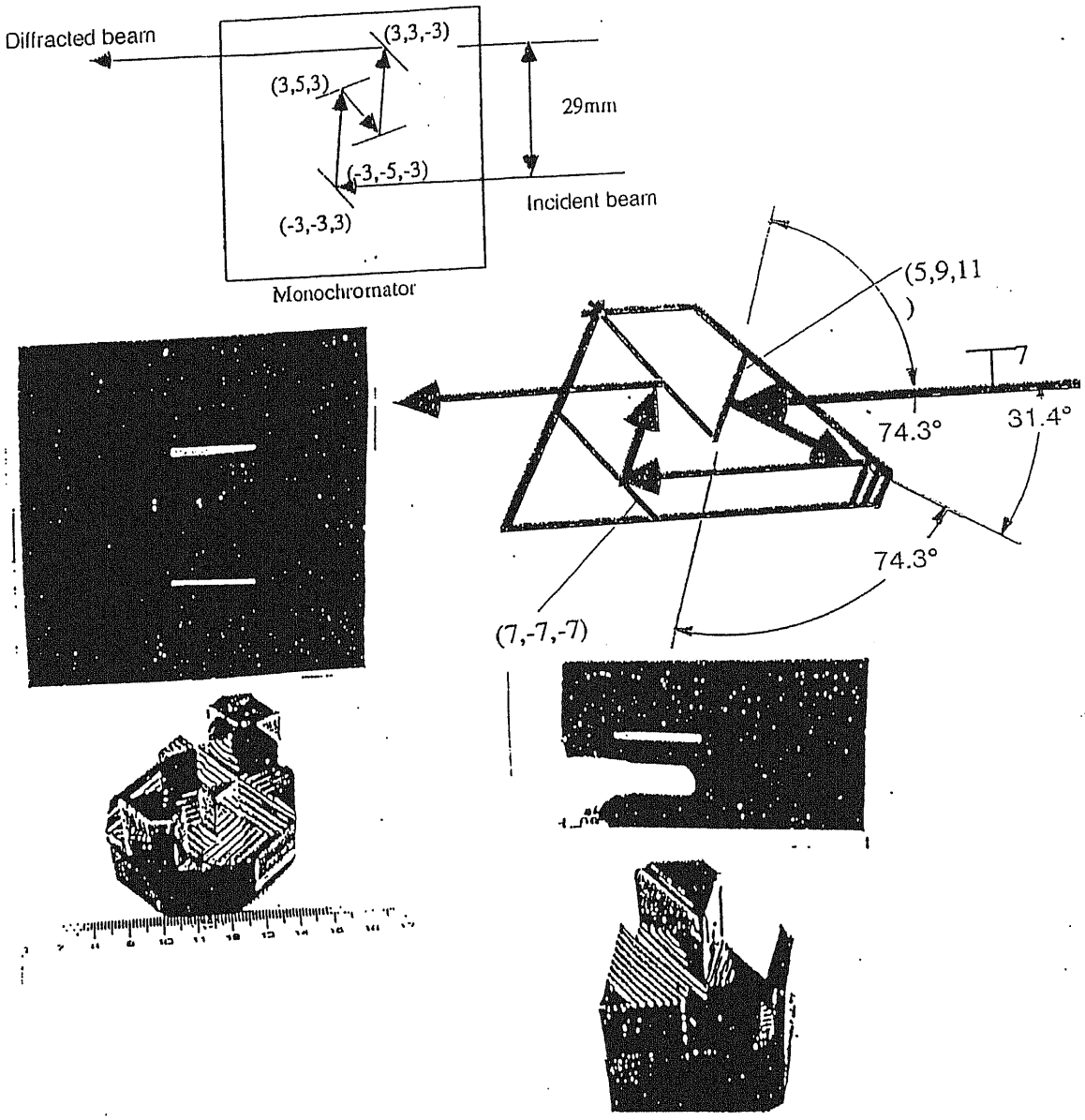

FIG 3 X-ray photograph from 0.0694 and 0.1542nm Monochromators showing the agreement between the incident and diffracted beam gap with designed value.

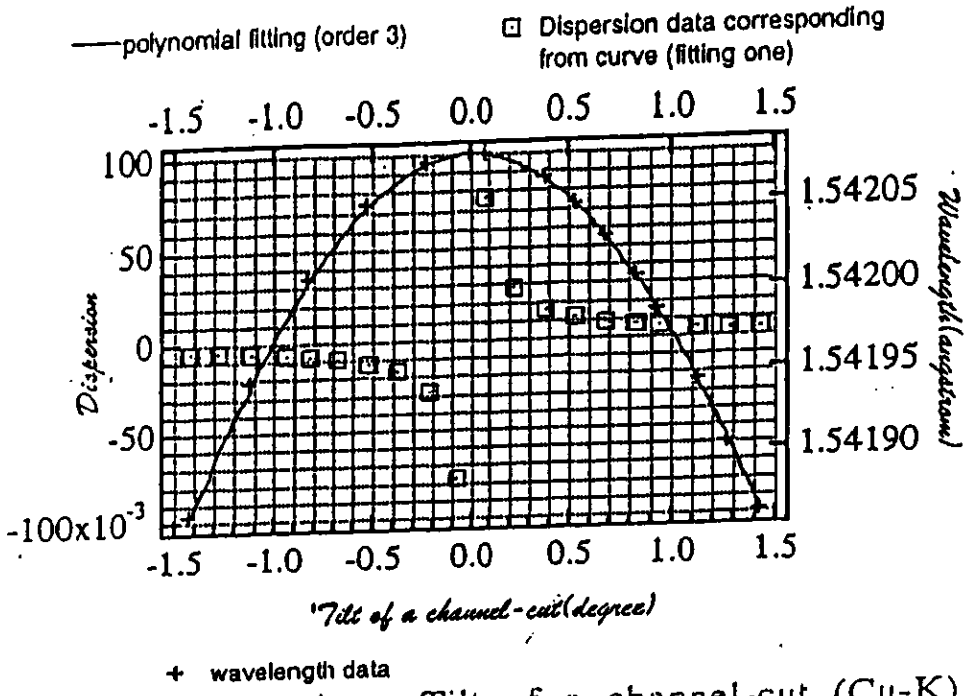

Fig 3b Dispersion and wavelength vs Tilt of a channel-cut (Cu-K)

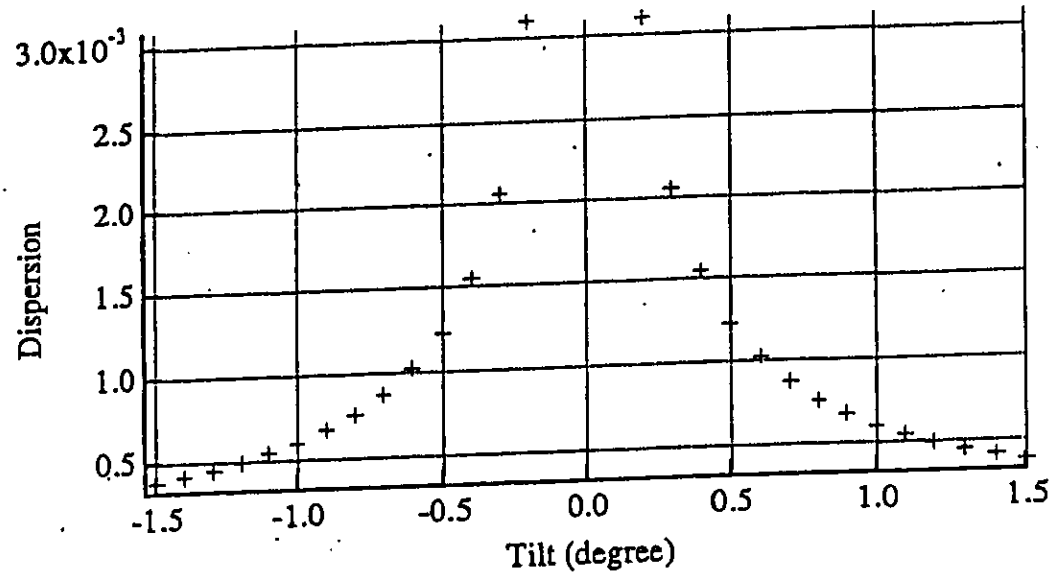

Fig 3c Singularity at maximum wavelength position for 0.0694MM

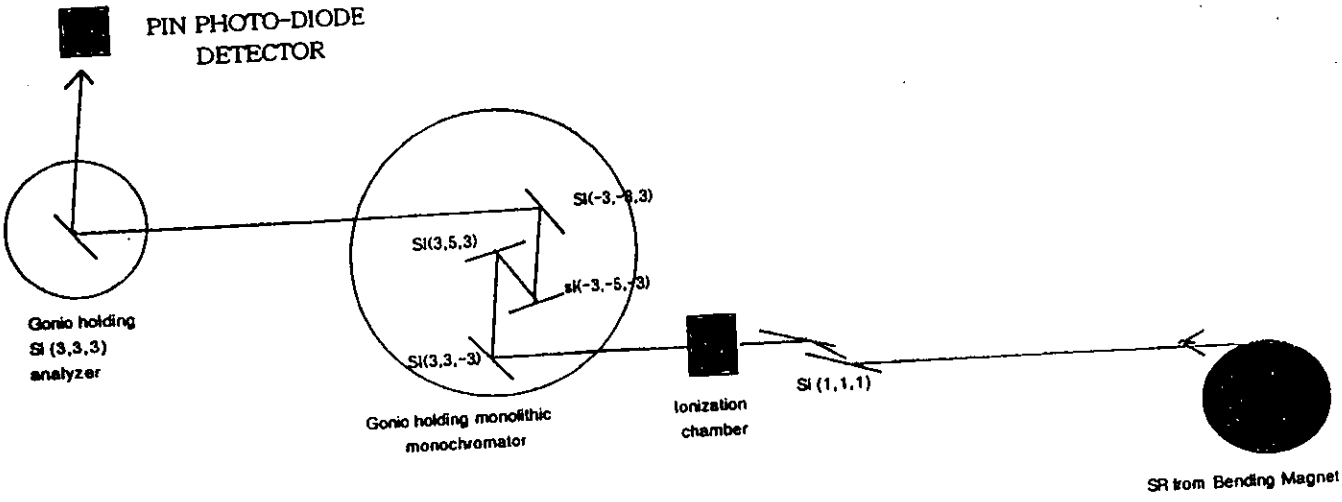

Fig 3d Analyzer Crystal set-up for wavelength callibration of MM.

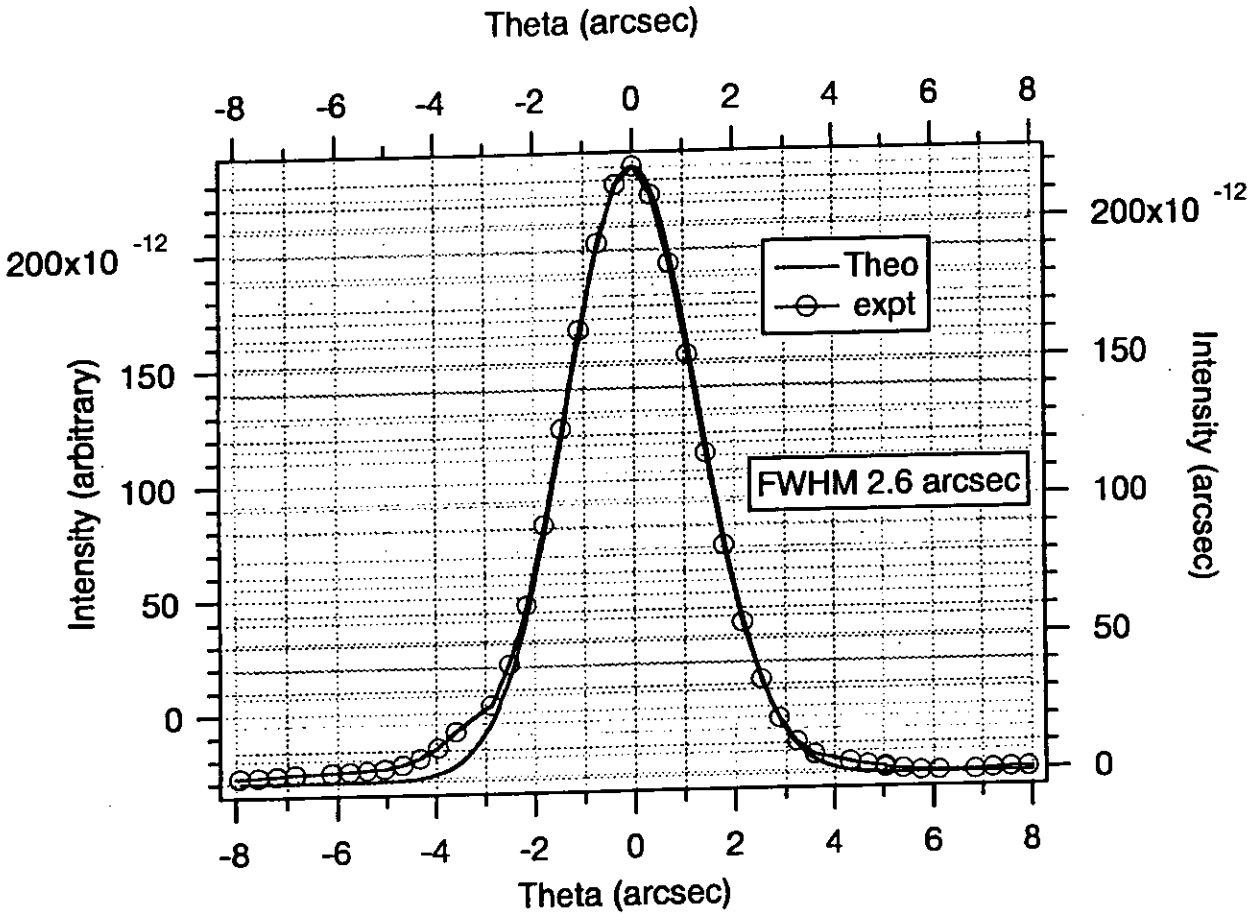

Fig 3e Rocking curves from (153) of MM 0.1612nm showing good agreement between theory and experiment

Table-3f

High Energy Resolution Crystal Monochromator for BL-3C2

Diffraction plane	$\Delta\lambda/\lambda$	λ (nm)	Beam size (mm) (VxH)	Input Current (μA)	Output Current (4th)	Throug-hput (out/in)	percent-age	CPS at sample
(5,9,11) ($\bar{7}$,7,7) (5,9,11) (7, $\bar{7}$, $\bar{7}$)	3×10^{-7}	0.009	1 x 16	7.56	13 pA = 13 $\times10^{4}$ cps	0.118 $\times10^{-3}$	.001	20000 Si (880)
(3,3,$\bar{3}$). ($\bar{3}$,3,3). ($\bar{3}$,$\bar{3}$,3). (3,5,3)	5.8×10^{-6}	.154	3x16	13.8	8.9 nA = 8.9 $\times10^{7}$ cps	0.809 $\times10^{-3}$	.089	9 $\times10^{6}$ Si(444)
(1,5,1). (1,1,7). ($\bar{1}$,3,1). ($\bar{1}$,1,$\bar{7}$).	5×10^{-6}	0.141	1 x 16	11	7 nA = 7 $\times10^{7}$ cps	0.636 $\times10^{-3}$	.063	4 $\times10^{6}$ GaAs (8,0,0)
(5,1,3). (1,5,3). ($\bar{5}$,1,3). ($\bar{1}$,3,3)	6×10^{-6}	0.161	1 x 11	10.87	10 nA = 1 $\times10^{8}$ cps	0.919 $\times10^{-3}$	.091	14 $\times10^{6}$ Si(5,3,1),(1,53)
(1,5,5) (5,1,3) (1,5,5) ($\bar{5}$,1,3)	4.4×10^{-6}	.135	1x1	14.3	6nA = 6×10^{7}	0.419 $\times10^{-3}$	.041	1×10^{6} Si(8,0,0)

4.2.1 Dumond diagram

Dumond diagram characterize monolithic monochromators in terms of their Energy and Angular resolution. Dumond developed a graphical technique for understanding the wavelength and angular distribution[36] of X-ray beam that results from the successive diffraction through various multiple- crystal face arrangements. The Dumond diagram for diffraction from the first four crystal faces is shown in Fig-3g. These diagrams is applicable only when all of these first four crystal faces are identical, and the x-ray beam undergoes the same bragg reflection at each crystal face. Figure 3g shows the intersection of the curves. The square shaped area represent the resulting x-ray beam. In Fig 3g four curves,O1,O2,O3,O4 represent the region of diffraction from crystal faces 1,2,3,and 4 in Fig3g, respectively. Curves O1 and O2 lie on top of one another, as do curves O3 and O4, so only two distinct curves are seen in Fig 3g. Curves O1 and O2 follow the functional dependence $\lambda = 2dsin\theta$ where d is the spacing of crystal planes. curves O3 and O4 are reflected about the λ axis and displaced by twice the Bragg angle, θ_B and so follow the functional dependence $\lambda = -2dsin(\theta - 2\theta_B)$. The enlargement of the intersection region shown in fig 3g shows that the O curves are actually bands of finite width , coerresponding to the band of narrow but finite angular width over which the Bragg diffraction is observed. The wavelength and angular distribution of the beam after the first four reflection is the product of the intensities of the bands in the intersection region. Suppose we know the angular dependence of the reflectivity[30] for a monochromatic x-ray beam that undergoes the specific bragg reflection. We are using with these first four crystal faces. We define that the line shape to be g(y). The maximum value of g occurs when y equals zero, and g gradually falls off to zero as y becomes large either positively or negatively. but g is not in general symmetric about zero. Then the intensity of band O1 across the line AC shown in Fig 3g would be $g(\theta - \theta_B)$. This is the intensity at λ_0, the central wavelength of the radiation emitted by x-ray. The

intensity of band O1 across line of constant wavelength λ slightly above or below λ_0 is the function g displaced slightly to the right or left by the difference between λ and λ_0 divided by the slope of O1 in this region,i.e

$$I = g[\theta - \theta_B - (\lambda - \lambda_0)/d\lambda/d\theta)] \quad (3.3)$$

$$I = g[\theta - \theta_B - (\lambda - \lambda_0)/2dcos\theta_B)] \quad (3.4)$$

We assume that the line shape does not change with small excursions in the wavelength.

The intensity of O2 is the same as for O1. The intensity of O3 along AC is the same function g, inverted and displaced. Thus the intensity of O3 along AC is $g(-\theta+\theta_B)$. On line of constant wavelength slightly above or below λ_0 the intensity of O3 is, by the logic used before,

$$I = g[\theta + \theta_B - (\lambda - \lambda_0)/2dcos\theta_B]$$

The intensity of O4 is the same as for O3. the angular and wavelength distribution of an x-ray beam that has undergone the first four successive reflections shown in fig-3g is therefore the product of four intensities,

$$I = g[\theta - \theta_B - (\lambda - \lambda_0)/2dcos\theta_B)]^2 \quad (3.5)$$

$$I = g[\theta + \theta_B - (\lambda - \lambda_0)/2dcos\theta_B]^2 \quad (3.6)$$

4.3 Analytical $\Delta\theta and \Delta\lambda/\lambda$

Here we have derived angular and wavelength spread in the dumond diagram for the two different h1,k1,l1 and h2,k2,l2 combinations. All symbols are labelled in Fig 3h. In triangle AMR (Fig-3h)

$tan\theta$'=AM/MR=AM/(MQ+QR)=AM/($\Delta\theta$+QR) (3.7)

In Triangle CQL

$tan\theta_1$=CQ/LQ=CQ/(MQ+LM)=CQ/($\Delta\theta$+LM).....(3.8)

from above

$tan\theta_1(\theta$+LM)=CQ.....(3.9)

$tan\theta_2^{'}(\theta$+QR)=AM.....(3.10)

Adding equation(3.7) and (3.8)

$tan\theta_1(\theta$+LM)+$tan\theta_2^{'}(\Delta\theta$+QR)=CQ+AM

$\Delta\theta(tan\theta_1 + tan\theta_2^{'})$ + $tan\theta_1$(LM)+$tan\theta_2^{'}$(QR)=AM+CQ.....(3.11)

In Triangle AOM

$tan\theta_1$=AM/OM=AM/(W1+LM).....(3.12)

In Triangle CQZ

$tan\theta_2^{'}$=CQ/(W2+QR).....(3.13)

From (3.12) and (3.13)

$tan\theta_1$(W1+LM)=AM.....(3.14)

$tan\theta_2^{'}$(W2+QR)=CQ.....(3.15)

adding (3.14) and (3.15)

$tan\theta_1$(W1+LM)+$tan\theta_2^{'}$(W2+QR)=AM+CQ.....(3.16)

Now comparing from (3.5) and (3.10)

$\Delta\theta(tan\theta_1+tan\theta_2^{'})+tan\theta_1(LM)+tan\theta_2^{'}(QR) = tan\theta_1(W1+LM)+tan\theta_2^{'}(W2+QR)$

$\Delta\theta = (tan\theta_1 W1 + tan\theta_2^{'} W2)/(tan\theta_1 + tan\theta_2^{'})$

from $tan(180 - \theta_2^{'}) = -\theta_2$

$\Delta\theta = (tan\theta_1 W1 - tan\theta_2 W2)/(tan\theta_1 + tan\theta_2)$.....(3.17)

$\Delta\lambda/\lambda = \Delta\theta cot\theta$ =[(tan$\theta_1 W1 - tan\theta_2 W2)/(tan\theta_1 + tan\theta_2)]1/tan(\theta_1+\theta_2)$.....(3.18)

4.4 Dumond diagram procedure:

(1) Dumond diagrams are functional dependance of $\lambda = 2dsin\theta$

(2) Dumond diagrams are curves of finite bandwidth corresponding to the angular width over which the Bragg-diffraction is observed and given by:

$$\Delta\omega_{1/2} = 2|C|\chi/sin2\theta_B .....(3.19)$$

$$where\chi = -\gamma_e\lambda^2 F_h/\pi V_c .....(3.20)$$

γ_e is the classical electron radius.

F_h is the atomic structure factor

$|C|$=$cos2\theta_B$for π polarization and 1 for sigma polarization.

DUMOND DIAGRAM FOR WAVELENGTH 0.1410nm:

(1) for (1,1,5) index:

$\Delta\omega_{1/2} = 1.67arcsec$ Band width for (1,1,5) represented by OI,OII (2) for (1,7,1) index: $\Delta\omega_{1/2} = 1.54arcsec$ Band width for (7,7,7) represented by HI,HII and following the same procedure ,the slope for OI,OII is37.79degree and slopefor HI,HII is 15.83 degree.

DUMOND DIAGRAM FOR WAVELENGTH 0.06940nm:

(1) for (5,9,11) index:

$\Delta\omega_{1/2} = 0.14arcsec$ Band width for (5,9,11) represented by OI,OII (2) for (7,7,7) index: $\Delta\omega_{1/2} = 0.19arcsec$ Band width for (7,7,7) represented by HI,HII and following the same procedure ,the slope for OI,OII is 5.5 degree and slopefor HI,HII is 15.8 degree.

DUMOND DIAGRAM FOR WAVELENGTH 0.1359nm:

(1) for (5,3,1) index:

$\Delta\omega_{1/2} = 1.26arcsec$ Band width for (5,3,1) represented by OI,OII (2) for (1,5,5) index:

$\Delta\omega_{1/2} = 1.22 arcsec$ Band width for (1,5,5) represented by HI,HII and following the same procedure ,the slope for OI,OII is 31.69 degree and slopefor HI,HII is 18.96 degree.

Dumond diagrams drawn are shown in Fig 3i, 3j 3K. Thus the draw of dumond diagram for MM provides the understanding of the intuitive energy spread and angular spread of each MM.

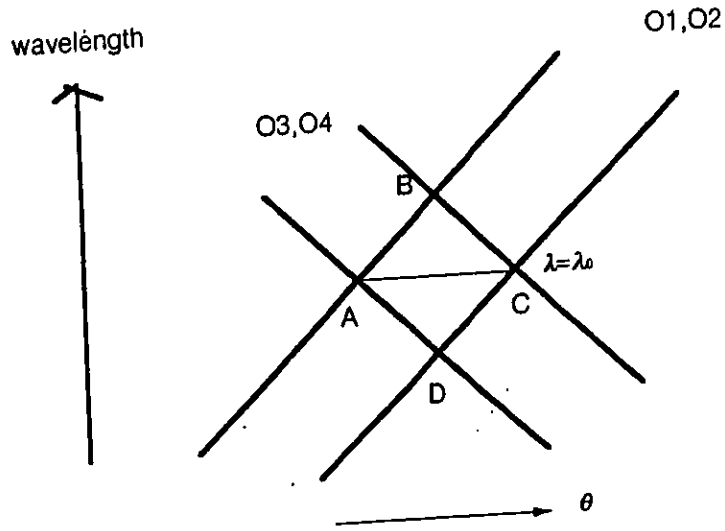

Fig 3g Enlarged view of the intersection region.

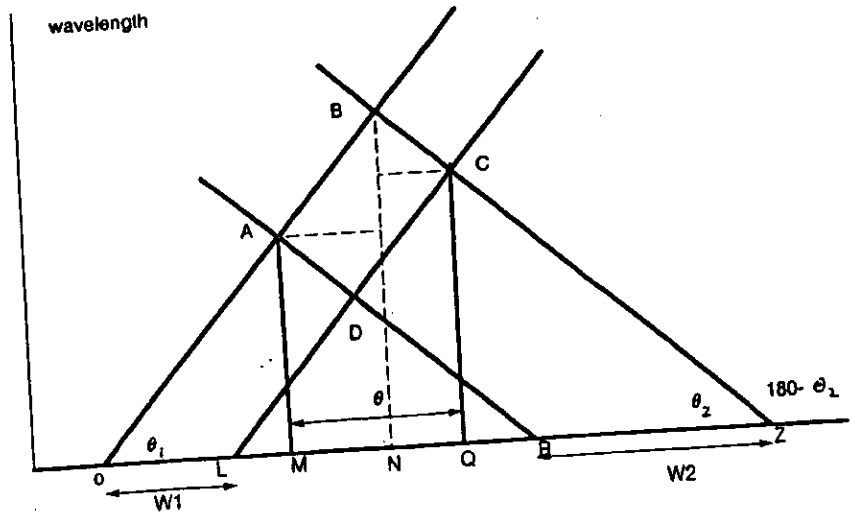

Fig-3h Analytical description for Dumond diagram

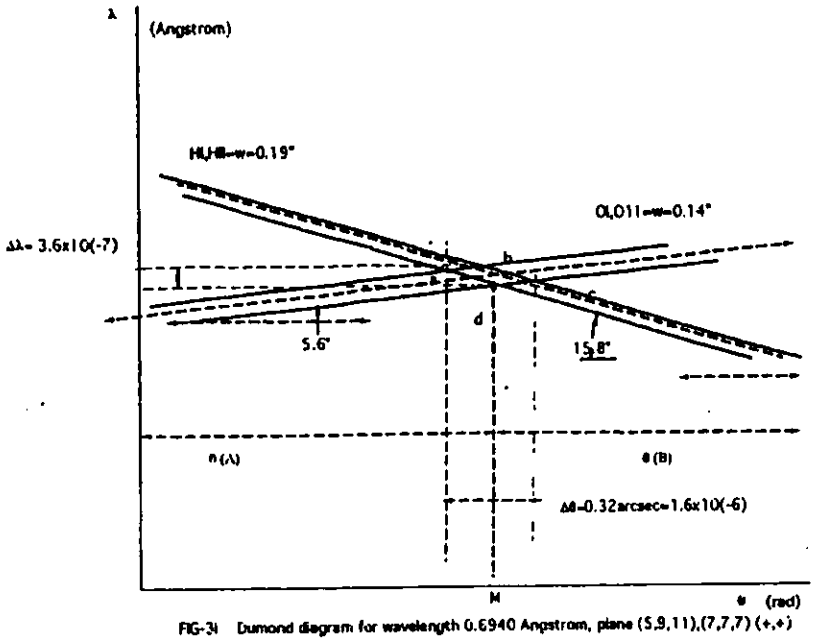

FIG-3i Dumond diagram for wavelength 0.6940 Angstrom, plane (5,9,11),(7,7,7) (+,+) set up

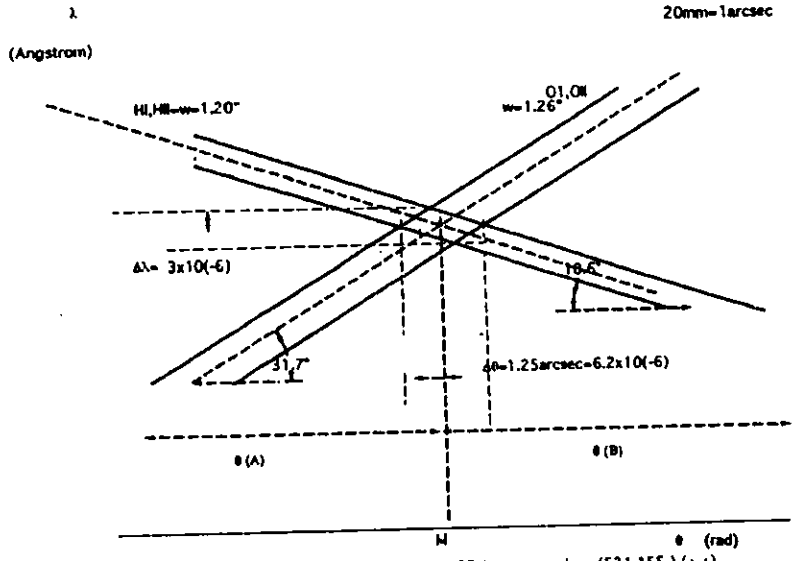

FIG-3j Dumond diagram for wavelength 1.35 Angstrom, plane (531,155) (+,+)

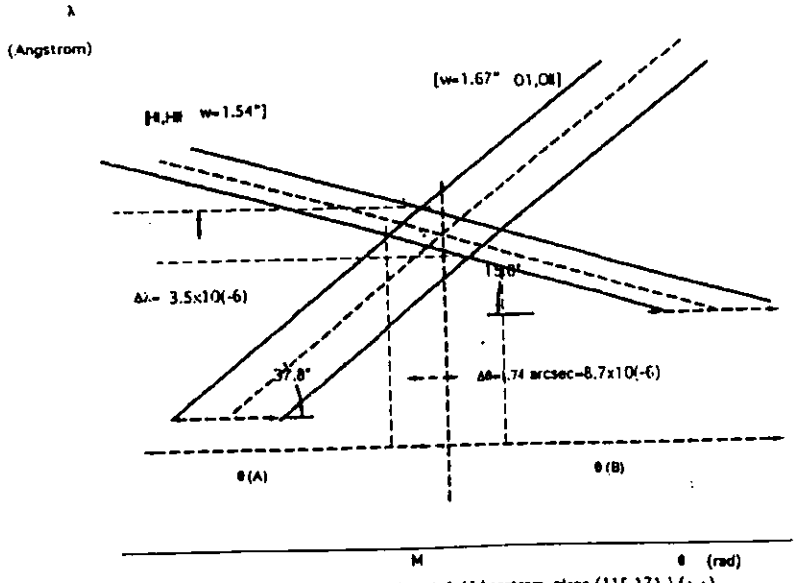

FIG-3k Dumond diagram for wavelength 1.41Angstrom, plane (115,171) (+,+)

4.7.1 2-beam Rocking curves

Two beam rocking curves is shown in Fig-1 , Comparing with Fig 1 with Fig 2 to 10 , it is estimated that overall Bragg peak shift is 12 micro radian.

4.8 3 -beam Rocking curves

Further effort has been made to calculate the 3-beam diffraction from a finite crystal using the Takagi-taupin [62,63], approach considering the natural parameter (η) of a crystal which is the ratio of the crystal dimension to the extinction length and u parameter which is the product of the crystal dimension to the excitation error (deviation from the Bragg peak) and is dimension less. In these calculations Φ is the product of the three structure factors involved in three beams [62,63,64,66,70]. By using on the Takagi-Taupin equations for three coupled waves in a perfect crystal it has been possible to obtain general boundary-value green functions for the wave fields D_0, D_h, D_g. For a crystal shaped as a parallelepiped the integral power P_h is calculated by suitable integration over one divergence angle and over the entrance and exit surfaces. The result which is expressed as a function of the deviation from the Bragg condition for the third wave, is continuous through the three-beam point, and gives the expected assymetry associated with the invariant phase Φ of the product of the three structure factors involved. Non zero value of X corresponds to the movement of reciprocal lattice point relative to the Ewald sphere.

In the expression for the integrated power the dimensions of the crystal [70] , scaled to appropriate extinction lengths, occurs as parameters. The movement of the reciprocal latrtice point owing to the rotation of the crystal when calculating the integrated power. When this movement is small it shows oscillations in the integrated power, both Umweganregung and Aufhellung situations is observed.

In the result, Fig 17, shows invariant phase of three-beam Φ=0 shows the relative change in integrated power as a function of u,(parameter which is the product of the crystal dimension to the excitation error (deviation from the Bragg peak)) corresponds to usually called Umweganregung case, Fig 17.

Fig 18 with Phase $\Phi = 180$ corresponds to the Aufhellung case Fig 18, others $\Phi = 90, 270$degrees are intermediate case. Other intermediate case shown in Fig 19 , Fig 20.

Non zero value of X corresponds to the movement of reciprocal lattice point relative to the Ewald sphere when the crystal is rotated to measure the integrated power. Splitting in Fig 21, Fig 22 is attributed to the two excitation errors usually occurs due to the 3-beam case as we have calculated in the earlier calculation. In these calculations It has been proved that the diffraction power is symmetric in case of phase 90 degree and 270 degree Fig 19 and Fig 20 in agreement with the plane wave of dynamical theory.

From experimentally observed curve it seems that there are some resonant errors occurs enlarged in Fig 14, Fig-15. Fig 16 shows the diffraction curves after the fourth reflection - this is perhaps due to the narrow angular window and narrow energy window after the fourth diffraction.

4.8.1 Bragg-Peak shift

Detailed calculation Fig 1-Fig 11 shows that the overall Bragg angle-shift is about 12 micro radian in case of (513) and (153) diffraction with wavelength 1.612607 angstrom monochromator.

4.8.2 Structure factor:

In general for the direction of the spectrum hkl, the structure factor F(hkl) is given by

$$F(hkl) = \sum f_j e^{2\pi i(hu_j + kv_j + lw_j)} .....(1)$$

where u, v, w being the fractional co-ordinates of the centre of the atom whose scattering factor is f_j and summation being all over the atoms in the unit cell. To show the phase factor we know that a complex amplitude includes the phase factor, for example in $f = f^{'} + if^{''}$ then we can write

$$f^{'} + if^{''} = |f|(cos\Phi + isin\Phi) = |f|e^{i\Phi}$$

where

$$tan\Phi = \frac{f^{''}}{f^{'}}.$$

$$|f| = \sqrt{(f^{'2} + f^{''2})}$$

corresponds to a real amplitude factor equal to the modulus of f and a phase factor $e^{i\Phi}$

The structure factor of the unit cell can be written as

$$F = (F^{'} + iF^{''})$$

and the phase is defined by the ratio of the imaginary part of the structure factor to the real part and can be written as:

$tan\Phi = \frac{F^{''}}{F^{'}}$.

Detailed structure factor for co-planar three beam (0,0,0),(-5,-1,-3),(-1,-5,-3) can be calculated for Si using the equation, square of F(hkl):

$$|F^2_{hkl}| = 16[2f^2 + 2f^2 cos\pi/2(h + k + l)]$$

for Si has 8 atoms with positions (0,0,0) (0,1/2,1/2),(1/2,1/2,0),(1/2,0,1/2) and at (1/4,1/4,1/4), (1/4,3/4,3/4), (3/4,1/4,3/4),(3/4,3/4,1/4). Using the tables of International Union of Crystallography F(000)=112, F(-5,-1,-3)=30.00 and F(-1,-5,-3)=30.00. the coupled reflections F(-4,4,0)=44.80

Some more values of structure factors for various indexes of Si is given in appendix.

The triplet phase of $\Phi_{(000)}\Phi_{(-5-1-3)}\Phi_{(-1,-5,-3)}$ the co-planar three beam (000),(-5,-1,-3),(-1,-5,-3) is 0 degree.

4.9 Discussion

We have calculated the Bragg peak shift for the (513) and (153) simultaneous diffraction, estimated 12 micro-radians in comparison with 2-beam case. There is a split in Bragg peaks-the physical reason for the split peaks is that, when there two or more Bragg reflections simultaneously excited, it is possible, depending on the particular scanning scheme adopted, that the Bragg nodes may go through the Ewald sphere not exactly all at the same time -for the same theta value, in our case. Further Unwegenregung, Aufhellung situations have been covered in the 3-beam calculations. Structure factor and triplet phase have been determined to be F(000)=112, F(513)=30.00, F(153)=30.00 and phase 0^0.(zero degree).

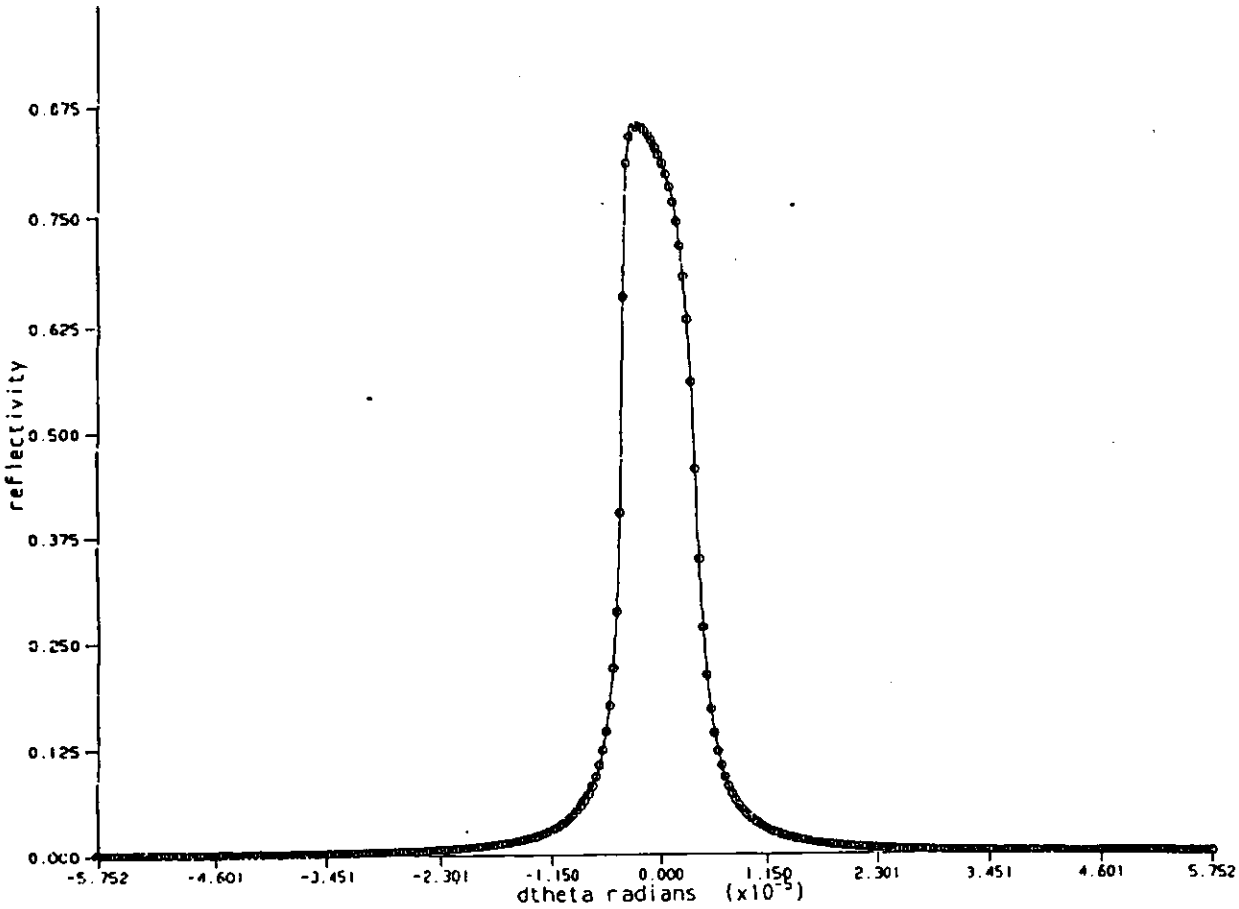

FIG 1 Rocking curve with wavelength 1.612597 , N=2

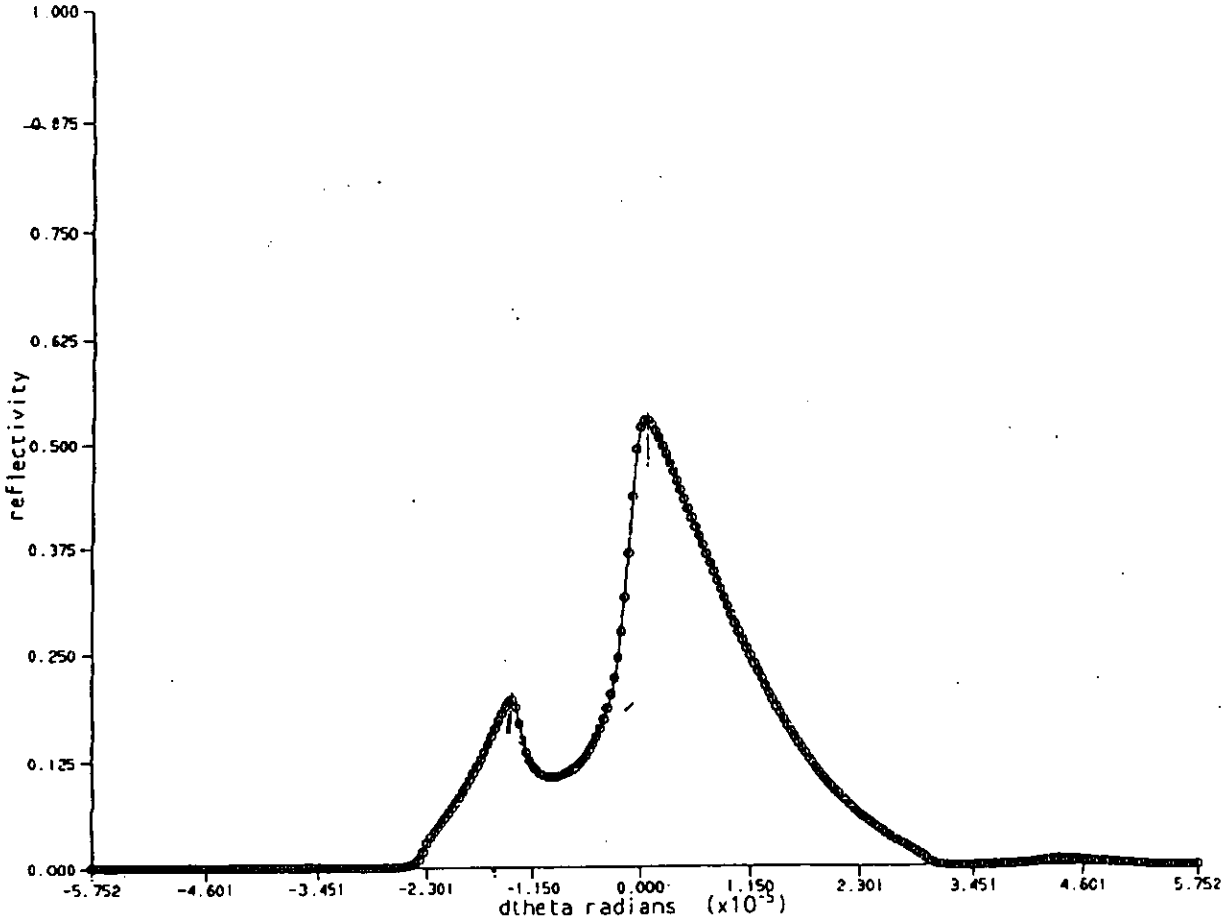

FIG 2 Rocking curve with wavelength 1.612582 , N>2

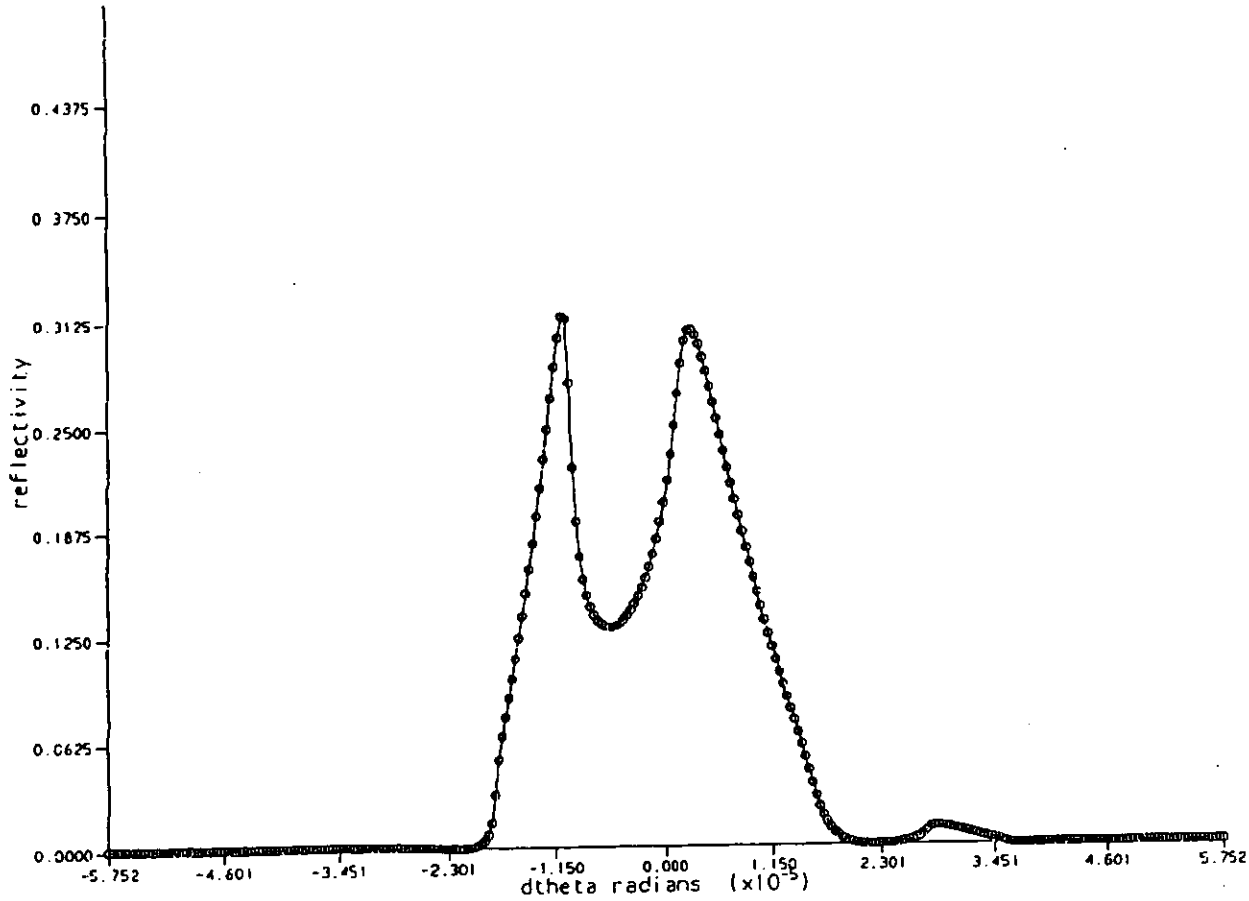

FIG 3 Rocking curve with wavelength 1.612587 , N>2

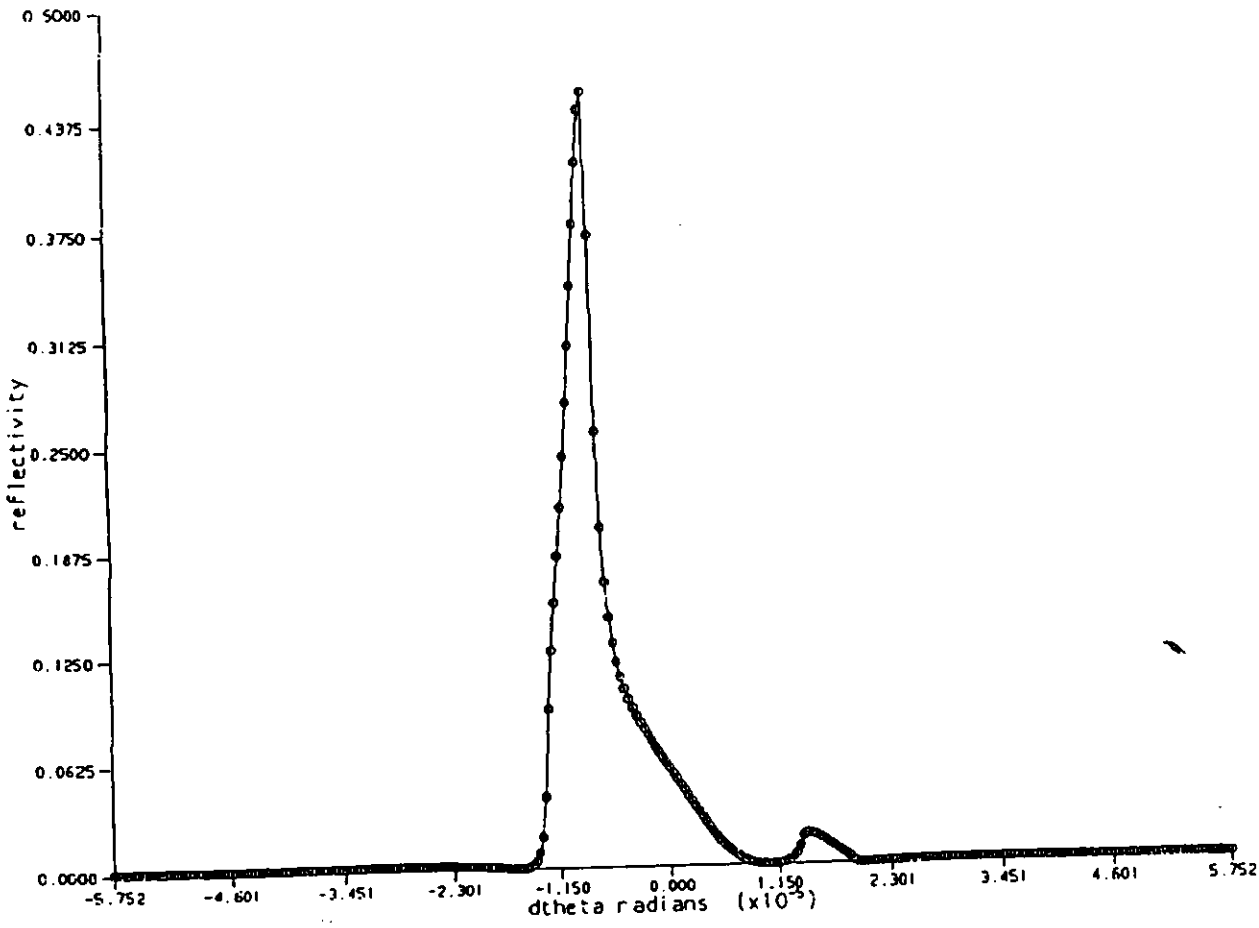

FIG 4 Rocking curve with wavelength 1.612592 , N>2

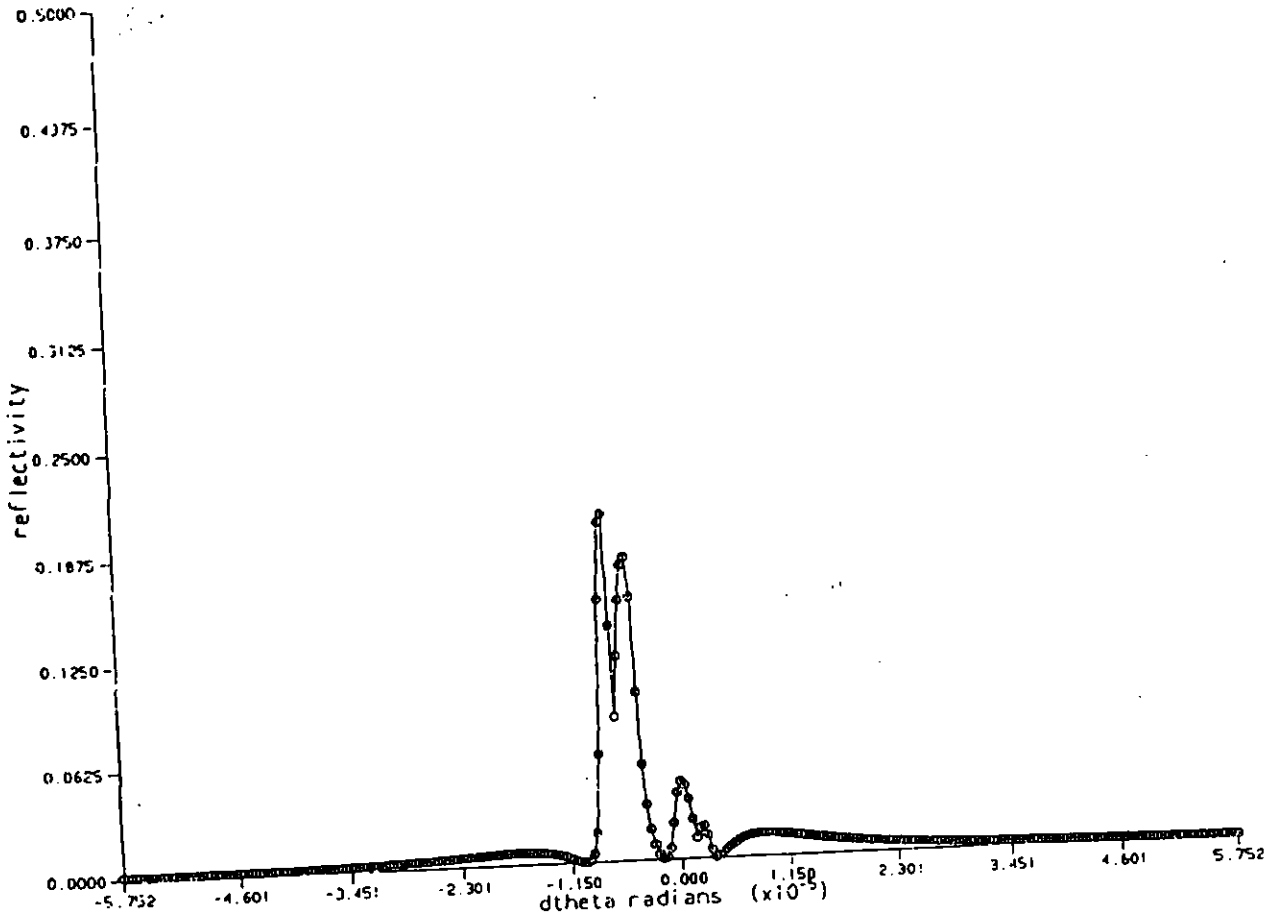

FIG 5 Rocking curve with wavelength 1.612597 , N>2

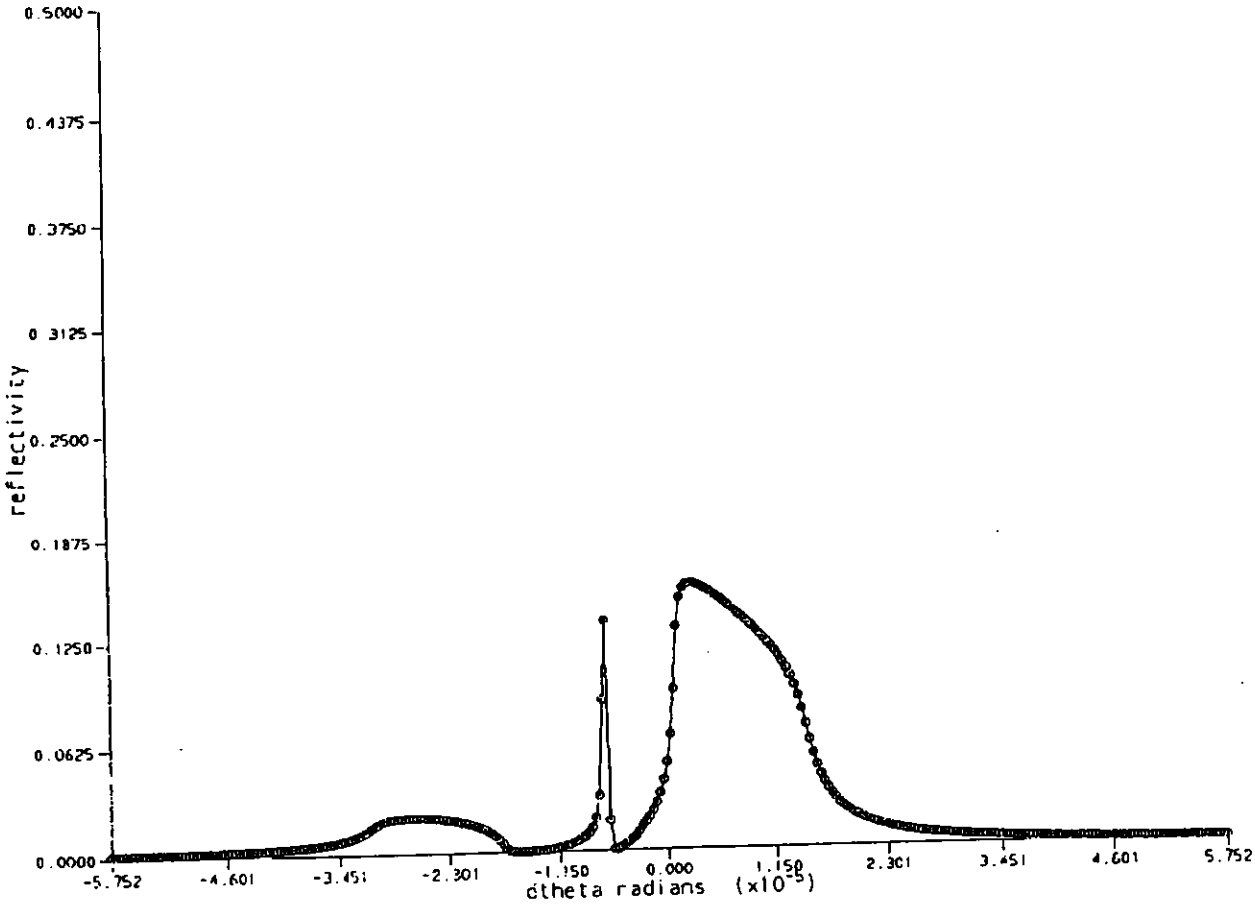

FIG 6 Rocking curve with wavelength 1.612602, N>2

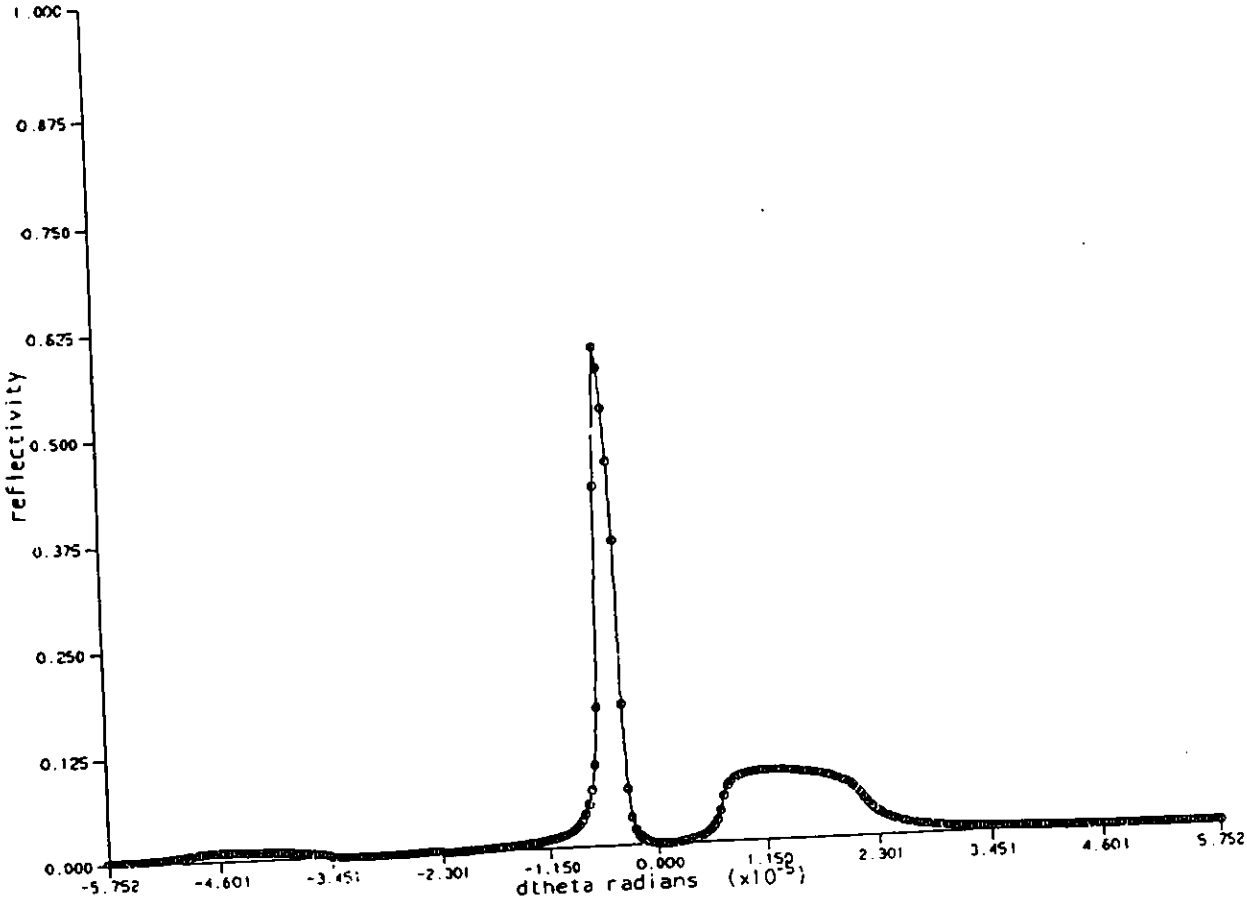

FIG 7 Rocking curve with wavelength 1.612607 , N>2

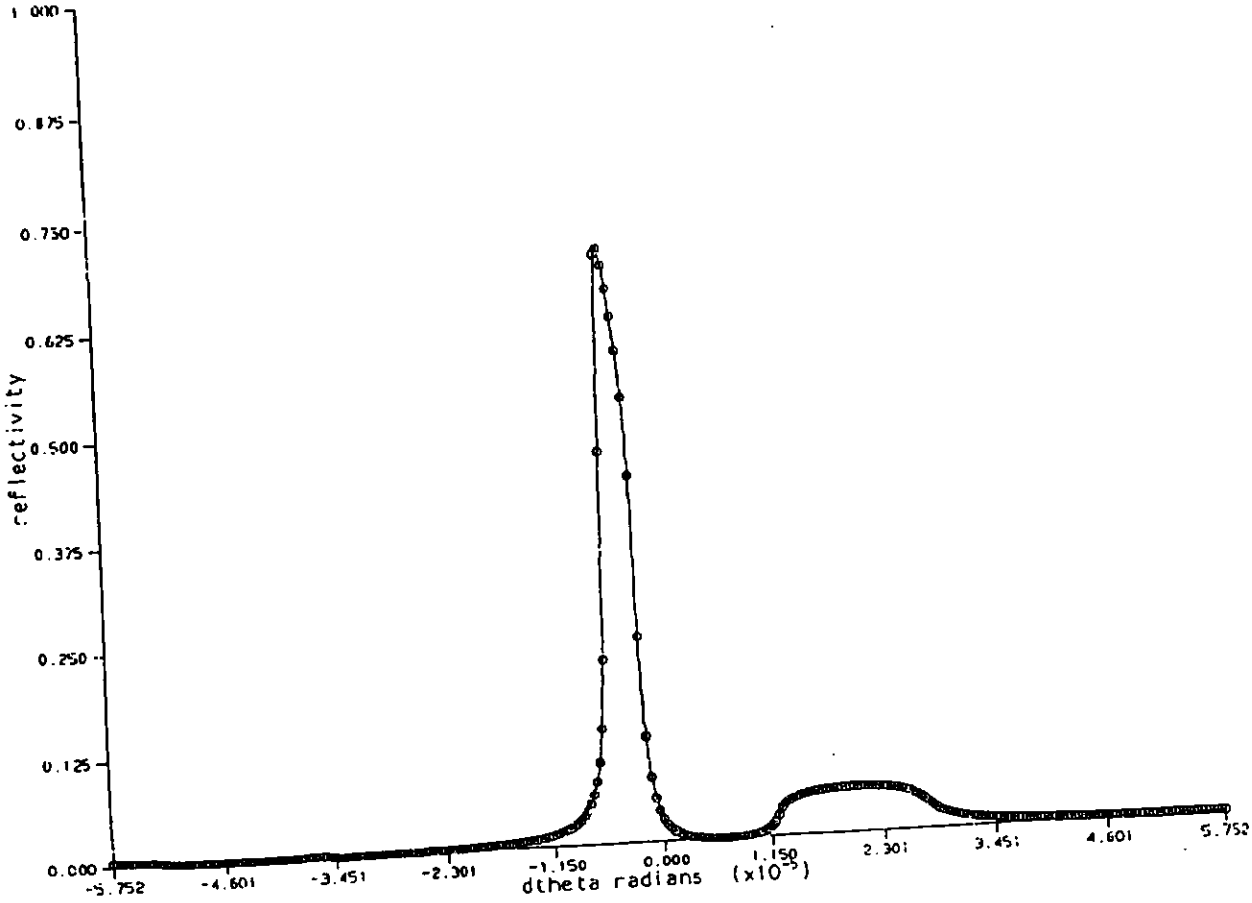

FIG 8 Rocking curve with wavelength 1.612612 , N>2

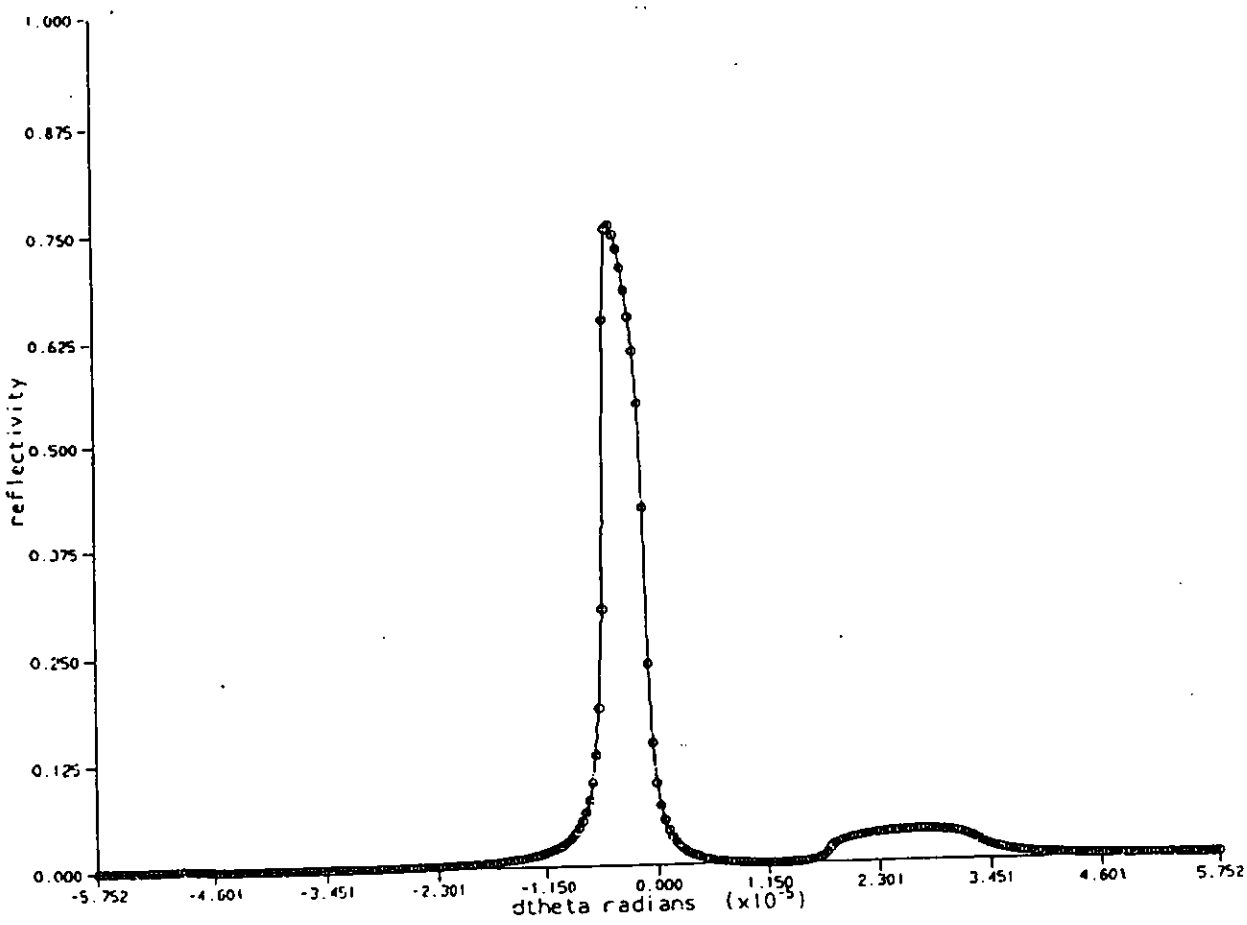

FIG 9 Rocking curve with wavelength 1.612617 , N>2

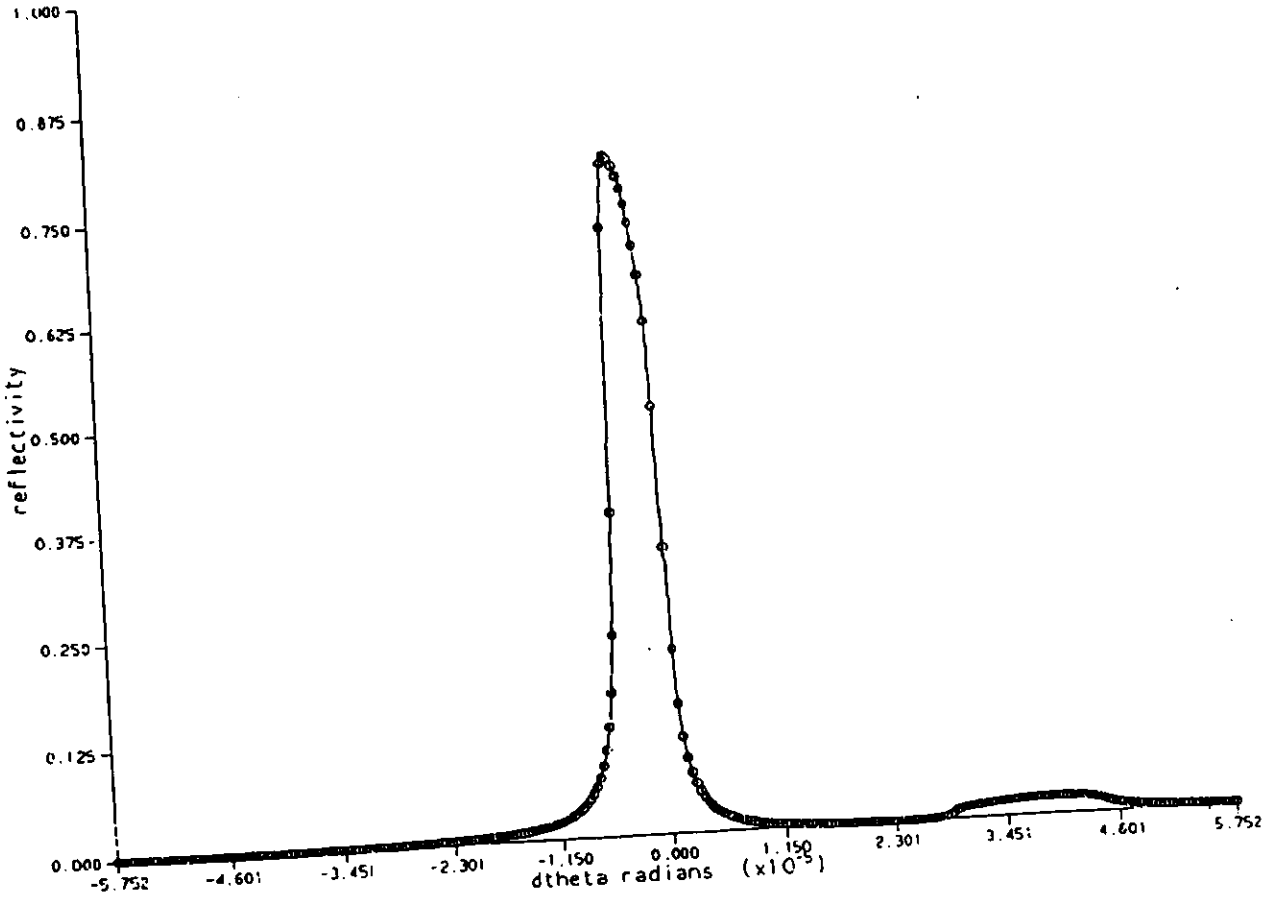

FIG 10 Rocking curve with wavelength 1.612627 , N>2

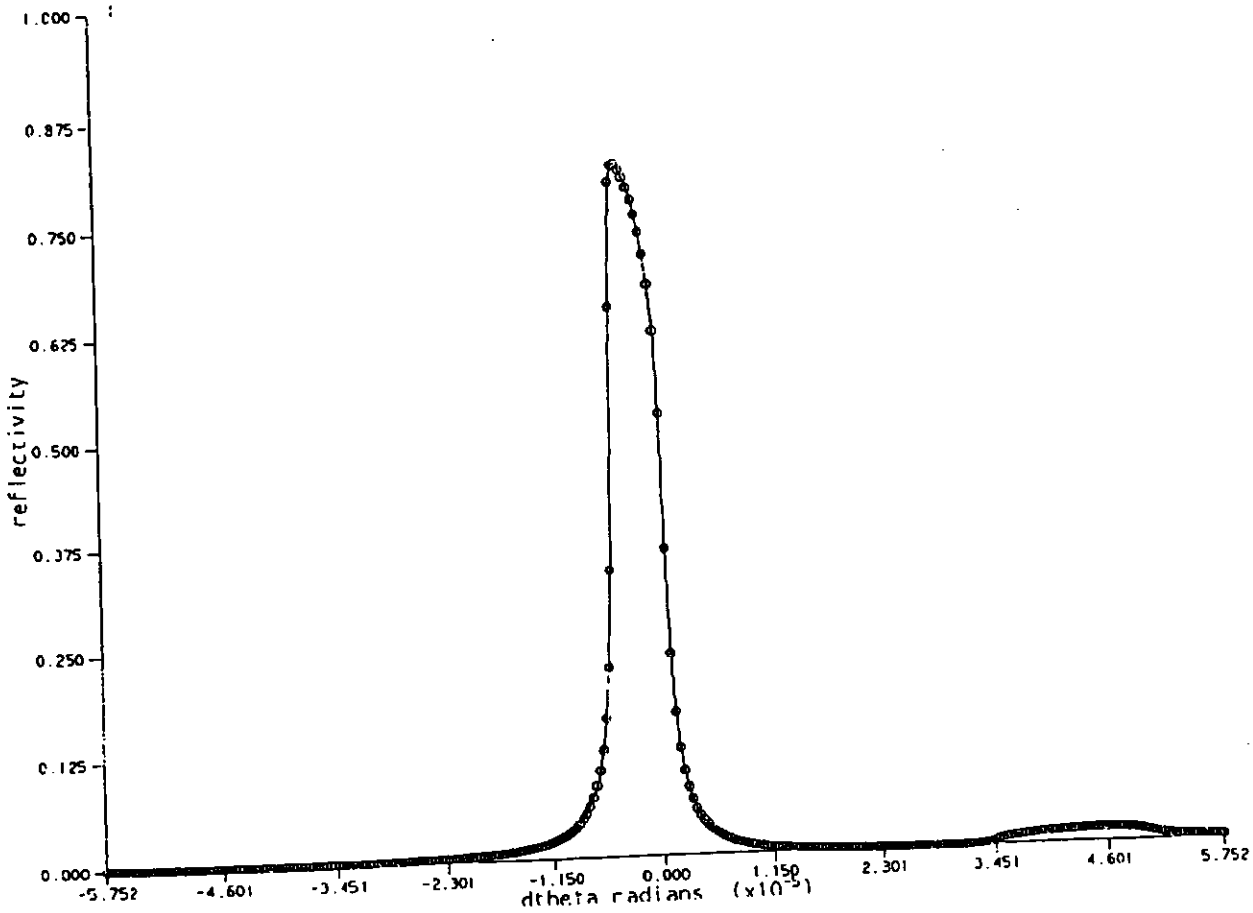

FIG 11 Rocking curve with wavelength 1.612632 , N>2

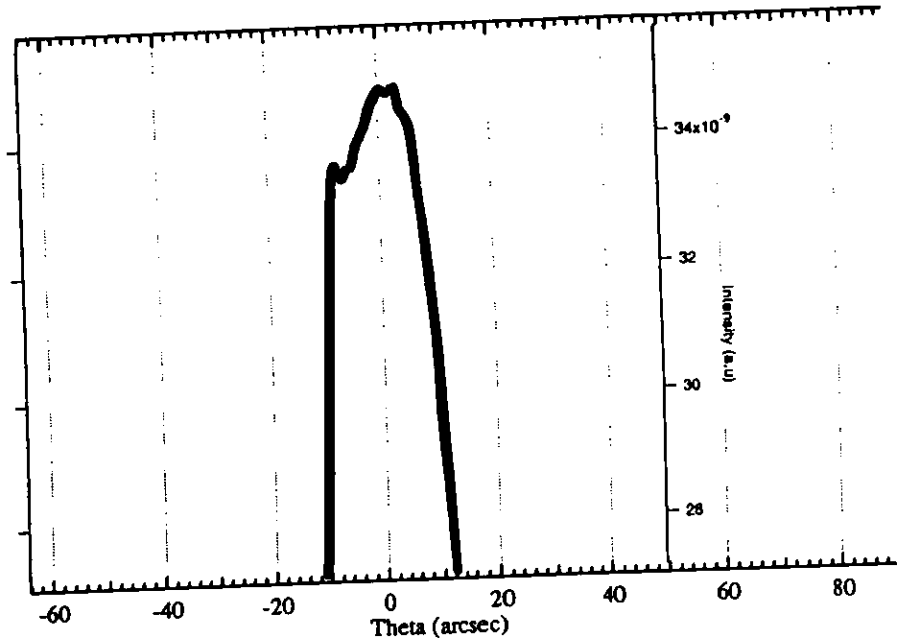

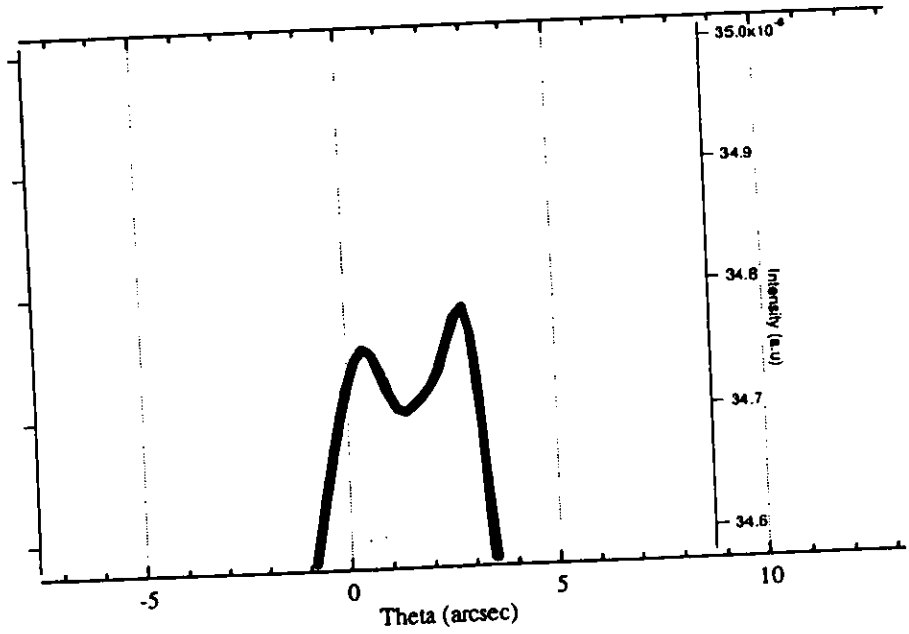

FIG 14, 15 Experimentally observed first diffraction (513) curves.

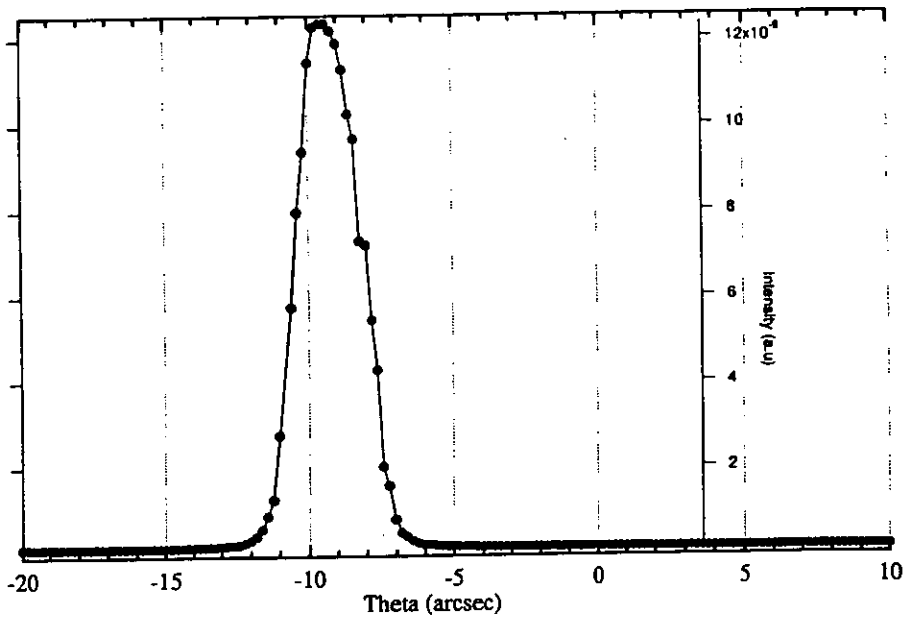

FIG 16 Experimentally observed curved after Fourth reflection.

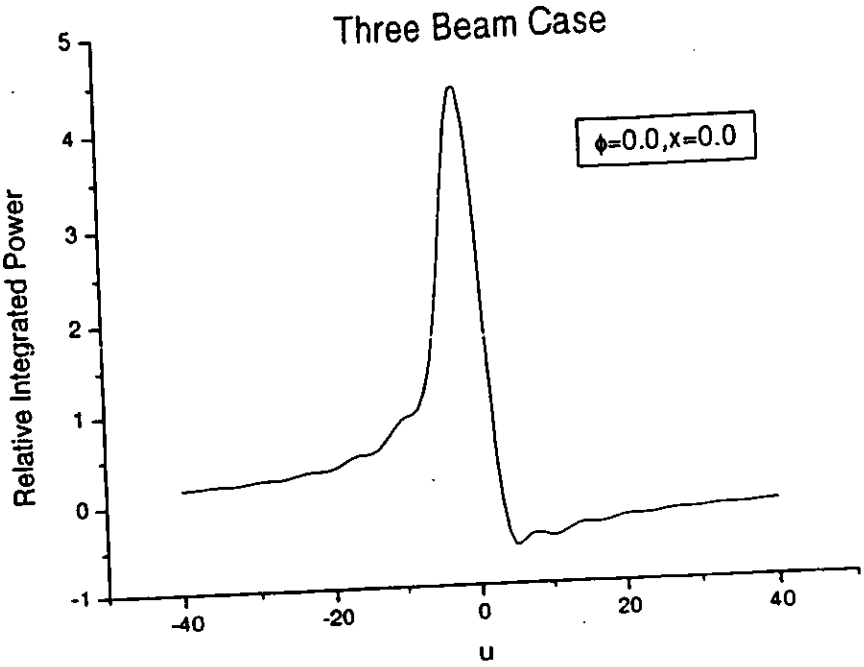

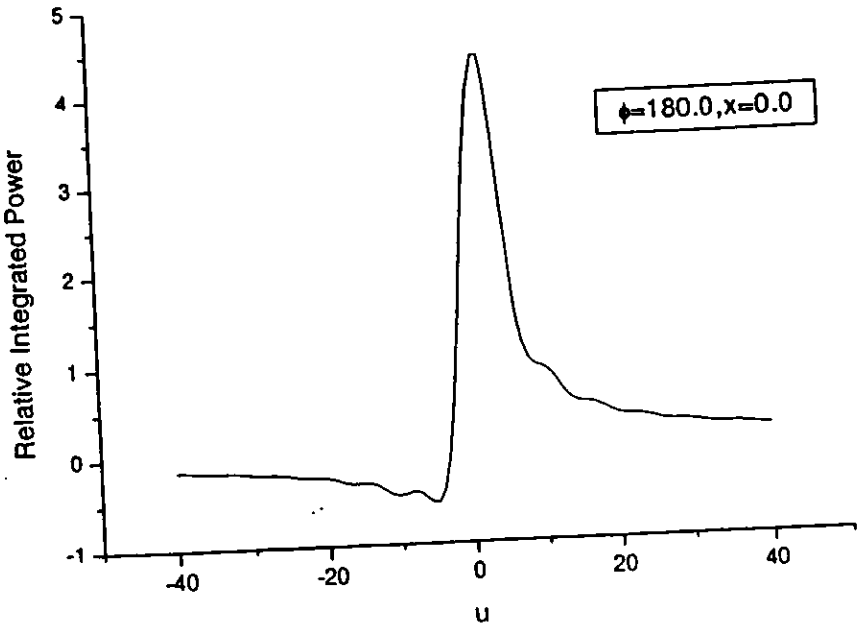

Fig 17, 18 Relative integrated power for Unwegenregung case and Aufhellung case.

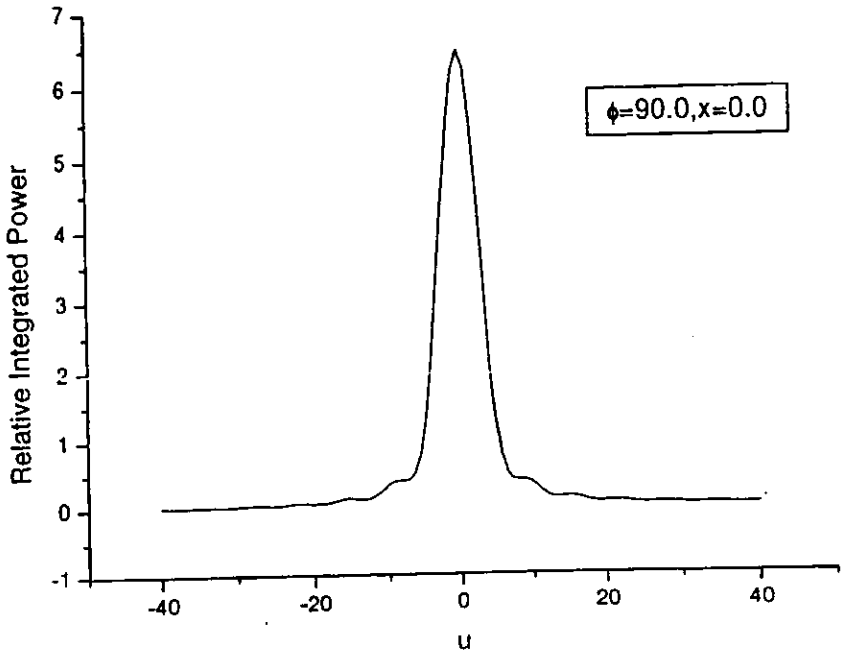

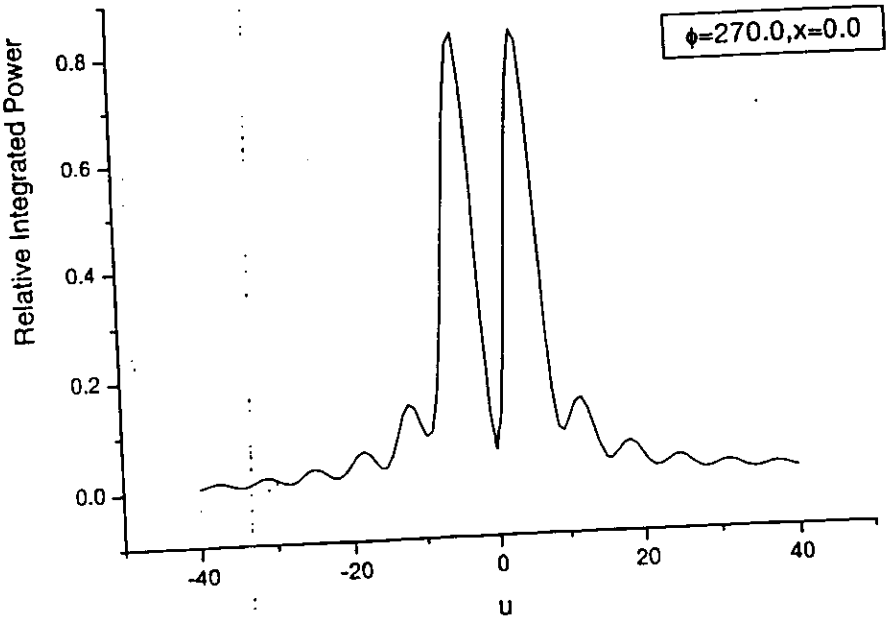

Fig 19 20 Relative Integrated power for Phase factor 90 and 270 degree showing symmetry.

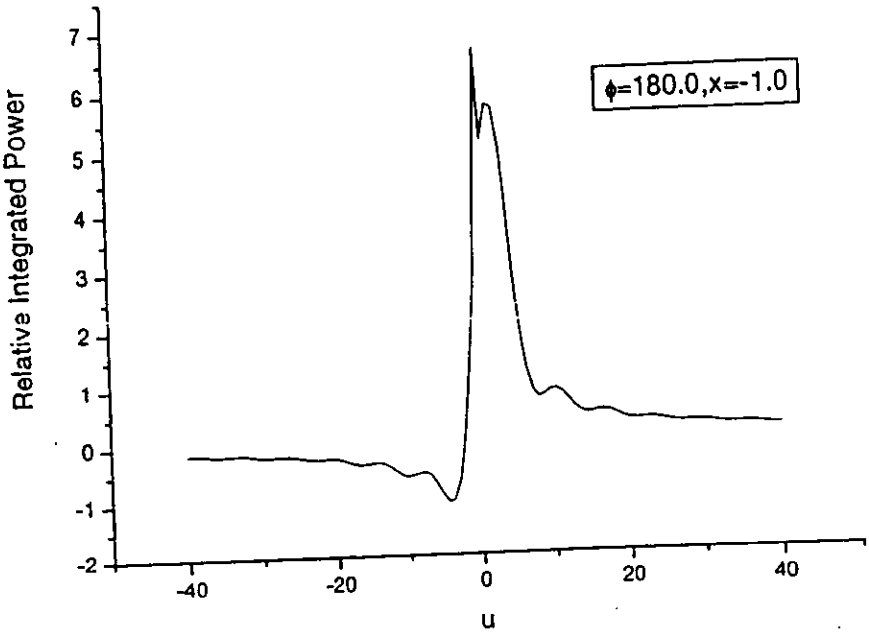

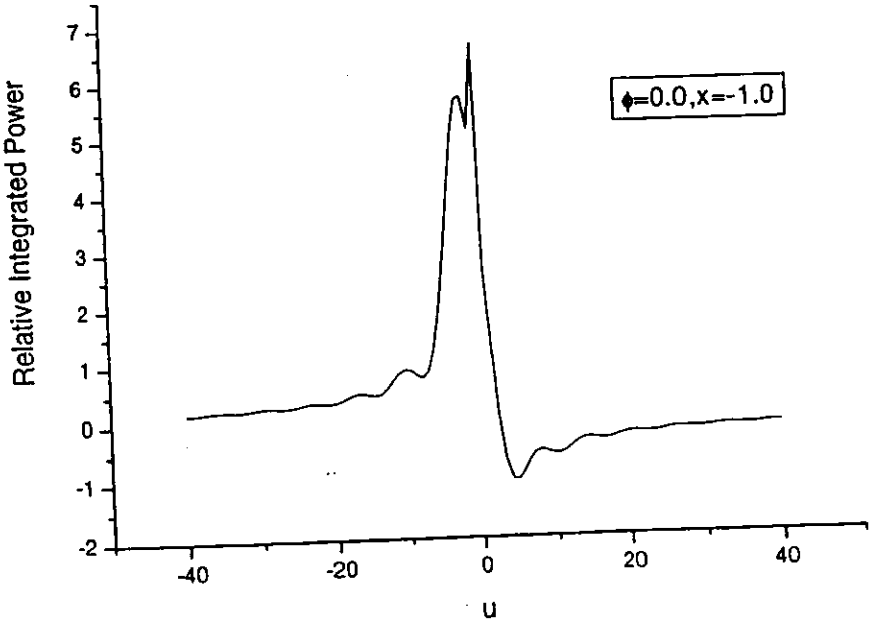

Fig 21 22 Relative integrated power for Unwegenregung and Aufhellung case showing resonance.

Chapter 5

Lattice spacing Measurement : (1) Scheme-1 with monochromator diffraction index $d_1 \neq d_2$ (2) Scheme-2 with monochromator diffraction index $d_1 = d_2$

X-ray optic systems have been developed at beam line BL-3C2 of Photon factory,KEK for the study of the relative lattice spacings of Si-wafers using synchrotron radiation (SR). Since, unlike a X-ray tube, SR has no characteristic [wavelength] spectral lines, a new tool of (+,+) high resolution channel-cut monolithic monochromators (MM) are introduced in the systems as a wavelength selective device. Using two types of MM, two schemes are proposed and applied to the study of the lattice spacings of Si-wafers. The lattice spacing differences are determined in the range of sub ppm level, for example in scheme-1 we obtain 0.6 ppm and 0.2 ppm in scheme-2. One of the practical advantages of this system is that it can be applied for a fast and

precise measurement of the lattice spacing changes due to the doping and defects in Si, GaAs and other single crystals.

5.1 Introduction

Lattice spacing measurements of Si and other single crystals is of importance both for fundamental solid state physics and applications. For decades, especially since Si is routinely used in the semiconductor industry as well as commonly employed in beamline optics of synchrotron radiation facilities and other x-ray experiments. Much of the works on lattice spacing measurement has been reported using well defined wavelength of laboratory x-ray sources [1-8]. In contrast relatively few works have been reported using the state-of the art SR x-ray source [54-56].

Unlike X-ray tube data for which tables of wavelengths of the characteristic spectral lines are available, there are no lines in the synchrotron radiation (SR) spectrum. Thus it demands to make schemes and data available for precise determinations of lattice spacing which utilize the SR source. Thus one of our main motivation is to develop a high precision relative lattice spacing measurement system using SR for synchrotron radiation users. In addition the methods can be applied for other applications, such as for example, the measurement of relative lattice spacing changes due to the Boron [B] doping in Si, B doping in VBG LEC GaAs , As and In doping in GaAs crystals, to mention a few. One of the nice advantages is that these systems do not rely on a high accurate absolute value of wavelength and relative high precision value is sufficient for most of the applications puposes using these systems.

To this end, we have constructed two X-ray optics systems for relative high precision lattice spacing measurement of single crystal using synchrotron radiation at BL-3C2 of Photon factory, KEK. In our new optics energy selective (+,+) channel-cut monolithic monochromator together with higher angle resolution goniometer with a precision of 0.36 arc sec has been introduced. We have designed and fabricated several kinds of MM that give a fixed exit beam position and provide a convenient setting of the whole X-ray optics. With the current set-up it is simple to make another d-spacing measurement, if need be by simply replacing the monochro-

mator with another. In addition to the measurements of Si crystals, measurements for other materials such as GaAs crystals can easily be performed. The monolithic double crystal monochromator is obtained from a single perfect crystal as a means of obtaining an X-ray beam of well defined wavelength. Monolithic monochromator (MM), is in effect a single perfect crystal where two sets of Bragg planes play the role of two seperate crystals. As the interplanar angle between the concerned diffraction plane is fixed in the MM therefore the wavelength emerging from this device is highly stable and is extremely stable against temperature variations. The two types of MM allow us to propose two schemes for the lattice spacing measurement. Approximately, the precision achieved in $\Delta d/d$ in these systems is in the range of 10^{-7} to 10^{-8}. The method has been applied [53,54-57] for the Boron doped Si and B doped VBG LEC GaAs single crystals. From these measurements we can see that the lattice spacing changes can be modelled by Vegard's law. The method can be applied to study the lattice spacing changes due to the doping, defects in the single crystal and further to study photon-phonon energy transfer in inelastic scatteing experiments. The two proposed systems are ready for use at SR facilities.

The layout of this chapter is as follows. In the next section we discuss the MM. This is followed by experimental details of our proposed schemes and the measurements made. We then briefly mention computer control employed in our set-up and applications. Applications will be undertaken in more detail in a later note. Section VI is devoted to results and discussion. Finally conclusions are stated.

5.2 Monolithic Monochromator:

The starting point of monolithic monochromator (MM) design is the Bragg's law. In order to obtain suitable wavelength for experiments from MM, we consider the following three equations:

$$\lambda_1 = \lambda = 2d_1 sin\theta_1(1 - \delta/\sin^2\theta_1)$$

$$\lambda_2 = \lambda = 2d_2 sin\theta_2(1 - \delta/\sin^2\theta_2)$$

$$\theta_1 + \theta_2 + \beta_0 = \pi$$

where δ represents the real part of refraction index and β_0 is the interplanar angle between the two planes, θ_1 and θ_2 are the Bragg angles for two diffraction planes d_1 and d_2 respectively.

(1) Solving the three equations, yields after simple algebra:

$$\lambda = \frac{2d_1 sin\beta_0}{[(\sqrt{(h_2^2 + k_2^2 + l_2^2/h_1^2 + k_1^2 + l_1^2)} - \cos\beta_0)^2 + \sin^2\beta_0]^{1/2}} \quad (1)$$

(2) if $d_1 = d_2 = d$ Eq. 1 further reduces to :

$$\lambda = \frac{2d\sin\beta_0}{[(1 - \cos\beta_0)^2 + \sin^2\beta_0]^{1/2}} \quad (2)$$

Using Eqs. 1 and 2 a simulation code MMCD [Monolithic Monochromator Crystal Design] has been realized which can generate different wavelengths using (h_1, k_1, l_1) and (h_2, k_2, l_2) combinations . Our code relies on the Deslatte's [28] lattice spacing of silicon wafer of $d_{220} = 1.9201715 \pm 0.0000006$ angstrom at 25^0C.

Two types of Monolithic monochromator [MM] have been designed and fabricated on the basis of Eqs. 1 and 2. These are notated by Type-1 and Type-2. Type-1 is used in the experimental set-up, refered to as scheme-1 and similarly Type-2 is utilized in the set-up called scheme-2.

Figs. 1 and 2 show the MM that have been made for the wavelength defined by Eqs. 1 and 2 respectively. Some of the simulated wavelengths from MMCD code is given in Table I for both types of MM with refraction correction δ, given by $\delta = 4.48 \times 10^{-6} n_0 \lambda^2$. Here n_0 is the number density, for example for Si $n_0 = 699nm^{-3}$, and λ is the wavelength of x-rays.

For illustration, we reproduce the following two examples here:

1. Type-1: MM diffraction planes $d_1 \neq d_2$, wavelength $\lambda = 0.1410846$ nm
   This monolithic monochromator has been made using the reflection indexes (1,1,7), (1,5,1),(-1,-1,-7),and (-1,-5,-1)which is an implementation of equation (1). The motivation behind for fabrication of this monochromator is to study the d-spacing of Si as well as GaAs(800) single crystal. As the high Bragg angle provides high precision therefore we found the above indexes from the MMCD code provides 86.5 degree for GaAs(800) sample. Table II represents some of the monochromator wavelengths that we have made together with their design parameter.

2. Type-2 MM diffraction plane $d_1 = d_2$, wavelength $\lambda = 0.1612607$ nm
   This monochromator has been designed having same Bragg angle for $(h_1, k_1, l_1)$and (h_2, k_2, l_2), the index being used are (5,1,3) and (1,5,3), which is an implementation of equation (2). The reason of choosing this wavelength and these indexes originates from the advantage of precision lattice spacing measurement for Si. Conventional Bond method usually provides high precision value but we need a rotation of the sample in the Bond method. If we choose (5,1,3) and (1,5,3) indexes of the samples and wavelength 0.16126 nm we can achieve quasi-simultaneous diffraction instead of rotation of the sample and thus the effect of temperature will be smaller, measurement time will be shortened and more precise data than conventional Bond method at room temperature can be obtained.

5.2.1 Resolution provided by the Monolithic Monochromator

The FWHM of the reflecting range of MM is determined by the dynamical theory of diffraction and is given by :

$$\Delta\theta = 2C\chi_g(\gamma_g/\gamma_0)^{1/2}/\sin 2\theta_B$$

$$\chi_g = -\gamma_e\lambda^2 F_h/\pi V_c$$

where γ_e is the classical electron radius, F_h is the atomic structure factor, V_c is the volume of the unit cell, λ is the wavelength C is the polarization factor, it is 1 for σ polarization and $\cos 2\theta_B$ for π polarization. We note that $(\gamma_g/\gamma_0) = 1$ for symmetric reflection. The energy resolution is given by

$$\Delta E/E = cot\theta\Delta\theta$$

As an example of MM designed for wavelength 0.1410846 nm , calculated angular divergence and wavelength spreads are given by: $\Delta\lambda/\lambda = 2.5 \times 10^{-6}$ and $\Delta\theta = 8 \times 10^{-6} rad$. All monochromators were well characterized in terms of their throughput, wavelength and angular resolution. The experiment was carried out at beamline BL-3C2 [26,27] which is located at the Photon Factory's 2.5 GeV ring.

5.2.2 Synchrotron x-rays

As is well-known some of the advantages of SR compared to conventional x-ray generator tubes are, higher intensity, the wavelength selectivity and well-colliminated beam. Many devices have and are being developed to further increase the intensity such as wigglers and undulators and x-ray FEL's. We used the standard bending magnet radiation which gave at least an order of magnitude higher intensity and better resolution than the X-ray tube. The much higher statistics and lower background obtained with SR are important factors in precision measurements. The

question arises as how to extract exact values for wavelength. For x-ray tubes there is a guiding principle, since tables of wavelengths of the characteristic spectral lines are readily available. In contrast there are no lines in the SR spectrum. Only the absorption edges of elements in the speciman or of thin foils placed in the beam can be measured. The accuracy of such measurements is not as high as desired because of the uncertainty as to what feature of the edge should be used as a measure of wavelength.

The wavelength problem could be avoided by using the ratio of the lattice parameters of the specimen to an accurately known standard. The limitation is of course the accuracy of the standard. A discussion of the extraction of standard for exact wavelength determination will be discussed elsewhere. For the purpose of current work we limit our discussion to the following: For determination or the callibration of wavelength we use FZ Si(444) as a reference, which is oxygen free and the lattice parameter change has been determined to about 2×10^{-8}. The callibration was performed before and after a series of experiments and no change was detected, showing the stability of our measurement technique. The wavelength was callibrated by using an FZ silicon wafers of

5.3 EXPERIMENTAL

5.3.1 Measurement of lattice spacing of Si -wafers single crystals

Scheme-1 with Type-1 MM diffraction planes $d_1 \neq d_2$

This scheme is a modification of the Bond method with MM X-ray optics. We have carried out an experiment for the precision lattice spacing measurement of Si using SR from bending magnets. Fig. 3a shows the schematic diagram of the

experimental set-up. The novelty of the scheme is that we can replace the MM and sample in each experiment. Several experiments have been carried out using the above scheme. We describe here the case where MM of wavelength 0.1410846 nm , and sample Si(444) FZ are used. The experiments for the other cases i.e. with different MM wavelengths follows the almost same procedure and only the results will be reported. As can be seen in Fig. 3a a channel-cut MM has been introduced using the geometry of successive lattice planes (1,5,1) and (1,1,7) and a wavelength of 0.1410846 nm was obtained. In the experimental scheme of Fig. 3a, SR x-ray beam from the channel-cut monochromator is diffracted from a sample crystal Si(444) at a crystal angle W1 (diffraction maxima) into detector PIN #1 of left side. The same Bragg reflection is also observed at a crystal position W2 (diffraction maxima) with a detector PIN #2 of right side. The change in crystal angle $(180 - 2\theta_B)$ is independent of the goniometric errors and now one can obtain the Bragg-angle using the Bond formalism [47]. Necessary tilt adjustment both for channel-cut crystal and sample crystal has been made. The center of the goniometer, holding the sample Si(444) fixed was adjusted by taking X-ray photos so that the center of the beam from the monochromator will hit the center of rotation axis of the goniometer. We also used the laser (He-Ne) beam to adjust the beam height and position. A rotary encoder with a digit of 0.36 arcsec were used to record the W1 and W2 values.

An automated computer system has been installed to run the experiment and to store the data, see below, section IV. Table III shows the W1 and W2 values for Si(444). The average value for 9 measurements of a Si-wafer is reported as $d_{obs} = 0.078390564nm \pm 3 \times 10^{-8}$ at 25^0C. The average $\Delta d/d$ was obtained as 6.2×10^{-7} calculated from d(cal) and d_{obs}. The results of $\Delta d/d$ for Si FZ, and GaAs(800) samples are reported in Table IV.

Scheme-2 with Type-2 MM diffraction planes $d_1 = d_2$

In this Scheme a two equivalent lattice planes have been chosen for the sample for a particular wavelength, thus providing the two almost simultaneous diffraction with a few arc sec rotation of the sample. The scheme of the system is shown in Fig-4a. In this scheme, a monolithic monochromator (MM) of 4-reflection type having $d_1 = d_2$ diffraction planes has been introduced as a fixed wavelength device. A monolithic monochromator that uses (5,1,3),(1,5,3),(-5,-1,-3),(-1,-5,-3) reflections has been made from channel-cut Si-crystal grown along [1,1,1] direction provides the wavelength of $\lambda = 0.16126nm$ The wavelength 0.16126nm satisfies the simultaneous Bragg condition for the indexes (5,1,3), (-5,-1,-3),(1,5,3),and (-1,-5,-3). The Bragg angles for both indexes is 61.4392 degree and the interplanar angle is 57.1216 degree. In this set up MM crystal faces are arranged in a (+,+,-,-,) dispersive setting. The four crystal faces of the monochromator are the inner faces of channel-cut crystals of Si. The method has been applied for the d- spacing of FZ Si wafer measurement, the sample index was choosen being the (5,1,3) and (1,5,3) which provides the same Bragg angle. The sample was selectecd Fz Si orientation flat of 110, normal direction of 111. When a x-ray beam of wavelength 0.16126 nm is projected on the sample along 111 direction, Bragg conditions for (5,1,3) and (1,5,3) is satisfied and thus we observed the two diffraction simultaneously. The measured Bragg angle is determined by geometry of the experiment and is given by $\theta_B = 90^0 - \beta_0/2 - D$, where D is the peak difference between the two rocking curves (5,1,3)and (1,5,3) [Fig 4b]. For two such measurements $\Delta\theta \propto \Delta D$, thus ΔD is a direct measure of change in relative lattice spacing from the differential of the Bragg's law $\Delta d/d = -cot\theta\Delta\theta$.

5.3.2 Assymetry:

In order to incorporate the refraction and assymetry the additional term to the Bragg angle can be written more explicitly by the formula

$$\theta_{Assym} = 90^0 - \beta_0/2 - \delta/4[2 + 1/b + b] - D$$

where b is the assymetry factor. In another form in terms of small correction (ϵ) due to the assymetry arises from the miscut can be written as $\epsilon = \frac{\delta}{sin2\theta_b}[1+sin\theta/sin(2\theta_b - \theta)]$ where θ and θ_b are glancing angle of incidence and Bragg angle.

In this experiment the polarization of the SR is choosen as horizontal and the diffraction plane is chosen vertical. Two goniometers has been used for the monochromator and sample crystal. The axis of the goniometer has been adjusted perpendicular to the x-ray beam by laser. The goniometer containing the MM has two tilt axis, one parallel to the first diffraction plane and the other is perpendicular to the plane. Fig 4c shows the Photographic view of the Scheme. In our system several thermistor probes were used for temperature measurement both at MM and at sample. The entire experimental hutch was covered by the Styler foam, and the temperature fluctuation was controlled to within $\pm 0.01^o$ C. Refraction correction has been taken into account to d with $\delta = 4.48 \times 10^{-6} n_0 \lambda^2$, where $n_0 = 699 nm^{-3}$ for Si. The measured d_{153} value in our experiment on the average was 0.091801632 nm$\pm 2 \times 10^{-8}$.

5.4 Computer control:

An automated computer system has been installed to run the experiment and to store the data. During the measurement, the computer automatically drove pulse motors for the goniometers, counted x-ray intensities, and saved data in the memory. The block diagram for the control system is shown in Fig 6. In this system 8 motor control system has been used to run the MM and sample goniometer stage and

several GPIB interface has been used to run the beam line optics and experimental optics. Multimeter and pico-ammeter is used to record the intensity from PIN photodiode. Two 16 channel pulse motor controller system connected with motor driving system which are further connected to several goniometer stage holding the sample (GMS) and monochromator stage (GMM). Therefore sample scanning and MM setting are controlled from outside the hutch. Temperature controlled system has been developed to monitor the temperature by 7015 multiplexer coupled with 2000 multimeter. Fig 5 shows one of the temperature record before and after the lattice spacing measurement as an example . Ten temperature probe has been installed to monitor the temperature at MM, at sample and at various position of the hutch. The entire hutch was covered by the styler form . Further vibration spectrum has been recorded by Fourier spectrometer. Fig 8 shows the spectrum when the accelerometer sensor is placed on the sample goniometer stage and Fig. 9 shows the spectrum when the sensor is put on the sample holder during the goniometer movement by motor, we observed from the both spectrum that there is no significant changes, the peaks are due to the a.c line signal in the experimental hutch, thus the lattice spacing values are error free.

5.5 Applications

Applications of the methods for lattice spacing changes to Boron doped Si and VBG LEC GaAs crystals have been reported elsewhere [53], the results demonstrate that the lattice spacing changes can be modelled by $\Delta a = a_0 \times (r_i - r_s)/r_s \times (N_i/N_s)$ where r_i and r_s are the radii of impurities and silicon atoms respectively and N_i andN_s are the concentration of impurities and silicon. This is in good agreement with Vegard's law. Further, several new states has been observed in addition to the Vegard's states in case of B doped VBG LEC GaAs crystal . The presented methods are useful in the study the lattice spacing changes induced by the defects,

and doping in single crystals. Moreover, it is possible to study phenemenon such as photon-phonon energy transfer in inelastic scattering due to the high resolution x-ray optics, used in the current set-up. A more detailed discussion of the applications of the mentioned methods will be discussed elswhere.

5.6 Results and Discussion

As mentioned above, two relative lattice spacing measurement methods using two types (i.e scheme-1 and scheme-2 based respectively on the diffraction plane conditions $d_1 \neq d_2$ and $d_1 = d_2$) of (+,+) energy selective MM with SR have been developed. Results of the two schemes are summarized in this section.

In scheme-1 we applied our method to several MM, as shown in Table III and Table IV. The novelty of the method is that in each case MM and sample can be changed. For the Si sample grown by FZ and for the plane (444) a MM wavelength of 0.1410 nm is utilized. Fig. 3b shows the pair of diffraction curves for this case. The results for this case are summarized in Table III. Nine measurements were taken at different position of Si wafer and the corrected d values are listed. The average value of $\Delta d/d$ is 6.2×10^{-7} as mentioned before. Table IV shows the results of our lattice spacing measurement for Si grown by CZ, and FZ methods where the planes (800) and (444) are considered in addition to GaAs grown by CZ method for the plane (800). We can see that the average value of $\Delta d/d$ is higher for GaAs compared to that of Si. Temperature and refraction corrections have been taken into account. For scheme-1 several temperature probes were installed at sample and MM. The true value of d is given by $d_{obs} + \Delta d_r + \Delta d_t$, where Δd_r and Δd_t are the refraction and temperature corrections respectively. The refraction correction is calculated for wavelength .1410 nm as $0.0000019\mathring{A}$ and temperature correction was $0.000006\mathring{A}$ to the d-value. The calculated d -value has been taken at 25°C from Deslattes [28]; the measured d_{444} value obtained on the average from nine measurement points is

0.078390564 nm $\pm 2 \times 10^{-8}$.

In scheme-2 two equivalent planes and a few arc sec rotation (D) of the samples provide two quasi-simultaneous Bragg diffraction. This method is fast. Several scans were performed for a Si wafers prepared with FZ method and two diffraction profiles were recorded from the (5,1,3) and (1,5,3) planes. Fig. 4b shows this scheme with pair of diffraction from the (5,1,3) and (1,5,3) planes. Fig. 6 shows the results of seventy measurements taken at different positions of Si(153) FZ prepared wafer. From this graph we can see that the approximate average value of $\Delta d/d$ is 1.1×10^{-7}. Temperature variation has been carefully monitored. For scheme-2 several temperature probes were installed at sample and MM. The true value of d is given by $d_{obs} + \Delta d_r + \Delta d_t$, where Δd_r and Δd_t are the refraction and temperature corrections respectively. The refraction correction is calculated for wavelength .16126 nm as 0.00000749$\AA$ and temperature correction was0.00000291$\AA$ to the d-value. The calculated d -value has been taken at 25°C from Deslattes. The measured d_{153} value obtained on the average from seventy measurement points is 0.091801632 nm $\pm 2 \times 10^{-8}$. As Fig. 10 shows for 70 measurement the $\Delta d/d$ obtained from ΔD is within 0.2 ppm level. The standard deviation calculated from 100 measurement of differential peak difference D at one point was 2×10^{-8}.

5.7 Conclusions

In conclusion keeping in mind the unique features of SR such as high intensity, tunability, high resolution d-spacing 2-measurement systems have been developed at Photon factory, KEK and successfully operated and tested. The system can be used in a routine d-spacing measurement of Si and other single crystals with a precision of 10^{-7} to 10^{-8}. Both systems are inexpensive and each measurement takes only few tens of seconds. The accuracy of the both methods is determined by the tilt adjustment of the MM, geometric misalignment, peak determination of the profiles

and the fluctuation of the wavelength and the stability of SR. In scheme-2 we have demonstrated a method for Si lattice spacing measurement which only requires few arc sec rotation of the sample thus bypassing the larger rotation [on the order of few degrees] of the sample required in the conventional Bond method. As the two pair of diffractions occur almost simultaneously, therefore each measurement takes only few seconds. Thus our new system is speedy, accurate and highly stable. The method is suitable for improving the accuracy of measuring the lattice parameter, which in turn is needed for the determination of the exact wavelength used. The applications of the methods for lattice spacing changes to Boron doped Si and VBG LEC GaAs crystals have been reported elsewhere [9,10,12]. The results demonstrate that the lattice spacing changes can be modelled by $\Delta a = a_0 \times (r_i - r_s)/r_s \times (N_i/N_s)$where r_i and r_s can be regarded as a radius of impurities and silicon atoms and N_i andN_s are the concentration of impurities and silicon. This is in agreement with Vegards law. Further, several new states have been observed in addition to the Vegard's states in the case of B doped VBG LEC GaAs crystal . The presented methods open up a new direction in the solid state research, in particular to the study of changes in the lattice spacing due to the defects, and doping in single crystals.This is made possible due to the high resolution x-ray optics used in the set-up described here.

It is hoped that the method can be applied in a wide variety of application in the condensed matter research especially where high resolution is of prime importance.

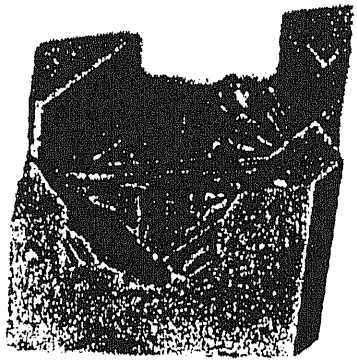

Figure 1
Type 1 monolithic monochromator designed for a wavelength of 0.1410 nm with index $(1, 5, 1)$, $(1, 1, 7)$, $(\bar{1}, \bar{5}, \bar{1})$, $(\bar{1}, \bar{1}, \bar{7})$.

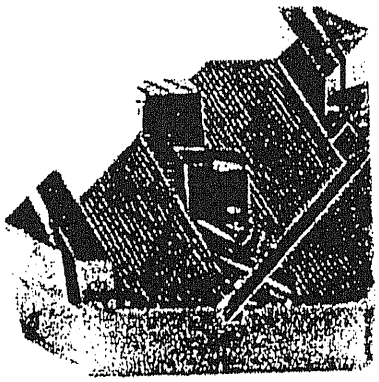

Figure 2
Type 2 monolithic monochromator for a wavelength of 0.1612 nm with index $(5, 1, 3)$, $(1, 5, 3)$, $(\bar{5}, \bar{1}, \bar{3})$, $(\bar{1}, \bar{5}, \bar{3})$.

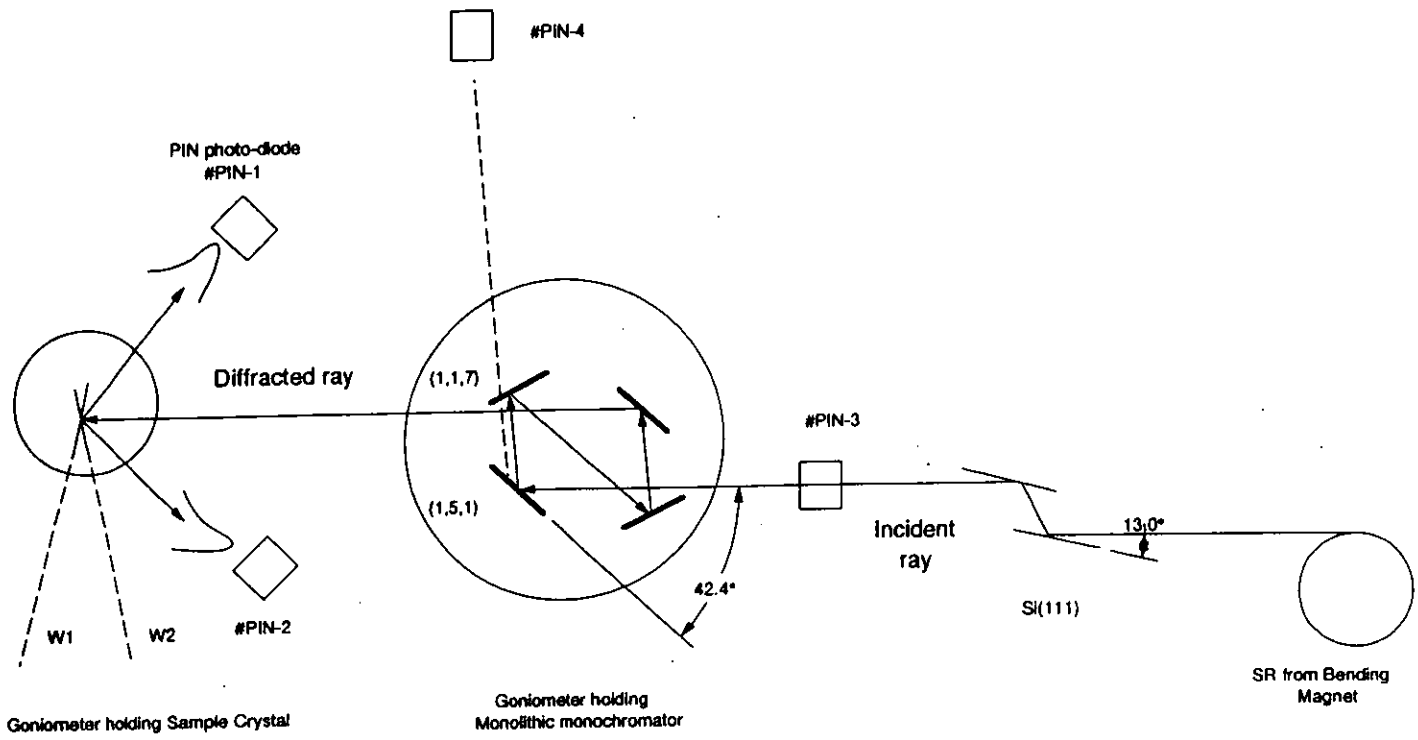

Fig 3a Scheme-1 SR from BM with MM 0.1410nm and sample Si(444)

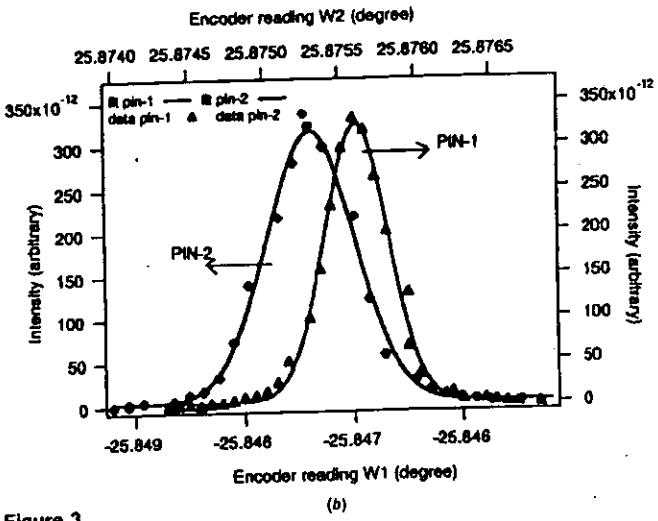

(b)

Figure 3
(*a*) Scheme 1: SR from the bending magnet incident on the Si(111) double-crystal monochromator and, after four reflections from the MM (0.1410 nm), impinges on sample Si(444). Two diffractions are recorded at the PIN #1 and PIN #2 detectors. *W*1 and *W*2 values are recorded using a Heiden heigh encoder. (*b*) Pair of diffraction curves observed in scheme 1 from the Si +(444) and −(444) planes.

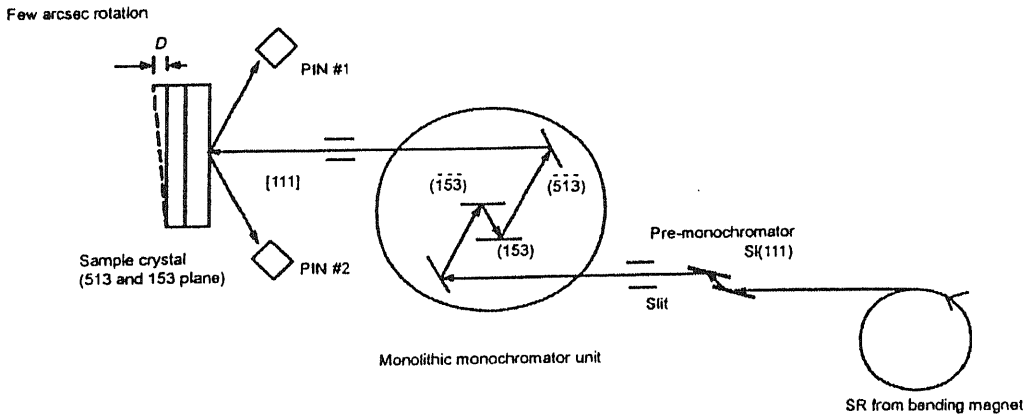

(a)

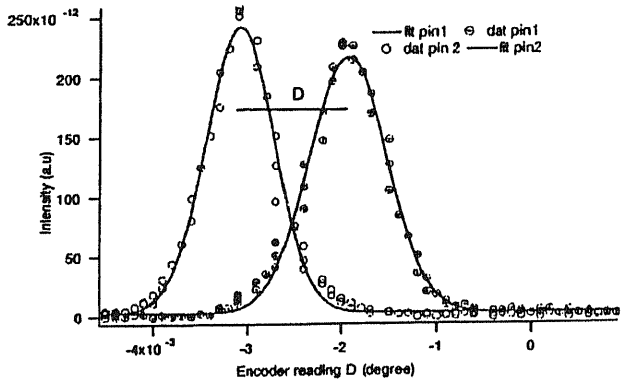

(b)

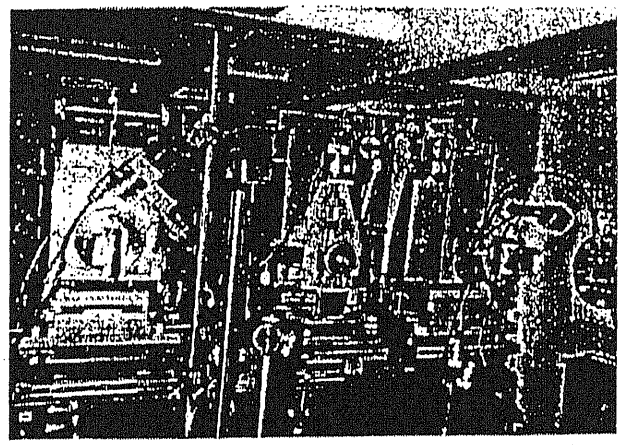

(c)

Figure 4
Scheme 2: SR from the bending magnet incident on the Si(111) double-crystal monochromator and, after four reflections from the MM (0.1612 nm), impinges on sample Si(153). Two diffractions are recorded at the PIN #1 and PIN #2 detectors. The differences between the two peaks' *D* values are recorded using a Heidenheigh encoder. (*b*) Pair of diffraction curves observed in scheme 2 from the Si (513) and (153) planes. (*c*) Photographic view of scheme 2. A goniometer near to the beam port is used for the MM with two tilt stages; a third goniometer is used for the Si(153) sample wafer; two PIN detectors are set to record the two quasi-simultaneous diffractions.

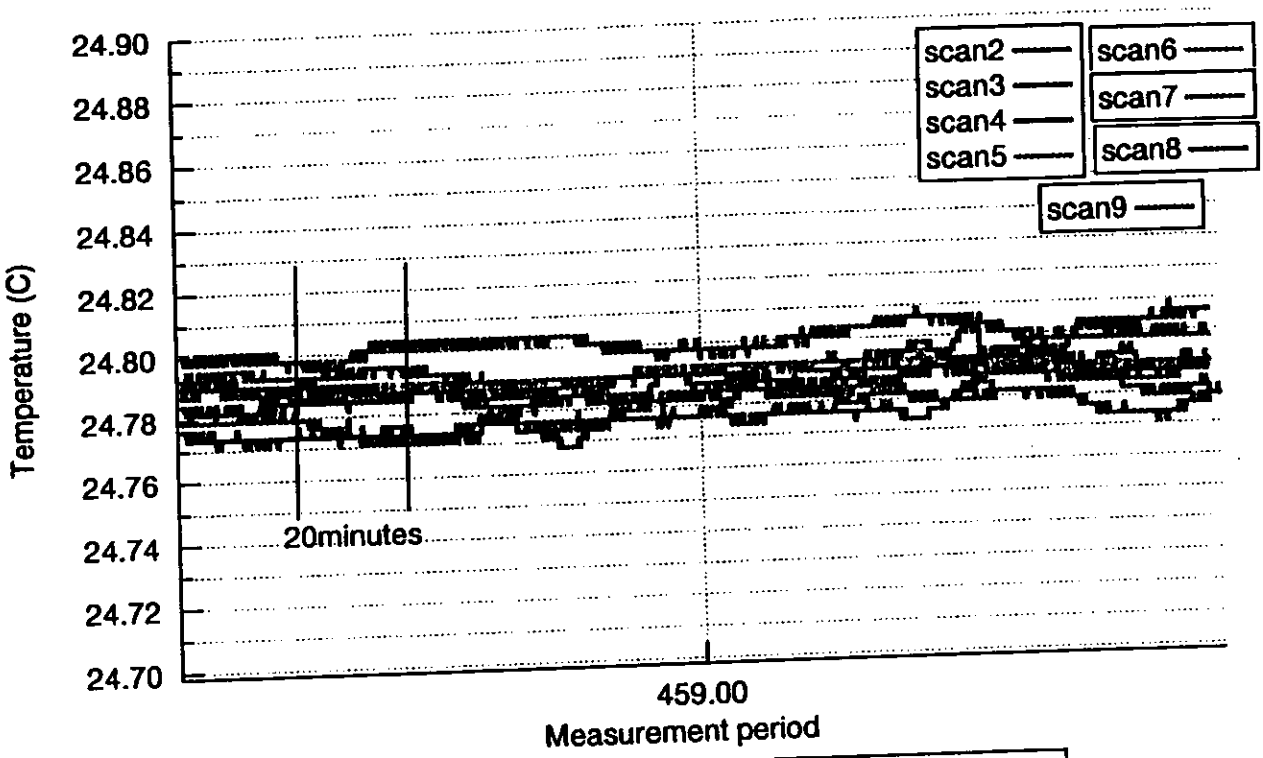

Fig 5 Temperature record during various scan

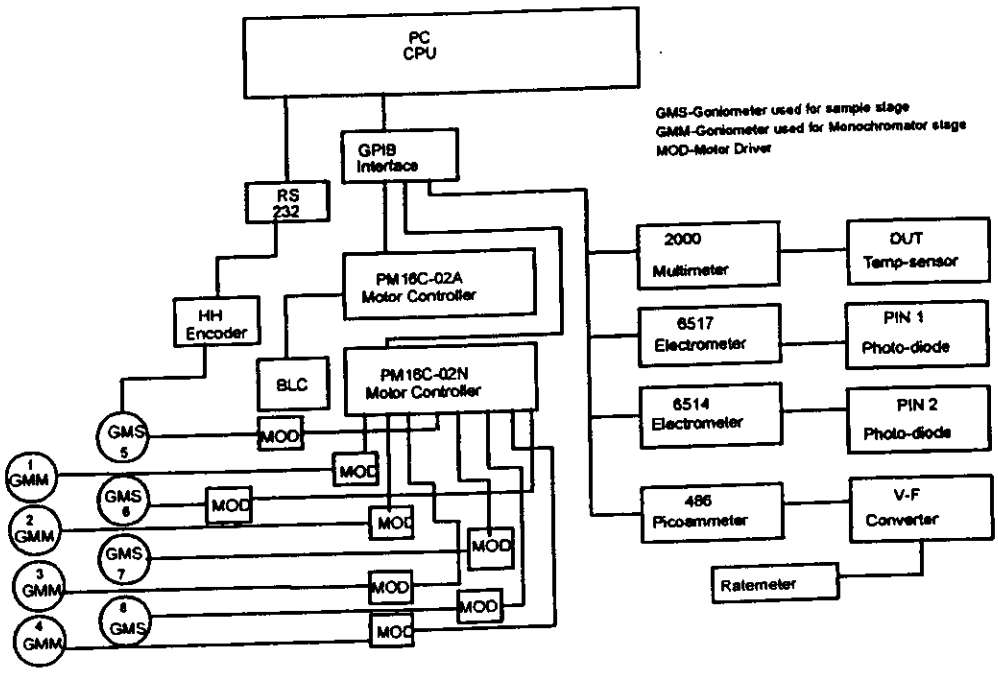

Figure 6
Computer-controlled block diagram for the relative lattice-spacing measurement system.

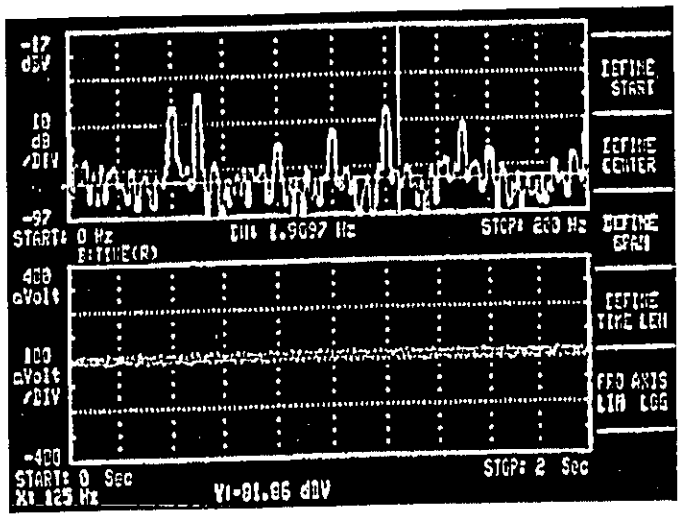

Figure 8
Vibration spectrum in db when the accelerometer sensor is placed on the sample stage of the goniometer. The peak signals are due to the line signal in the hutch.

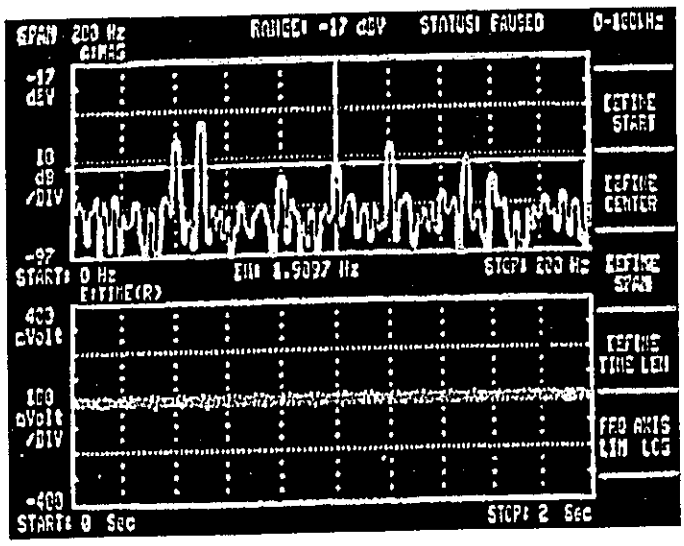

Figure 9
Vibration spectrum in db when the accelerometer sensor is placed on the sample holder. The peak signals are due to the line signal in the hutch.

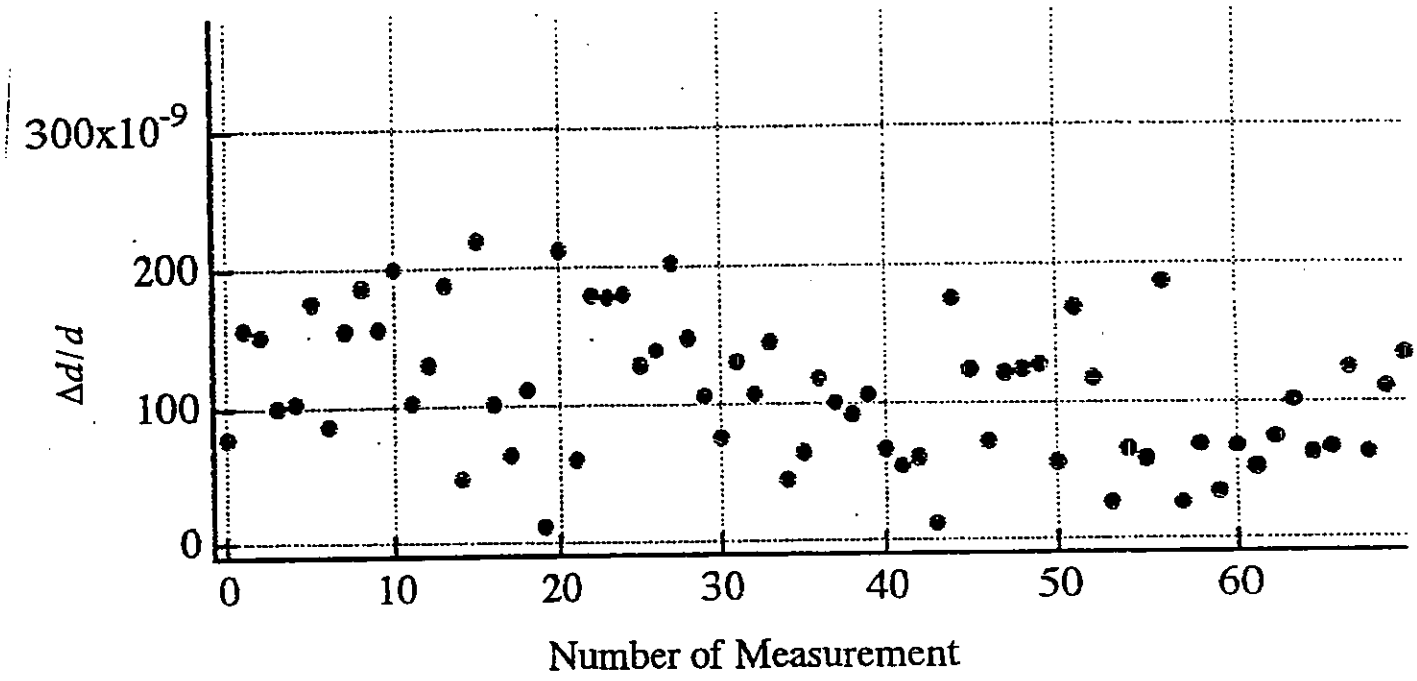

Figure 10
The relative lattice-spacing changes for 70 measurement points of an Si(153) wafer. The precision is within 0.2 p.p.m.

Table I. Type-1 different indexes, MMCD Code generated wavelengths

$h_1k_1l_1$	$h_2k_2l_2$	HKL	β_0	θ_1	θ_2	λ	δ
1 5 5	-5 3 1	-4 8 6	69.2044	63.1437	47.6519	1.356950	.57719E-05
3 5 5	-3 3 1	0 8 6	70.8196	75.8031	33.3772	1.370938	.58915E-05
3 3 5	-3 5 1	0 8 6	73.5280	57.1730	49.2990	1.391940	.60734E-05
1 1 3	-5 -3 5	-4 -2 8	74.0515	25.2230	80.7255	1.395642	.61057E-05
1 1 3	-3 -5 5	-2 -4 8	74.0515	25.2230	80.7255	1.395642	.61057E-05
1 5 5	5 1 5	6 6 10	46.6641	66.6680	66.6680	1.396621	.61143E-05
1 1 3	-5 3 1	-4 4 2	104.7631	25.3769	49.8599	1.403594	.61755E-05
3 5 5	1 5 -1	4 10 4	54.8119	83.0088	42.1792	1.403614	.61757E-05
1 1 5	1 1 7	2 2 12	42.4407	68.3502	69.2091	1.410846	.62686E-05

Table II. Type-2 same indexes, MMCD Code generated wavelengths

$h_1k_1l_1$	$h_2k_2l_2$	HKL	β_0	θ_1	θ_2	λ	δ
1 3 5	3-5 -1	4 -2 4	119.0593	30.4704	30.4704	.931039	.27172E-05
3 5 5	-5 -3 5	-2 2 10	94.8614	42.5693	42.5693	.956631	.28686E-05
1 3 5	5 -1 -3	6 2 2	111.8037	34.0981	34.0981	1.029302	..33210E-05
3 3 5	-3 5 -3	0 8 2	102.0815	38.9593	38.9593	1.041527	.34004E-05
1 5 5	-1 -5 5	0 0 10	91.1235	44.4382	44.4382	1.064914	.35548E-05
1 3 5	-5 -3 1	-4 0 6	104.9006	37.5497	37.5497	1.118970	.39249E-05
1 5 5	-5 5 -1	-4 10 4	72.8954	53.5523	53.5523	1.223493	.46924E-05
3 3 5	-3 -3 5	0 0 10	80.6311	49.6854	49.6854	1.263037	.50006E-05
1 3 5	-5 3 -1	-4 6 4	91.6373	44.1814	44.1814	1.279591	.51325E-05
1 5 5	5 5 1	6 10 6	46.6641	66.6680	66.6680	1.396621	.61143E-05
1 3 5	-3 5 -1	-2 8 4	78.4630	50.7685	50.7685	1.223493	.46924E-05
3 3 5	-3 -3 5	0 0 10	80.6311	49.6854	49.6854	1.422186	.63402E-05
1 1 5	-1 5 -1	0 6 4	92.1226	43.9387	43.9387	1.450516	.65953E-05
1 3 5	-1 -3 5	0 0 10	64.6231	57.6885	57.6885	1.551732	.75479E-05
1 3 5	5 3 1	6 6 6	57.1216	61.4392	61.4392	1.612607	.81517E-05

Table III. Monochromator made with some of their design parameter.

Diffraction Planes	Bragg-angles $\theta_1, \theta_2 (deg)$	Wavelength (nm)	L×B × H (mm)	Beam gap (mm)	$\Delta\lambda/\lambda$ ($\times 10^{-6}$)	$\Delta\theta$ ($\times 10^{-6}$)
(5 9 11),(7 -7 -7)	74.30; 50.77	0.0694067	45×40 × 40	7	0.5	1.6
(3 3 -3),(-3 -5 -3)	47.53; 68.58	0.1542067	55×52 × 50	29	2.8	9.2
(1 5 1),(1 1 7)	42.44; 68.06	0.1410846	35×42 × 35	15	2.5	8.7
(5 1 3),(1 5 3)	61.43; 61.43	0.1612607	60×55 × 37	35	4.3	0.1
(1 5 5),(-5 3 1)	62.78; 47.65	0.1352569	40×30 × 35	0	2.3	6.2

Table IV. Relative lattice spacing for wafer sample Si(444) with 0.1410 nm wavelength MM.

Measurement No	Left Peak W1 (degree)	Right Peak W2 (degree)	Difference W1-W2(degree)	d- value corrected (nm)	Average $\Delta d/d$ ($\times 10^{-7}$)
1	215.3518	163.6417	51.7101	0.078390514	
2	215.3526	163.6419	51.7107	0.078390713	
3	215.3516	163.6409	51.7107	0.078390713	
4	215.3525	163.6412	51.7113	0.078390912	
5	215.3525	163.6418	51.7107	0.078390713	6.2
6	215.3514	163.6428	51.7186	0.078390017	
7	215.3514	163.6410	51.7104	0.078390613	
8	215.3514	163.6423	51.7191	0.078390173	
9	215.3518	163.6411	51.7107	0.078390713	

Table V. Relative lattice spacing values measured using scheme-1 for Si and GaAs sample.

Sample No	Sample Type	Sample index	MM wavelength (nm)	Average $\Delta d/d$ ($\times 10^{-7}$)
Si	FZ	(444)	0.1542	6.1
Si	CZ	(800)	0.1356	6.3
GaAs	CZ	(800)	0.1356	8.0

Chapter 6

Lattice spacing Measurement in GaAs(800)

6.1 Introduction

GaAs Crystals are heavily used in the semiconductor technology for IC and LSI circuits, therefore it is of great importance to understand its properties and structure. Since the crystal consists of Ga and As elements therefore it is difficult to growth the crystal uniformly . Lattice spacing is a non destructive measure to study the properties and quality of the GaAs crystals by which we can get the microscopic insight of the crystals [58,74].

6.2 Experimental arrangement

The experimental system is developed using the scheme-1 previously. The beam line covered the X-ray range 4-25 KeV X-ray . The Experimental hutch was covered by styler foam and thus thermally shielded . A steel base plate with a size of $1260 \times 1660 mm^2$was installed in to the hutch where two Kohzu type Goniometer

was put, one for the monochromator and the other for the sample. The Synchrotron radiation (SR) was introduced into the room. A beam height of 600 mm above the plate was obtained by adjusting all optical components. This was performed to a precision of 50 μmeter by taking x-ray pictures and using He-Ne lasers. This corresponds no error in the present lattice spacing measurement system. For further temperature control, fluorescent lamps were installed outside the ceiling of the hutch. The legs of the base plate were insulated by wooden plates from the floor and the inside hutch was completely thermally shielded. The SR is projected first onto a high precision monolithic monochromator (MM) and after 4 times of reflections it impinges on the sample. Prior Si(111) double crystal monochromator (DCM) was used to avoid the heat loading onto the monochromator.

6.2.1 Experiment with MM 0.1410nm wavelength

In this arrangement a channel-cut monolithic monochromator has been introduced in order to obtain valuable stability and a very narrow bandwidth of SR x-rays . This is achieved through the channel shaped MM using the geometry of successive lattice planes (151,117) and a wavelength of 0.1410 nm was obtained. By using the geometry of successive reflections, a highly collimated beam with a narrow band width was produced. Its angular divergence and wavelength spread is described previously. The X-ray beam from the monochromator was monitored by the PIN photo-diode whose current was in the pico-amp range. The centre of the sample goniometer was adjusted by taking X-ray photos and with the help of laser beam so that the beam from MM heat the centre of the rotation axis. A Rotary encoder Heidenhein with a digit of 0.36 seconds of an arc was used in the sample goniometer. On the table of a sample goniometer, translational stage was mounted so that the sample can moved in x, y and z direction. The sample was 20mmx20mm GaAs wafer and was mounted vertically on a Aluminium holder. All the angular position

of the goniometer and linear positions of horizontal and vertical stages are readable in the computer. The X-ray diffraction from the sample was monitored by PIN photo-diode.

In the experimental schme, SR X-ray beam from the channel-cut monochromator [54]is diffracted at a crystal angle W1(peak position) into detector PIN of left side. The same Bragg reflection is also observed at a crystal position W2(peak position) with a detector PIN of right side in the scheme -1. The change in crystal angle ($180-2\theta_B$) is independent of the goniometric errors and now one can obtain the Bragg-angle using the Bond formalism [47] $\theta_B = [180 - (W1 - W2)/2]$.We monitored the SR X-ray from the channel-cut crystal by anPIN detector . Ncessary tilt adjustment both of channel-cut crystal and sample crystal has been made. The centre of the goniometer ,holding the sample was adjusted by taking X-ray photos so that the centre of the Monochromator beam will hit the centre of rotation axis. A rotary encoder with a digit of 0.36 arcsec were used to record the W1 and W2 values.

6.3 MM of 0.1410nm Setting

The MM with wavelength 0.141 nm is shown in Fig-1 . The MM uses the index of (151) and (171) and their conjugates, the Bragg angles for them are 42.4 and 68.1 degrees respectively and thus the wavelength transmitted by the MM was 0.1410846nm. The wavelength was set by tilting the MM cross tilting stage of the goniometer and the MM was set at its maximum wavelength, the wavelength has a double check once by the tuning of a Si(111) downstream monochromator and later by Bond method without MM and further fine tuning after the installment of MM and recording the consecutive diffraction from 1st and 4th diffraction plane of MM recorded by PIN detector. Experiments were carried out using some of the MM, such as 0.141nm MM and sample and 0.135nm MM and GaAs(800) samples. The novelty of the method is that in each case MM and sample can be changed.

We applied A monochromatic beam with wavelength $\lambda = 0.135659nm$, after 4 times of reflection projected onto the sample. The X-ray beam size of approximately $1mm \times 1mm$ locates on a sample crystal surface. Using this system, precise lattice spacing measurements of GaAs single crystals were carried out , samples (800) specimans were put on a precision goniometer. .Bragg angles of GaAs(800) was 86.5 degrees.

Fig 2, 3,4 shows the pair of diffraction in the method from sample crystal GaAs(800) . Relative lattice spacing have been measured by measuring the differencec in bragg angle using the differential Bragg's law $\Delta d/d = -cot\theta\Delta\theta$. Fig 5 shows shows experimental scan fitting well with the theory. Fig 6 shows the variation of the measured Bragg-angle , both for CW and CCW motion of the goniometer.

6.4 Results and discussions

We have achieved the both relative and absolute measurement of GaAs (800) lattice spacing, the estimated $d(800) = 0.0706584nm \pm 2 \times 10^{-6}$ and relative lattice spacing have been measured by measuring the differencec in bragg angle using the differential Bragg's law $\Delta d/d = -cot\theta\Delta\theta$. Relative lattice spacing values are 2 parts per million. Using the described scheme, defects in GaAs can be studied and the method can be applied for other condensed matter research especially where high resolution is of prime importance.

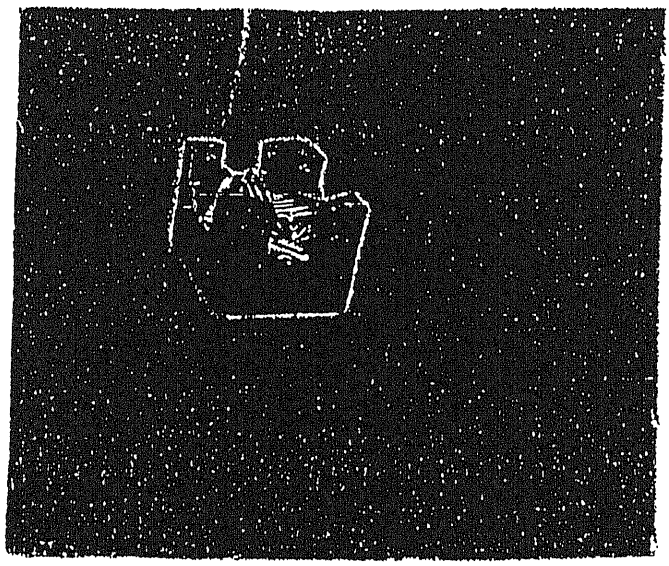

Fig 1 Type-1 Monochromator designed for wavelength 0.1410 nm

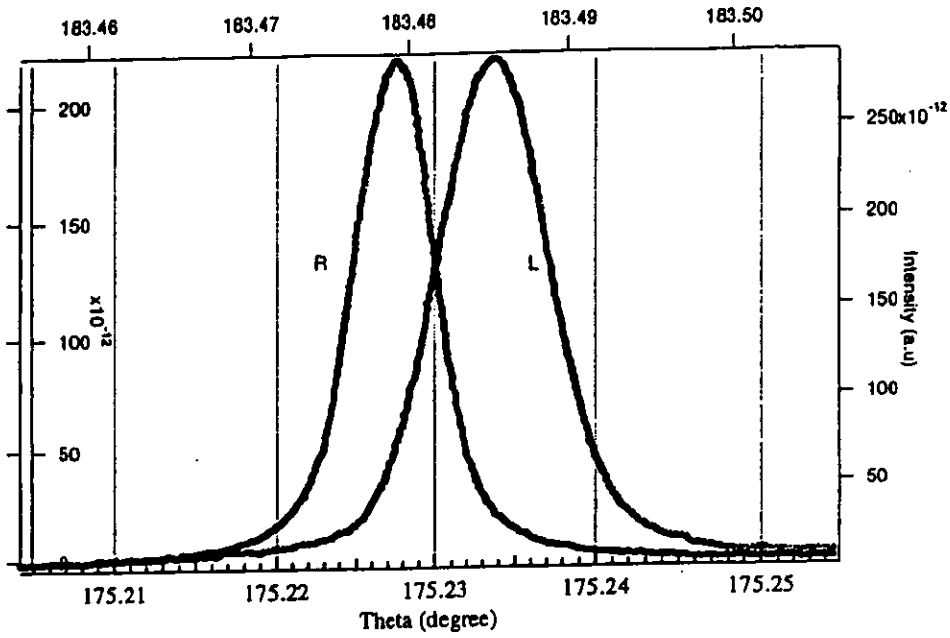

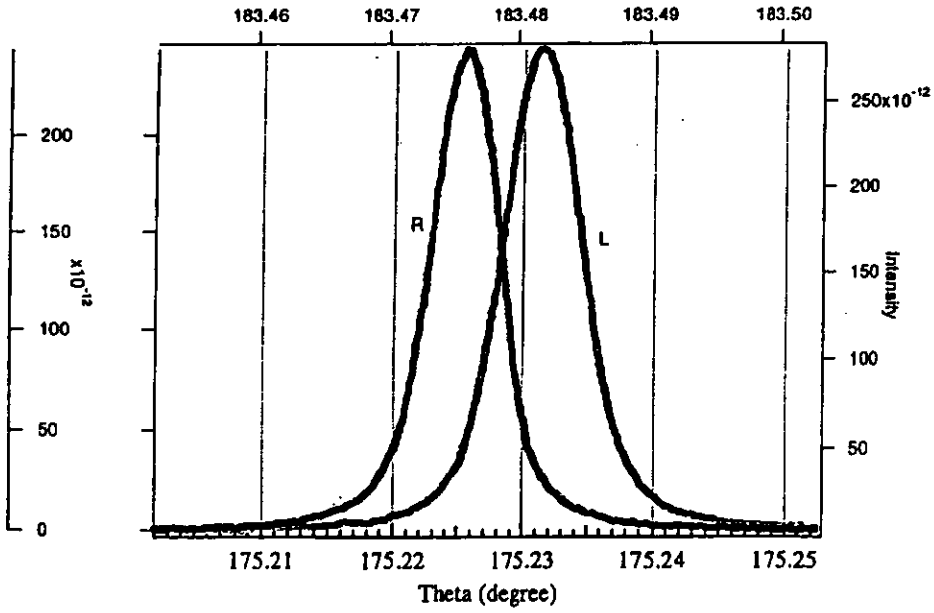

Fig 2 3 Pair of diffraction from GaAs(800) wafer sample.

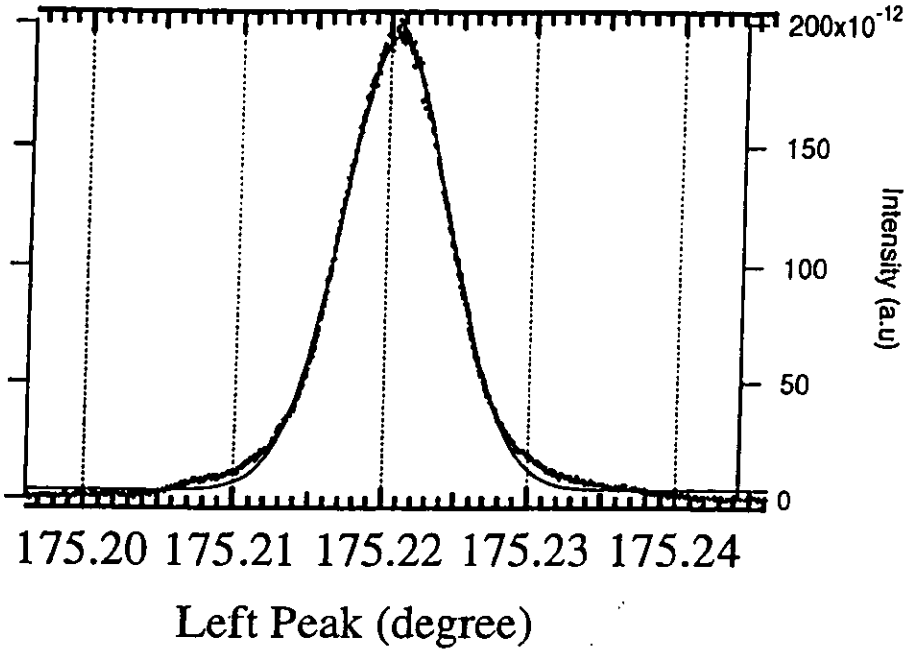

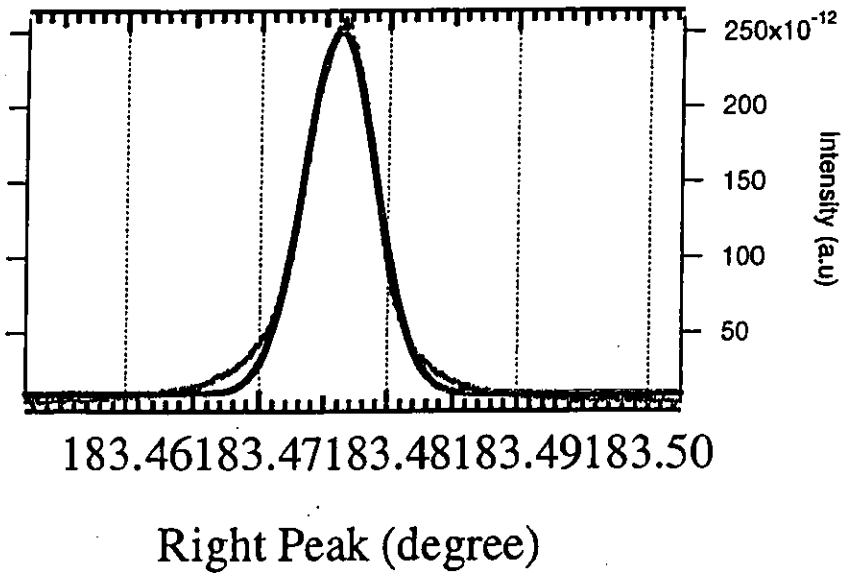

Fig 4 Diffraction from +(800) and -(800) of GaAs sample.

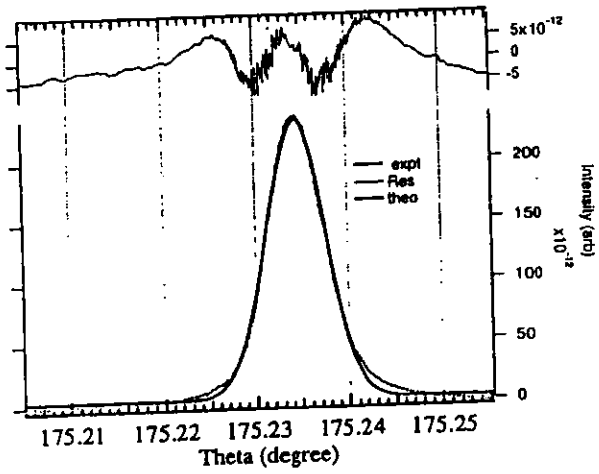

Fig 5 Diifraction from left peak showing good fit , upper half shows the residual.

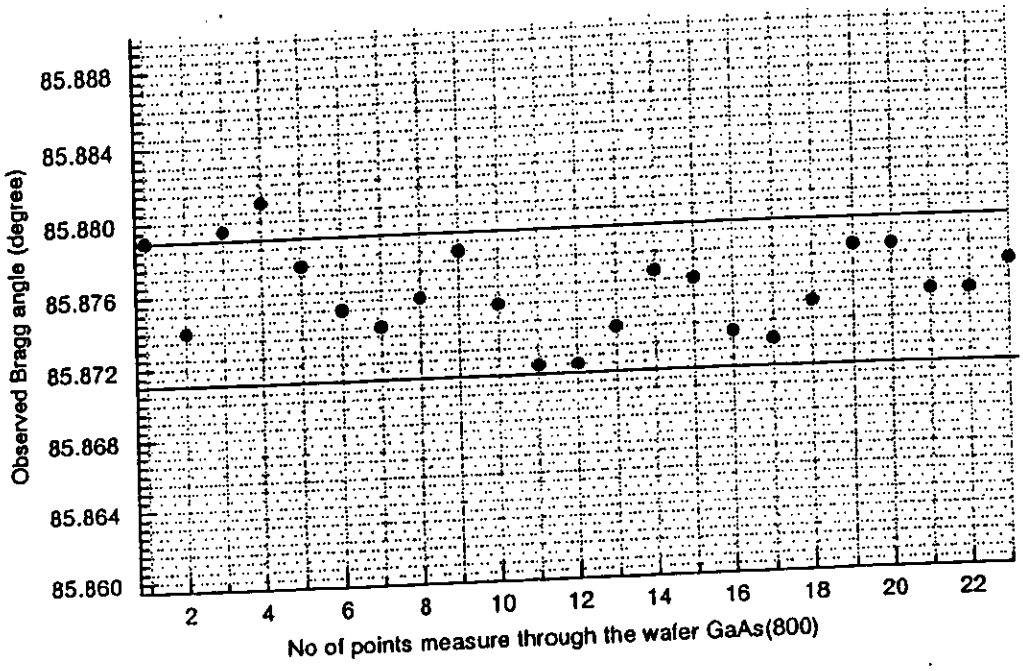

Fig 6 Measured Bragg angle from GaAs(800).

6.5 References

[1]Wilson A.J.C Appl.Phy **16,** 665 (1948)

[2] Buerger M.J precision method .New York,John willey (1964)

[3] Taupin D J Appl.Crys C **6,** 266 (1973)

[4] Wolf P.M de Acta Crysta 1 **1,** 207(1948)

[5]Powls .Acta cryst **12,** 483 (1979)

[6] Wilson,A.J.C J appl.phy **36,** 929(1980)

[7]M Hart .Phys. E.Sci Instrum **12,** 911 (1979)

[8] S.E.G.Slusky and A.T.Macrander Appl.Cryst. **20,** 522 (1987)

[9] D.Hausermann and M Hart J Appl.Cryst **23,** 63(1990).

[10]Peter Becker ,Klaus Dorenwendt et'al Phys.Rev Letter **46,** 1540 (1981)

[11] M Hart and D.P.Siddons Instruments and Methods

[12]Peter Becker ,Klaus Dorenwendt et'al Phys.Rev Letter **46,** 1540 (1981)

[13] Beaumont, J.H. Hart,M. (1974). J.Phys.E **7**823.

[14] Cermek.J. (1960). Acta.Cryst. **13,** 832.

[15] Cernohorsky.M.(1960). Acta.Cryst. **13,** 823.

[16] Compton, A.H. Allison, S.K., London:MacMillan (1935).

[17] Deslattes,R.D. Henins,A.(1973).Phys. Rev. Lett. **31,** 972.

[18] De Wolf.P. M. (1960).Acta.Cryst. **13,** 835.

[19] Hart,M Siddons,D.P.(1982). Instruments and Methods **204,** 219.

[20] Y.Okada and F.Orito, Appl.Phy.Lett,52,1998,582

[21] M.Ando, Y.Higashi, K.Usuda, S.Yasuami and H.Kawata: Rev.Sci.Instr**60-7**, 2410-2413(1978).

[22] Bond,W.L.,,Acta.Cryst. **13,** 814 (1960)

[23] Y.Okada ,Y Tokumura and Y kadota ,Appl.Phy.Lett,52,1998,582

[24] M.Ando,D.Bailey and M Hart. Acta Crya tallography A **A34**, 484-489 (1982).

[25]Buras B Appl Crysta **11,**137(1978)

[26] RAHMAN Mohammed Obaidur, OKADA Yasumasa, ZHANG Xiaowei, SUGIYAMA Hiroshi, IMAI Yasuhiko, NAKAYAMA Kan, FUJIMOTO Hiroyuki , TAKANO Yukio, YODA Yoshitaka and ANDO Masami.
KAZUKA Silicon Forum Proceedings. **1,** (1999)

[27] M.O.Rahman, H.Sugiyama, X.W.Zhang, K.Hyodo, and M.Ando JSSRR proceedings. **12,** 210 (1999)

[28] Deslattes,R.D.,Henins,A., Phys.Rev.Lett. **31,** 210 (1999)

[29] B.KAgarwal X-ray spectroscopy, springer Verlag. (1991)

[30] Y Yabashi private communication 2000]

[31] Nakayama, K., Hashizume H., Miyoshi A., Kikuta S., and Kohra K. Z Naturforsch teil **A28,** 632(1973)

[32] Y Saito, T Nakatani, T Matsushita, T Miyahara, et'al J .Sync rad **5,** 542 (1998)

[33] H.Miyazawa,Y.Ishii,S.Ishida and Y.nanishi Appl.Phy.Lett **43,** 853 (1983)

[34] A.S.Jordan,R.Caruso and A.R.Von Neida Bell sys. Tech J. **59,** 593(1980)

[35] T Matsushita and H Hashizume Hand book on synchrotron Radiation **vol 1,** 261 (1983)

[36] J.W.M Dumond Phys.Rev **52,** 872(1937)

[37] W.J.Bartels Philips tech .Rev **41,** 183 (1983)

[38] B.K.Tanner X-ray diffraction Topography,Pergomon press,Oxford (1981)

[39] H.Kuwamoto and D.E.Holmes J .Appl.Phy **59,** 656 (1986)

[40] S.Ozawa J .Cryst.Growth **76,** 323 (1986)

[41] I.Fujimoto J .J.Appl.Phy **23,** L287 (1984)

[42] G.Marienko J.Res.Natl bur.stn **A81,** 1 (1977)

[43] J.Harris,Y.Nannichi and G.Pearson J .Appl.Phy **40,** 4575 (1969)

[44] D.T.J.Hurle J .phy.Chem.solids **40,** 613 (1997)

[45]Oleg gang .J.Appl.cryst. **30,** 7-15(1997)

[46]Buras B Appl Crysta **11,**137(1978)

[47] W.L.Bond Acta crysta **13,** 814 (1960)

[48]Y.Takano,Y.ishida,N.Matsunaga Jpn.J.Appl.Phys **24,** L239(1985)

[49] Y.Okada and Y.Tokumaru Appl.Phys.Lett **48,** 1253 (1986)

[50] O.Lagerstedt and B.Monemar Phys.Rev B **19,** 3064 (1979)

[51] Bragg W.H An introduction to crystal structure analysis,london,Bell (1928)

[52]Parrish.W, Acta.Cryst.(1960). **13,** 838.

[53] Rahman,M.O. Ando,M.(2001). SPIE **4407,** 141

[54] Rahman,M.O., Okada.Y., Zhang, X.W. Sugiyama, H., Imai,Y., Nakayama,K., Fujomoto, H., , Takano, Y., Yoda, Y., Ando, M. (1999)KAZUKA Silicon Forum Proceedings. **1,** 175

[55] Rahman,M.O., Sugiyama,H., Zhang,X.W. Hyodo, K., Ando,M.(1999). JSSRR proceedings. **12,** 210.

[56]Matsushita, T., and U kaminaga (1980) Appl.Crystallogra. **13,** 465,472

[57] Kikuta,S and K.Kohra (1970) Phy.Soc Jpnl.Cryst. **29,** 1322.

[58] Matsushita,T., S.Kikuta and K.Kohra (1971) Phy.Soc Jpnl.Cryst. **30,** 1136.

[59] Usuda,K., PhD thesis (1994)Graduate University for Advanced studies,PF,KEK.

[60] James R W (1958) The Optical Principle of the Diffracation of x-rays (Bell, london)

[61] Materlik G V O kostrum (1980) Sci Inst. **51,** 86

[62] Takagi S(1962). Acta Crysta **B 15,** 1311

[63] Takagi S(1969). J.Phys.Soc Jpn **26,** 1239

[64] Slusky ,S.E.G. and A.T.Macrander, A.T.(1987) Appl.Cryst. **20,** 522.

[65] Staumanis.M.E.(1960).Acta.Cryst. **13,** 818.

[66] Weyerer.H.(1960).Acta.Cryst. **13,** 821.

[67] Wilkens.V.M.(1960). Acta.Cryst. **13,** 826.

[68] Kato N (1976). Acta Crysta **A 32,** 453

[69] W H Zachariasen Theory of x-ray diffraction in crystals,Dover (1994)

[70] Thorkildsen,G.(1987). Acta Cryst **A43,** 361

[71]Q. Shen, R.Colella Acta Crysta **A 44,** 17 (1988)

[72]R.Colella Acta Crysta **A 30,** 413 (1974)

[73] O.Pachakova, R Bubakova Acta Crysta **A 43,** 161 (1987)

[74] S L Chnag: Multiple Diffraction of X-rays in Crystals Solid State Series, Springer Verlag (1984).

0.0.1 Appendix:3 beam programme and MMCD code

0.0.2 Acknowledgment

```
      program three_beam
      real nog,nhg,noh,y1,y2
      common /c1/nog,nhg,noh
      open(1,file='data1.dat',status='unknown')

      pi=3.1415926
      noh=0.05
      nog=0.4
      nhg=0.4
      write(1,'(4a12)')  'phi','x','u','y'

      do i=1,4
        phi=(i-1)*90.0*pi/180.0

        x=0.0
        do j=1,101
          u=-40.0+(j-1)*80.0/100.0
          y1 =y(u,x,phi)
          write(1,100) phi*180.0/pi,x,u,y1
        end do

100     format(4f12.6)

        x=1.0
        do j=1,101
          u=-40.0+(j-1)*80.0/100.0
          y2 =y(u,x,phi)
          write(1,100) phi*180.0/pi,x,u,y2
        end do
        write(1,*)
      end do
      end

      function y(u,x,phi)
      real nog,nhg,noh,u,x,phi,y
      common /c1/nog,nhg,noh
        y=-2.0*abs(nog*nhg/noh)*(cos(phi)*f2(u,x)-sin(phi)*f1(u,x))
     *    -nog**2*f1(u,x)-nhg**2*(f1(u,x)+f4(u,x))
     *    +2.0*nog**2*nhg**2/noh**2*f3(u,x)
      end

      function f1(u,x)
       if ( abs(u) > 0.0001) then
         f1= 1.0/u**2*(1.0-cos(u)) + x/u**2*(1.0+cos(u)-2/u*sin(u))
       else
         f1= 0.5 - x/6.0
       end if
      end

      function f2(u,x)
        if ( abs(u) > 0.0001) then
          f2= 1.0/u*(1.0-1.0/u*sin(u)) +
     *        x/u**2*(sin(u)-2/u*(1.0-cos(u)))
        else
          f2 =u/6.0 -x*u/6.0
        end if
      end

      function f3(u,x)
        if ( abs(u) > 0.0001) then
          f3= 1.0/u**2*( 1.0-1.0/u*sin(u) ) + x/u**2*(0.5+sin(u)/u
     *      - 3.0/u**2*( 1.0-cos(u) ))
        else
```

```
      f3=1.0/6.0-x/6.0
    end if
  end

  function f4(u,x)
    if (abs(u) > 0.0001) then
      f4=x/u**2*(1.0+cos(u) - 2.0/u*sin(u)-x*(cos(u)-4.0*sin(u)/u
*        +6.0/u**2*(1.0-cos(u))))
   else
     f4 =-x/6.0-x**2/6.0
   end if
  end
```

Appendix: Structure Factor values of Si.

i j	h k l	esse	F(hkl)
1 2	-5-1-3	.5447	30.0208
1 3	-1-3-5	.5447	30.0208
1 4	-1-5-3	.5447	30.0208
1 5	-3-5-1	.5447	30.0208
1 6	-5-3-1	.5447	30.0208
1 7	-3-1-5	.5447	30.0208
2 1	5 1 3	.5447	30.0208
2 3	4-2-2	.4510	50.7968
2 4	4-4 0	.5208	44.5353
2 5	2-4 2	.4510	50.7968
2 6	0-2 2	.2604	69.5585
2 7	2 0-2	.2604	69.5585
3 1	1 3 5	.5447	30.0208
3 2	-4 2 2	.4510	50.7968
3 4	0-2 2	.2604	69.5585
3 5	-2-2 4	.4510	50.7968
3 6	-4 0 4	.5208	44.5353
3 7	-2 2 0	.2604	69.5585
4 1	1 5 3	.5447	30.0208
4 2	-4 4 0	.5208	44.5353
4 3	0 2-2	.2604	69.5585

```
*****************************************************************cc
.......................MMCD.......................................c
.....................MONOLITHIC MONOCHROMATOR CRYSTAL DESIGN.....c
.........THIS PROGRAM AUTOMATICALLY GENERATE THE TWO DIFFRACTION PLANES FOR cc
FABRICATION OF V-CUT MONOLITHIC MONOCHROMATOR AND THEIR WAVELENGTH. cc
*****************************************************************cc

-----------------------VERSION UNIX_98.6-----------------------cc

:cccccccccccccccccccccccccccccccccccccccccccccccccccccccccccccccccccc

      program MMCD
      parameter(a=5.431061,pi=3.1415926,n=3000)
      integer h1,k1,l1,h2,k2,l2,h,k,l,mark1,mark2
      integer list(n,6),ii,indx(n),indx2(n)
      real angle1,angle2,angle3,lamda,x,lamda_list(n),angle_list(n,3)
      real lamda2,lamda3,lamda_list2(n),lamda_list3(n)
      real theta1,theta2,theta10,theta20
      real d1,d2,lmbda,lmalp,lmphai,beta0,alpha,lap,lph,lamda0
      common /dat/d1,beta0,d2
      open(20,file='vtestwt.dat',status='unknown')
      open(30,file='vtestw1.dat',status='unknown')
      open(40,file='vtestw2.dat',status='unknown')
      open(50,file='vtestw3.dat',status='unknown')
: the following is a test for one paircccccccccccccccccccccccccccccccc
:cccccccccccccccccccccccccccccccccccccccccc
      h1=1
      k1=5
      l1=5
      h2=-4
      k2=4
      l2=4
      alpha=0.0
      phai=0.0
ccccccccccccccccccccccccccccccccccccccccccc
      write(40,*)'  alpha  ','  phai  ','  lamda'
      call bangle(h1,k1,l1,h2,k2,l2,angle3)
      write(*,*) 180.0-angle3
      call bangle(h1+h2,k1+k2,l1+l2,h2,k2,l2,angle1)
      write(*,*) angle1
      call bangle(h1+h2,k1+k2,l1+l2,h1,k1,l1,angle2)
      write(*,*) angle2
      call done(h1,k1,l1,d)
      write(*,*)'d=',d
      x=float(h1*h1+k1*k1+l1*l1)
      lamda=2.0*a/sqrt(x)*sin(angle1*pi/180.0)
      d1=a/sqrt(float(h1*h1+k1*k1+l1*l1))
      d2=a/sqrt(float(h2*h2+k2*k2+l2*l2))
      lmbda=(2*d1*sin(angle3))/((d1/d2-cos(angle3))**2+(sin(angle3))**2))**0.5
      lmalp=(2*d1*sin(angle3)*cos(alpha))/((d1/d2-cos(angle3))**2+
     * (sin(angle3))**2*(cos(alpha))**2)**0.5
      lmphai=(2*d1*sin(angle3)*cos(alpha+phai))/((d1/d2-cos(angle3))**2+
     * (sin(angle3))**2*(cos(alpha+phai))**2)**0.5
      write(*,*) lamda
      write(*,*) lmbda,angle3,d1,d2
      write(*,*) lmbda,lmalp,lmphai,alpha,phai
      pause
      ii=1
      do h1=0,5
        do k1=h1,5
          do l1=k1,5
            do h2=-5,5
              do k2=-5,5
                do l2=-5,5
```

```
                if (mod(abs(h1),2).eq.1.and.mod(abs(k1),2).eq.1
     *              .and.mod(abs(l1),2).eq.1) then
                    mark1=1
                    goto 1
                else
                    mark1=0
                end if
                if (mod(h1,2).eq.0.and.mod(k1,2).eq.0
     *              .and.mod(l1,2).eq.0) then
                    if (mod(h1+k1+l1,4).eq.0) then
                        if (h1*h1+k1*k1+l1*l1.gt.0) then
                           mark1=1
                        else
                           mark1=0
                        end if
                    else
                        mark1=0
                    end if
                else
                    mark1=0
                end if
:cccccccccccccccccccccccccccccccccccccccccccccccccccccccccccccccccccccc
                continue
                if (mod(abs(h2),2).eq.1.and.mod(abs(k2),2).eq.1
     *              .and.mod(abs(l2),2).eq.1) then
                    mark2=1
                    goto 2
                else
                    mark2=0
                end if
                if (mod(h2,2).eq.0.and.mod(k2,2).eq.0
     *              .and.mod(l2,2).eq.0) then
                    if (mod(h2+k2+l2,4).eq.0) then
                        if (h2*h2+k2*k2+l2*l2.gt.0) then
                           mark2=1
                        else
                           mark2=0
                        end if
                    else
                        mark2=0
                    end if
                else
                    mark2=0
                end if
:cccccccccccccccccccccccccccccccccccccccccccccccccccccccccccccccccccccc
!               continue
                if (mark1*mark2.eq.1) then
                    h=h1+h2
                    k=k1+k2
                    l=l1+l2
                    call bangle(h1,k1,l1,h2,k2,l2,angle3)
                    call bangle(h1,k1,l1,h,k,l,angle2)
                    call bangle(h2,k2,l2,h,k,l,angle1)
                    x=float(h1*h1+k1*k1+l1*l1)
                    lamda=2.0*a/sqrt(x)*sin(angle1*pi/180.0)
                    if (lamda.ge.0.5.and.lamda.le.1.5) then
                       list(ii,1)=h1
                       list(ii,2)=k1
                       list(ii,3)=l1
                       list(ii,4)=h2
                       list(ii,5)=k2
                       list(ii,6)=l2
                       angle_list(ii,1)=angle1
                       angle_list(ii,2)=angle2
                       angle_list(ii,3)=180.0-angle3
                       lamda_list(ii)=lamda
```

```
                    beta0=(180.0-angle3)*pi/180.0
                    d1=a/sqrt(float(h1*h1+k1*k1+l1*l1))
                    d2=a/sqrt(float(h2*h2+k2*k2+l2*l2))
                    lamda2=flamda(0.0,0.0)

                    beta0=(angle3)*pi/180.0
                    lamda3=flamda(0.0,0.0)
                    lamda_list2(ii)=lamda2
                    lamda_list3(ii)=lamda3
                    ii=ii+1
                    write(*,10) h1,k1,l1,h2,k2,l2,h,k,l,
                                180-angle3,angle2,angle1,
     *                          angle1+angle2+180-angle3,lamda
     *              write(30,10) h1,k1,l1,h2,k2,l2,h,k,l,
                                180-angle3,angle2,angle1,
     *                          angle1+angle2+180-angle3,lamda
     *

                 end if
              else
                 write(*,*) h1,k1,l1,h2,k2,l2
                 pause
              end if
           end do
        end do
      end do
    end do
  end do
  format(1x,3i2,'   ',3i2,'   ',3i3,'   ',4f9.4,f12.6)
  call indexx(n,lamda_list,indx)
  call indexx(n,lamda_list2,indx2)
  do i=1,n
     ii=indx(i)
     ii2=indx2(i)
     if (lamda_list(ii).ne.0.0) then
        h1=list(ii,1)
        k1=list(ii,2)
        l1=list(ii,3)
        h2=list(ii,4)
        k2=list(ii,5)
        l2=list(ii,6)
        h=h1+h2
        k=k1+k2
        l=l1+l2
        angle1=angle_list(ii,1)
        angle2=angle_list(ii,2)
        angle3=angle_list(ii,3)
        lamda=lamda_list(ii)
        write(20,10) h1,k1,l1,h2,k2,l2,h,k,l,
                     angle3,angle2,angle1,
     *               angle1+angle2+angle3,lamda
     *
     end if
     if (lamda_list2(ii2).ne.0.0) then
        h1=list(ii2,1)
        k1=list(ii2,2)
        l1=list(ii2,3)
        h2=list(ii2,4)
        k2=list(ii2,5)
        l2=list(ii2,6)
        h=h1+h2
        k=k1+k2
        l=l1+l2
        angle1=angle_list(ii2,1)
        angle2=angle_list(ii2,2)
        angle3=angle_list(ii2,3)
        lamda2=lamda_list2(ii2)
```

```
      lamda3=lamda_list3(ii2)
      if (mod(h+k+l,4).ne.0.and.lamda2.ge.0.5.
     *  and.lamda2.lt.1.5.and.lamda3.ge.0.5.and.lamda3.lt.1.5
     *    .and.mod(abs(h),2).eq.0.
     *  and.mod(abs(k),2).eq.0
     *   .and.mod(abs(l),2).eq.0) then
     *     write(40,10) h1,k1,l1,h2,k2,l2,h,k,l,
     *                  angle3,angle2,angle1,
     *                  angle1+angle2+angle3,lamda2
      d1=a/sqrt(float(h1*h1+k1*k1+l1*l1))
      d2=a/sqrt(float(h2*h2+k2*k2+l2*l2))
      theta1=asin(lamda2/(2.0*d1))*180.0/pi
      theta2=asin(lamda2/(2.0*d2))*180.0/pi
      theta10=asin(lamda3/(2.0*d1))*180.0/pi
      theta20=asin(lamda3/(2.0*d2))*180.0/pi
      write(50,11) h1,k1,l1,h2,k2,l2,h,k,l,
     *             angle3,theta1,theta2,
     *             theta1+theta2+angle3,lamda2,
     *             180.0-angle3,theta10,theta20,
     *             180.0-angle3+theta10+theta20,lamda3
     *
      end if
    end if
    format(9i3,3f9.3,1f7.1,1f8.4,3f9.3,1f7.1,1f8.4)
1
      do j=0,15
        alpha=float(j)*pi/180.0
         lap=flamda(alpha,0.0)
c     lap=(2.0*d1*sin(beta0)*cos(alpha+phai))
     *  /sqrt((d1/d2-cos(beta0))**2
     *  +(sin(beta0))**2*(cos(alpha+phai))**2)
        write(40,100) alpha/pi*180.0,0.0,lap
c     end do
      do j=0,15
c        do k=1,5
c           alpha=float(j)*pi/180.0
c           phai=0.1*float(k)*pi/180.0
c           lph=flamda(alpha,phai)
c           write(40,100) alpha/pi*180.0,phai,lph
c        end do
c     end do

    end do
100 format(3e16.8)
    end

    function flamda(alpha,phai)
    parameter(pi=3.1415926)
    real alpha,phai,d1,d2,beta0
    common /dat/d1,beta0,d2
    flamda=(2.0*d1*sin(beta0)*cos(alpha+phai))
   * /sqrt((d1/d2-cos(beta0))**2
   *       +(sin(beta0))**2*(cos(alpha+phai))**2)
    end

    subroutine bangle(h1,k1,l1,h,k,l,angle)
    parameter(pi=3.1415926)
    real x,y,z,angle
    integer h1,k1,l1,h,k,l,n1,n2,n3
    n1=h1**2+k1**2+l1**2
    n2=h**2+k**2+l**2
    n3=h1*h+k1*k+l1*l
    x=float(n1)
    y=float(n2)
    z=float(n3)
    if (n1*n2.eq.n3*n3) then
       angle=acos(1.0)*180.0/pi
```

```
      else
         angle=acos(z/sqrt(x*y))*180.0/pi
      end if
      end
*************************************************************************
      subroutine done(h1,k1,l1,d)
      real h1,k1,l1,d
      parameter(a=5.431061)
      d=a/sqrt(float(h1*h1+k1*k1+l1*l1))
      return
      end

cc this is a subroutine for writing the wavelength in order cccccccccccc

      SUBROUTINE indexx(n,arr,indx)
      INTEGER n,indx(n),M,NSTACK
      real  arr(n)
      PARAMETER (M=7,NSTACK=1000)
      INTEGER i,indxt,ir,itemp,j,jstack,k,l,istack(NSTACK)
      real  a
      do j=1,n
        indx(j)=j
      end do
      jstack=0
      l=1
      ir=n
1     if(ir-l.lt.M)then
        do 13 j=l+1,ir
          indxt=indx(j)
          a=arr(indxt)
          do i=j-1,l,-1
            if(arr(indx(i)).le.a)goto 2
            indx(i+1)=indx(i)
          end do
          i=l-1
2         indx(i+1)=indxt
13      continue
        if(jstack.eq.0)return
        ir=istack(jstack)
        l=istack(jstack-1)
        jstack=jstack-2
      else
        k=(l+ir)/2
        itemp=indx(k)
        indx(k)=indx(l+1)
        indx(l+1)=itemp
        if(arr(indx(l)).gt.arr(indx(ir)))then
          itemp=indx(l)
          indx(l)=indx(ir)
          indx(ir)=itemp
        endif
        if(arr(indx(l+1)).gt.arr(indx(ir)))then
          itemp=indx(l+1)
          indx(l+1)=indx(ir)
          indx(ir)=itemp
        endif
        if(arr(indx(l)).gt.arr(indx(l+1)))then
          itemp=indx(l)
          indx(l)=indx(l+1)
          indx(l+1)=itemp
        endif
        i=l+1
        j=ir
        indxt=indx(l+1)
        a=arr(indxt)
3       continue
```

```
  i=i+1
if(arr(indx(i)).lt.a)goto 3
continue
  j=j-1
if(arr(indx(j)).gt.a)goto 4
if(j.lt.i)goto 5
itemp=indx(i)
indx(i)=indx(j)
indx(j)=itemp
goto 3
indx(l+1)=indx(j)
indx(j)=indxt
jstack=jstack+2
if(jstack.gt.NSTACK)pause 'NSTACK too small in indexx'
if(ir-i+1.ge.j-1)then
  istack(jstack)=ir
  istack(jstack-1)=i
  ir=j-1
else
  istack(jstack)=j-1
  istack(jstack-1)=l
  l=i
endif
endif
goto 1
END
```

Acknowledgment:

I am extremely grateful to my honourable supervisors Professor Masami Ando, Professor Yoshitaka Kimura , Professor Tadashi Matsushita, Professor Kazumasa Ohsumi, Professor Atsuo IIda, Professor Hiroshi kawata, Professor Masaharu Nomura for jointly supervising me during my difficult time. I am extremely grateful to Professor Yoshitaka Kimura, Head, Department of Material Structure Science, Graduate University for Advanced Studies and Director, Institute of Material Structure Science, High Energy Accelerator Research Organization-KEK, Japan for his constant encouragement, indispensable guidance, thoughtful suggestions throughout my research works. I am very grateful to Professor Tadashi Matsushita, Chairman of my doctoral degree Committee and Deputy Director Of the Institute of Material Structure Science, High Energy Accelerator Research Organization-KEK , Graduate University for Advanced Studies for his kind suggestions, discussions, valuable guidance and encouragements during my rersearch works and introducing me with the N-beam dynamical diffraction problem. I would deeply thank Professor Masami Ando for his kind guidance, supervision and constant encouragement and providing me the opportunity for my higher studies in Japan. His deep love for science will encourage me in future to develop my career further.

I would like to thank Professor Keiichi Kodaira, President of the Graduate University for Advanced Studies for his kind guidance, encouragement and special care about my academic progress.

I would also like to thank Dr X W Zhang, Dr K Hyodo, Dr H Sugiyama, for their continuous help during the experiment, data takaing and analysis, crystal cutting procedure , etching and overall guidance. I am grateful to Dr Y Higashi for helping in understanding the design , fabrication and performance of the precision goniometer and to build up the temperature system made of styro foam.

I would llike to thank again to Professor Kazumasa Ohsumi, Professor Atsuo IIda, Professor Hiroshi Kawata and Professor Masaharu Nomura for their continuous guidance, helpful discussions and suggestions which lead to write this thesis successfully. I would also wish to thank Professor Adolfo Savoia , Director of ELETTRA, Italy for introducing me the SR science.

I am highly grateful to Professor Sher Alam, Adavanced Institute of Science and Technology (AIST) for tremendous help in understanding and solving the Maxwells equations and for critical reading of my manuscript.

I am grateful to Professor Sadao Aoki, Departmental of Applied Physics

to provide me as his research student status in the University of Tsukuba and guiding me for the improvement of my thesis. I am grateful to Professor Seishi Kikuta for his encouragement and helping me to come to Japan. Thanks also goes to Professor Y Azuma, Prof K Koide, Prof Akira Yagishita, Prof K Nasu, Prof S Kamada, Dr S Yamamoto for their encouragment and helps during my research works.

I acknowledge my indebtedness and gratefulness to all honorable Faculty members of the the Department of Material structure science, Graduate University for Advanced Studies for their hearty cooperation and help in my research work when I faced problems and confusions.

Thanks also to Prof R Colella of Purdue University, USA and Prof S L Chang of SSRC Taiwan and Prof C T Chen director of SSRC Taiwan for their very kind comments and help.

I also feel to oblige thanks to our GUAS friends Mr Y Miyata, Mr O Morimoto Mr H Osawa and Mr Atsushi Mizusawa , Mr H Uchiyama and others. Thanks also goes to Reiko Ohtubo for various kind of help for my life in Japan.

Thanks to my father in law Mr Kazi Delwar Hossain, and mother in law Mrs Khurshida Hossain, for their affection, special thanks to my wife Halima for her great patience as well as to my sisters in laws Ameena, Mahera, Mahbuba, Bushra and brother in law Talha Hossain.

Thanks to my elder brother Mr Mahbubur Rahman, Mr Mominur Rahman, Mr Lutfur Rahman for their encouragement and supports. Also to my younger brothers Aziz, Murad, Murshed, Naeem and Jubaer.

Finally all thanks are due to Almighty Allah for making things and situations congenial and favourable for me for the task undertaken.